LONGITUDINAL CONTROL EFFECTIVENESS AND ENTRY DYNAMICS OF A SINGLE-STAGE-TO-ORBIT VEHICLE

Nguyen X. Vinh and Ching-Fang Lin
The University of Michigan
Ann Arbor, Michigan

Prepared for Langley Research Center
Under Grant NAG-1-86

TABLE OF CONTENTS

NOMENCLATURE

a	constant, Eq.(86); parameter in the confluent hypergeometric equation, Eq.(236); parameter in the hypergeometric equation.
A	square matrix, Eq.(76); constant of integration, Eq.(153).
b	parameter in the confluent hypergeometric equation; parameter in the hypergeometric equation.
$b(\tau)$, $b_1(\tau)$	varying coefficients in the equations for the angle-of-attack.
B	inertia parameter, Eq.(194).
c	flight path angle parameter, Eq.(126).
$c(\tau)$, $c_1(\tau)$	varying coefficients in the equations for the angle-of-attack.
$\bar{c}$	mean aerodynamic chord.
C_D	drag coefficient.
C_L	lift coefficient.
C_N	normal aerodynamic force coefficient.
C_m	aerodynamic pitch moment coefficient.
$C_{m_{ac}}$	pitch moment coefficient about the aerodynamic center.
C_{m_t}	thrust moment coefficient.
$C_{m_{tot}}$	total pitch moment coefficient.
$C_{D_\alpha} = \partial C_D / \partial \alpha$	slope of drag curve.
$C_{L_\alpha} = \partial C_L / \partial \alpha$	slope of lift curve.
$C_{m_\alpha} = \partial C_m / \partial \alpha$	static stability derivative.
$C_{m_{\dot{\alpha}}} = (V_o/\bar{c})(\partial C_m / \partial \dot{\alpha})$	downwash effect stability derivative.
$C_{m_q} = (V_o/\bar{c})(\partial C_m / \partial q)$	damping in pitch stability derivative.
D	drag force.
E	lift-to-drag ratio.
f	average thrusters force.

F_N	normal component of the combined aerodynamic and propulsive force.
F_T	tangential component of the combined aerodynamic and propulsive force.
$\vec{F}$	total force applied to the vehicle.
g	acceleration of the gravity.
$\vec{G}$	total moment of force.
h	constant parameter, Eq.(224).
h, h_{ac}	location in fraction of $\bar{c}$ of the center-of-gravity and mean aerodynamic center, Fig. 5.
H	altitude.
$\vec{H}$	angular momentum of vehicle.
I_x, I_y, I_z	moments of inertia about body axes.
I_{xz}	product of inertia.
k	constant parameter, Eq.(224).
k_1, k_2, k_3	constant coefficients, Eq.(223).
k_4, k_5	constant coefficients, Eq.(256).
k_y	dimensionless pitch moment of inertia, Eq.(194).
K	stability static margin.
$\bar{K}$	approximate value of K.
ℓ	body length.
ℓ_t	lever arm of thrusters force.
L	lift force.
m	mass of vehicle.
M	Mach number.
M	aerodynamic pitch moment about the center-of-gravity.
M_{ac}	aerodynamic pitch moment about the mean aerodynamic center.
M_t	thrusters pitch moment.

M_X, M_Y, M_Z	projections of total moment on body axes.
n	load factor; pitch frequency, Eq.(205).
N	number of oscillations.
p	roll rate; atmospheric pressure.
P	period.
q	pitch rate.
$\bar{q}$	dynamic pressure.
r	yaw rate.
R	radial distance from center of the Earth.
R*	gas constant.
s	speed parameter, Eq.(72).
S	reference area.
t	time.
T	power plant thrust magnitude; absolute temperature.
u	velocity component along x-body axis.
U	dependent variable, Eq.(185).
v	velocity component along y-body axis.
$\bar{v}$	dimensionless kinetic energy, Eq.(177).
V	speed.
$\vec{V}$	velocity vector.
w	velocity component along z-body axis.
W	weight of vehicle.
(x, y, z)	Cartesian coordinates.
(X, Y, Z)	components of combined aerodynamic and propulsive force on body axes.
x	speed variable, Eq.(115).
x_{ac}	distance from nose tip to aerodynamic center.
x_{cg}	distance from nose tip to center-of-gravity.

y	density dependent variable, Eq.(135).
y	angle-of-attack dependent variable, Eq.(224), Eq.(266).
Y	dimensionless atmospheric density, Eq.(115).
z	dependent variable, Eq.(181).
α	angle-of-attack; also denotes its perturbation.
β	sideslip angle.
$\bar{\beta}$	inverse of atmospheric height scale, Eq.(116).
γ	flight path angle.
δ	dimensionless atmospheric density, Eq.(67).
δ_e	elevon deflection angle.
δ_F	body-flap deflection angle.
ε	small perturbation, Eq.(93).
ζ	coefficient of proportionality, Eq.(60); speed independent variable, Eq.(146), Eq.(168), Eq.(260).
η	damping term, Eq.(205); density independent variable, Eq.(224).
θ	attitude.
λ	longitude; characteristic root.
μ	speed independent variable, Eq.(185), Eq.(266).
μ	density independent variable, Eq.(228).
ξ	constant, Eq.(79).
ρ	atmospheric density.
σ	density gradient, Eq.(72).
τ	firing time; dimensionless arc length, Eq.(65).
ϕ	bank angle.
Φ	flight path angle variable, Eq.(115).
ψ	heading; functions as defined in Eqs.(161), (164).
ω	phugoid frequency, Eq.(79).

$\bar{\omega}$	modified phugoid frequency, Eq.(110).
$\vec{\Omega}$	angular velocity of vehicle.

Subscripts

$_o$	reference condition; initial condition.
$_i$	initial condition.
$_g$	relative to ground system.

LIST OF FIGURES

SUMMARY

The classical theory of flight dynamics fcr airplane longitudinal stability and control analysis was extended to the case of a hypervelocity reentry vehicle. This included the elements inherent in supersonic and hypersonic flight such as the influence of the Mach number on aerodynamic characteristics, the effect of reaction control system and aerodynamic controls on the trim condition through a wide range of the speed.

Phugoid motion and angle-of-attack oscillation for three typical cases of cruising flight, ballistic entry and glide entry were investigated. In each case, closed form solutions for the variations in altitude, flight path angle, speed and angle-of-attack were obtained. These solutions displayed explicitly the influence of different design parameters and trajectory variables on the stability of the motion.

Aerodynamic and inertia characteristics of a Single-Stage-To-Orbit vehicle (SSTO) were used in the numerical application but the basic analytical theory developed can be used to assess entry dynamics of any lifting vehicle.

I. INTRODUCTION

A new Earth orbital transportation system could be required beginning in the last decade of this century provided that such system offers clear and significant cost/performance advantages over the existing system.

A proposal for such system is a Single-Stage-To-Orbit vehicle (SSTO) capable of performing space missions similar to that of the current space shuttle. After a direct ascent into orbit and completion of its space mission, the vehicle must sustain a reentry into the Earth's atmosphere at hypersonic speeds with lifting capability for a crossrange of 1100 n.mi., and perform a horizontal landing at speed not exceeding 170 knots.

Studies associated with the entry dynamics of this vehicle are now being conducted. Several excellent analyses have demonstrated the applicability of the control configured design approach to Advanced Earth Orbital Transportation Systems. It has been shown that, for the control-configured vehicle (CCV), the major design criteria are the hypersonic trim, the location of the center-of-gravity, the control surfaces heating and the mass of the system. Applicability and potential performance gains of CCV design concepts as applied to the development of a SSTO were globally analyzed in reference 1. One of the most significant applications of CCV concept is the reduction of the required vehicle static margins which can be used to reduce stabilizer and fin size, reduce trim drag, reduce wing size because of more favorable balancing tail loads. This may lead to significant weight savings. This problem has been analyzed by Freeman and Wilhite (ref. 2) using modern design analysis techniques (refs. 3-4). Starting with a baseline venicle with positive level of longitudinal stability, the vehicle was configured with the conventional stability requirements relaxed. The control-configured vehicle has an estimated gross lift-off mass 10 percent less than that of the baseline vehicle design. The largest single component weight reduction is a 33 percent reduction in the wing weight due to the 43 percent reduction in exposed wing area. Because of this, for the CCV, the ratio of body-planform to wing-planform area increases and the aerodynamic center is much more dependent on Mach number. From the aerodynamic characteristics deduced, it has been shown that the control-configured vehicle can be trimmed hypersonically over an acceptable angle-of-attack range, from 10° to 60°, by a combination of a body flap and elevon deflection.

On the other hand, for the SSTO vehicle, an aft center-of-gravity location resulting from large engine mass at the rear of the vehicle has created new stability problems during entry. The effect of center-of-gravity locations on hypersonic trim has been analyzed in reference 5. The results of this excellent study predict that control configuring of the reentry vehicle is definitely a requirement, and a combination of aerodynamic controls and reaction control system (RCS) would be adequate. While the location of the center-of-gravity can be easily evaluated, and by averaging, the RCS characteristics can be accurately modeled, the aerodynamic characteristics, and in particular, the aerodynamic center, can only be projected from wind tunnel tests before definite results can be obtained from flight tests data. This results in uncertainties to be incorporated in any analysis of dynamic stability and control of advanced transportation systems. These are analyzed

for the space shuttle orbiter in references 6 and 7 and can be extended to the SSTO design.

In this report, we shall extend the classical theory of flight dynamics for airplane stability and control analysis to the case of a SSTO vehicle. This will include the elements inherent in supersonic and hypersonic flight such as the influence of the Mach number on aerodynamic characteristics, the effects of RCS and aerodynamic controls on the trim condition through a wide range of the speed. Another important aspect of stability and control in hypersonic flight such as in the case of a SSTO vehicle which is not present in the case of airplane dynamics is the strong influence of the trajectory variables. While at low speeds one can always assess the stability dynamics using small perturbations theory about a steady reference flight path, reentry dynamics is an unsteady phenomenon in which the effects of the deceleration, the atmospheric density gradient and the curvature of the Earth are all important.

The organization of this report is as follows. After this introductory chapter, the classical Euler's equations of motion for airplane stability analysis are derived in Chapter II. For entry dynamics, these equations must be modified to include the effect of the variation of the vector acceleration of the gravity. As a first step, we introduce the modifying term to obtain the equations for longitudinal dynamics to be used for the analysis in this report. The effectiveness of reaction control system and aerodynamic controls on the trim condition during entry is analyzed in Chapter III. Entry dynamics of the SSTO is the subject of investigation in the following two chapters. In Chapter IV the phugoid, or trajectory oscillations for the three typical cases of cruising flight, ballistic entry and glide entry are investigated. In the analysis the important effects of atmospheric gradient, curvature of the flight path and deceleration are displayed explicitly. Chapter V investigates the angle-of-attack oscillations during entry for these cases. Resonance phenomena are analyzed and criteria for dynamic stability are established.

This study benefits from the wealth of aerodynamic data for the control-configured SSTO vehicle generated in references 2 and 8 and because of that it provides further understanding of the dynamic behavior of this advanced transportation system although the basic analytical theory can be used to assess entry dynamics of any lifting vehicle.

II. EULER'S EQUATIONS OF MOTION

The best description of the dynamic forces and moments connected with a rotating rigid body is given by Euler's dynamical equations based upon an axis system that remains rigidly fixed at the center-of-gravity of the moving body. On the other hand, the motion of the center-of-gravity is generally described by a differential system written with respect to inertial system.

In this chapter, we shall discuss the relationship between the two systems of equations.

Equations of Motion Over a Flat Earth

For a non rotating flat Earth, the variables involved are:

a) Position of the center-of-gravity with respect to a Cartesian ground system $Gx_g y_g z_g$ considered as inertial system

$$\begin{cases} x \\ y \\ z = -H \end{cases}$$

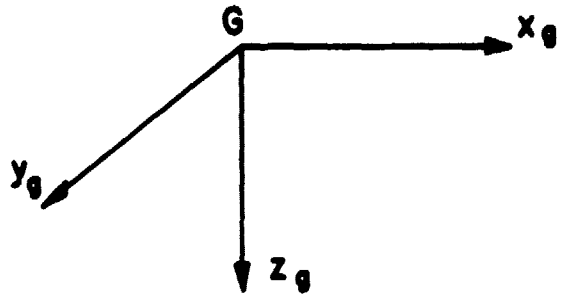

Notice that H is the altitude and subscript g has been omitted for convenience.

b) Components of the velocity vector $\vec{V}$ along the body axes

$$\vec{V} \begin{cases} u \\ v \\ w \end{cases}$$

c) Euler's angles

$$\begin{cases} \psi \\ \theta \\ \phi \end{cases}$$

d) Components of angular velocity $\vec{\Omega}$ of the vehicle along the body axes

$$\vec{\Omega} \begin{cases} p \\ q \\ r \end{cases}$$

With respect to the body axis system, the velocity vector $\vec{V}$ is defined in direction by the angle-of-attack α and the sideslip angle β with the relations (Fig. 1)

$$u = V\cos\beta\cos\alpha$$

$$v = V\sin\beta$$

$$w = V\cos\beta\sin\alpha$$

$$V = u\cos\alpha\cos\beta + v\sin\beta + w\sin\alpha\cos\beta \tag{1}$$

$$= \sqrt{u^2 + v^2 + w^2}$$

$$\tan\alpha = w/u$$

$$\tan\beta = v/\sqrt{u^2 + w^2}$$

where V is the magnitude of the velocity vector and u, v and w are the components of $\vec{V}$ along the body axes.

Using the body axes as reference system, the two vector equations

$$m\left(\frac{d\vec{V}}{dt} + \vec{\Omega}\times\vec{V}\right) = \vec{F}$$

$$\frac{d\vec{H}}{dt} + \vec{\Omega}\times\vec{H} = \vec{G} \tag{2}$$

for the forces and moments have projections

$$m[\dot{u} + qw - rv] = X - mg\sin\theta$$

$$m[\dot{v} + ru - pw] = Y + mg\cos\theta\sin\phi \tag{3}$$

$$m[\dot{w} + pv - qu] = Z + mg\cos\theta\cos\phi$$

and

$$I_x\dot{p} - I_{xz}(\dot{r} + pq) + (I_z - I_y)qr = M_X$$

$$I_y\dot{q} + (I_x - I_z)rp + I_{xz}(p^2 - r^2) = M_Y \tag{4}$$

$$I_z\dot{r} - I_{xz}(\dot{p} - rq) + (I_y - I_x)pq = M_Z$$

In Eqs.(3), X, Y and Z are the components along body axes of the combined aerodynamic and propulsive forces. In Eq.(4), it is assumed that, by symmetry the products of inertia $I_{xy} = I_{yz} = 0$. The three moments of force M_X, M_Y and M_Z are about the roll, pitch and yaw axes respectively.

We have, in addition, the kinematic relations

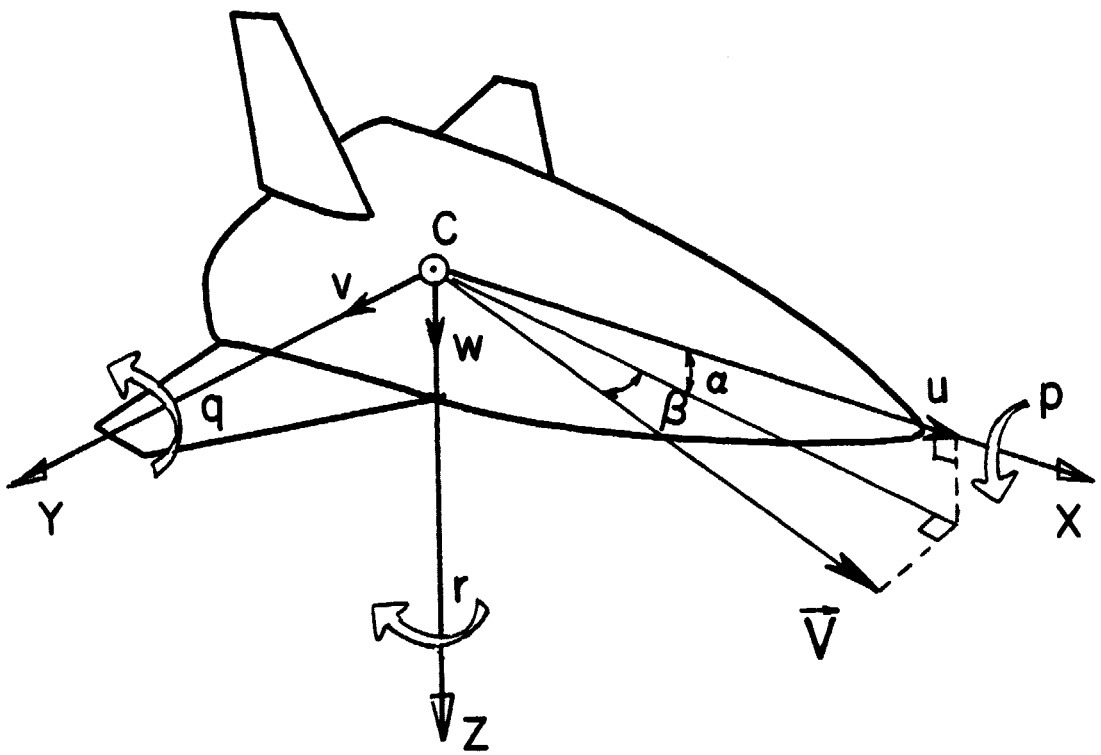

Fig. 1. Body axis system.

$$\dot{\psi} = (q \sin\phi + r \cos\phi)/\cos\theta$$

$$\dot{\theta} = q \cos\phi - r \sin\phi \qquad (5)$$

$$\dot{\phi} = p + (q \sin\phi + r \cos\phi)\tan\theta$$

The body system CXYZ is obtained from the ground system Gxyz by three rotations: ψ about z to Cx_1y_1z, then θ about y_1 and then ϕ about X, (Fig. 2). Hence, we have the transformation

$$\begin{pmatrix} x \\ y \\ z \end{pmatrix} = \begin{pmatrix} \cos\psi & -\sin\psi & 0 \\ \sin\psi & \cos\psi & 0 \\ 0 & 0 & 1 \end{pmatrix} \begin{pmatrix} \cos\theta & 0 & \sin\theta \\ 0 & 1 & 0 \\ -\sin\theta & 0 & \cos\theta \end{pmatrix} \begin{pmatrix} 1 & 0 & 0 \\ 0 & \cos\phi & -\sin\phi \\ 0 & \sin\phi & \cos\phi \end{pmatrix} \begin{pmatrix} X \\ Y \\ Z \end{pmatrix}$$

Carrying out the matrix multiplication

$$\begin{pmatrix} x \\ y \\ z \end{pmatrix} = \begin{pmatrix} \cos\theta\cos\psi & (\sin\theta\sin\phi\cos\psi - \cos\phi\sin\psi) & (\sin\theta\cos\phi\cos\psi + \sin\phi\sin\psi) \\ \cos\theta\sin\psi & (\sin\theta\sin\phi\sin\psi + \cos\phi\cos\psi) & (\sin\theta\cos\phi\sin\psi - \sin\phi\cos\psi) \\ -\sin\theta & \cos\theta\sin\phi & \cos\theta\cos\phi \end{pmatrix} \begin{pmatrix} X \\ Y \\ Z \end{pmatrix}$$

Putting (X,Y,Z) = (u,v,w) and (x,y,z) = (u_g,v_g,w_g), we deduce the projections of the velocity vector on the ground inertial axis system

$$\dot{x}_g = \dot{}'_g = u \cos\theta\cos\psi + v(\sin\theta\sin\phi\cos\psi - \cos\phi\sin\psi) + w(\sin\theta\cos\phi\cos\psi + \sin\phi\sin\psi)$$

$$\dot{y}_g = v_g = u \cos\theta\sin\psi + v(\sin\theta\sin\phi\sin\psi + \cos\phi\cos\psi) + w(\sin\theta\cos\phi\sin\psi - \sin\phi\cos\psi) \qquad (6)$$

$$\dot{z}_g = -\dot{H} = w_g = -u \sin\theta + v \cos\theta\sin\phi + w \cos\theta\cos\phi$$

The equations (3), (4), (5) and (6) completely describe the motion of the vehicle in the case of airplane dynamics.

The aerodynamic and propulsive forces and moments are functions of the control input, the speed and altitude. On the right-hand-side, we have 9 variables

$$H,\ u,\ v,\ w,\ \theta,\ \phi,\ p,\ q,\ r$$

It suffices to integrate the equations concerning these variables. Once they are known as functions of the time, the additional equations in x, y and ψ can be integrated.

Longitudinal Equations of Motion Over a Spherical Earth

For airplane dynamics, the equations above are adequate. For any vehicle configuration with known mass and engine properties, it suffices to tabulate

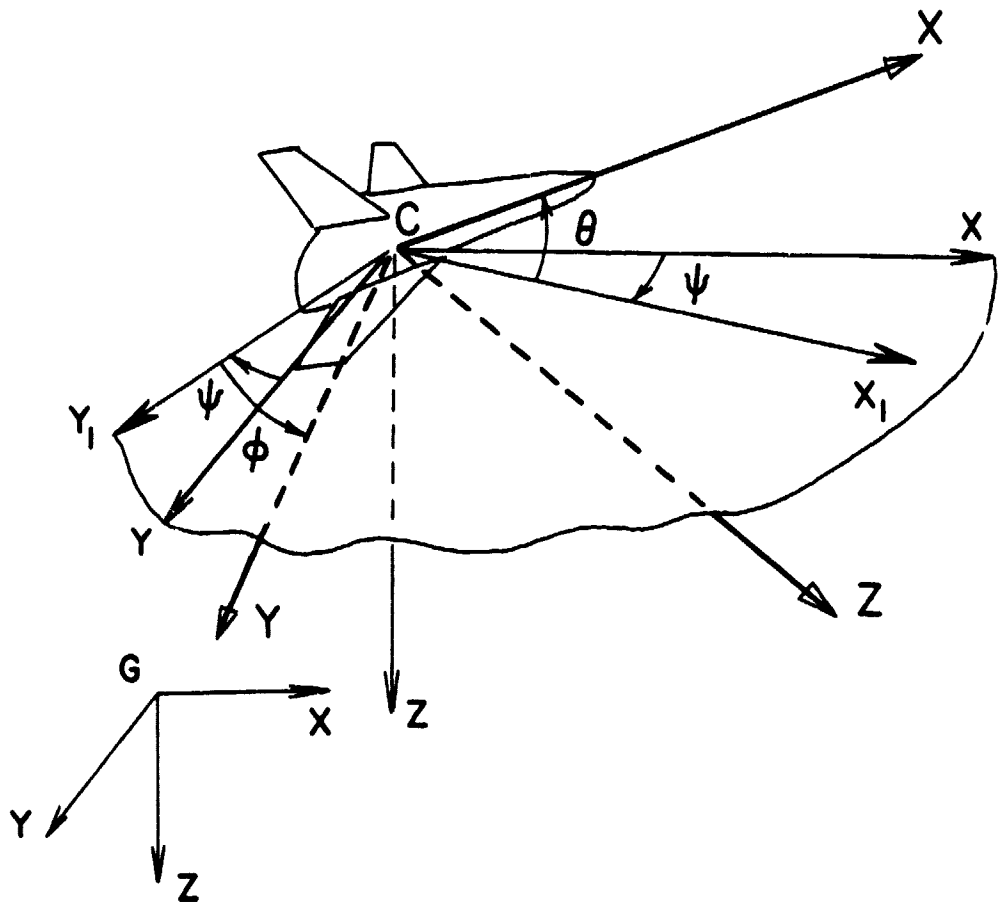

Fig. 2. Rotation of coordinate axes.

the aerodynamic characteristics for a simulation study to assess the dynamic response under any flight condition. This approach is illustrated in reference 9 where stall and post-stall characteristics of a high-performance fighter airplane, the F-16, with relaxed longitudinal static stability were analyzed.

For long-range hypervelocity vehicle, as in the case of the present SSTO vehicle, a flat Earth formulation is clearly inadequate because of the fact that the gravity acceleration changes its magnitude, and more importantly, its direction along the flight path.

We assume that the Earth is spherical but non-rotating and consider the fight in the plane of a great circle (Fig. 3). We first start with the equations for flight over a flat Earth by considering the relevant variables H, u, w, θ and q.

$$m[\dot{u} + qw] = X - mg \sin\theta \tag{7}$$

$$m[\dot{w} - qu] = Z + mg \cos\theta \tag{8}$$

$$I_y\dot{q} = M_\gamma \tag{9}$$

$$\dot{\theta} = q \tag{10}$$

$$\dot{H} = u \sin\theta - w \cos\theta \tag{11}$$

The original inertial ground system Gx_gz_g is now moved by translation to the geocentric inertial system Oxz with the origin at the center of the Earth. Let $\vec{R}$ be the position vector of the center-of-gravity with respect to the system Oxz. For airplane motion, the equations have been derived on the basis that the vector $\vec{g}$ is always directed along the ground axis Gz_g. In reality, this vector has rotated by an angle λ equal to the variation in the longitude. Let γ be the angle between the local horizontal and the velocity vector. This angle is termed the flight path angle. We have the kinematic relations

$$dR/dt = V \sin\gamma \tag{12}$$

$$d\lambda/dt = (V/R)\cos\gamma \tag{13}$$

Since the position vector $\vec{R}$ rotates with angular speed $\dot{\lambda}$, the angular rate $\dot{\theta}$ for the rotation of the body axes, referred to the fixed axes is

$$\dot{\theta} = q + (V/R)\cos\gamma \tag{14}$$

This equation replaces Eq.(10) and reduces to it in the case of flat Earth, $R \to \infty$. Since $\dot{R} = \dot{H}$, by comparing Eqs.(11) and (12), we have

$$V \sin\gamma = u \sin\theta - w \cos\theta \tag{15}$$

From Eqs.(1) for the case of zero sideslip angle, we have trivially

$$\begin{aligned} u &= V \cos\alpha \\ w &= V \sin\alpha \end{aligned} \tag{16}$$

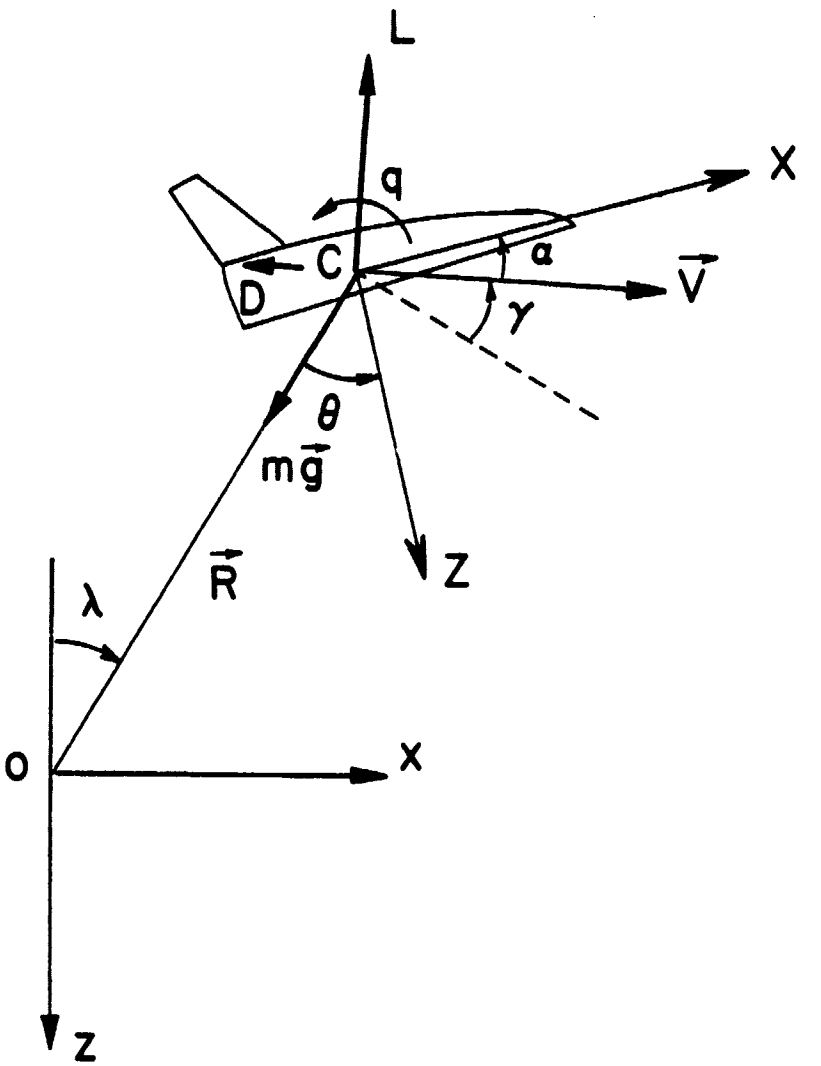

Fig. 3. Effect of the curvature of the Earth.

To this, we add the geometric relation

$$\theta = \gamma + \alpha \tag{17}$$

By taking the derivative of Eq.(15), using Eq.(14)

$$\begin{aligned}\dot{V}\sin\gamma + \dot{\gamma}V\cos\gamma &= \dot{u}\sin\theta - \dot{w}\cos\theta + (u\cos\theta + w\sin\theta)\dot{\theta} \\ &= (\dot{u}\sin\theta - \dot{w}\cos\theta) + (u\cos\theta + w\sin\theta)(q + \frac{V}{R}\cos\gamma)\end{aligned} \tag{18}$$

Now combining Eqs.(7) and (8)

$$m[(\dot{u}\sin\theta - \dot{w}\cos\theta) + q(u\cos\theta + w\sin\theta)] = X\sin\theta - Z\cos\theta - mg$$

Using Eq.(18) we write this equation as

$$m[\dot{V}\sin\gamma + \dot{\gamma}V\cos\gamma - (u\cos\theta + w\sin\theta)\frac{V}{R}\cos\gamma] = X\sin\theta - Z\cos\theta - mg$$

But

$$\begin{aligned}u\cos\theta + w\sin\theta &= V\cos\theta\cos\alpha + V\sin\theta\sin\alpha \\ &= V\cos(\theta-\alpha) = V\cos\gamma\end{aligned}$$

Hence

$$m[\dot{V}\sin\gamma + \dot{\gamma}V\cos\gamma - \frac{V^2}{R}\cos^2\gamma] = X\sin\theta - Z\cos\theta - mg \tag{19}$$

On the other hand, by eliminating q between the Eqs.(7) and (8)

$$m[u\dot{u} + w\dot{w}] = Xu + Zw - mgu\sin\theta + mgw\cos\theta$$

Therefore, since $V^2 = u^2 + w^2$ and $V\dot{V} = u\dot{u} + w\dot{w}$, we have

$$mV\dot{V} = XV\cos\alpha + ZV\sin\alpha - mgV(\sin\theta\cos\alpha - \sin\alpha\cos\theta)$$

or

$$m\dot{V} = X\cos\alpha + Z\sin\alpha - mg\sin\gamma \tag{20}$$

By observing that

$$F_T = X\cos\alpha + Z\sin\alpha \tag{21}$$

is the projection of the combined aerodynamic and propulsive force on the tangent to the flight patn, we have the force equation along the tangent to the flight path

$$m\dot{V} = F_T - mg\sin\gamma \tag{22}$$

Furthermore, using Eq.(20) in Eq.(19) and solving for $\dot{\gamma}$

$$m\dot{\gamma}V\cos\gamma = m\frac{V^2}{R}\cos^2\gamma + X\sin\theta - Z\cos\theta - mg$$
$$- X\cos\alpha\sin\gamma - Z\sin\alpha\sin\gamma + mg\sin^2\gamma$$

Hence

$$mV\dot{\gamma} = X\sin\alpha - Z\cos\alpha - m(g - \frac{V^2}{R})\cos\gamma$$

Observing that

$$F_N = X\sin\alpha - Z\cos\alpha \tag{23}$$

is the projection of the combined aerodynamic and propulsive force along the normal to the flight path, we have

$$mV\dot{\gamma} = F_N - m(g - \frac{V^2}{R})\cos\gamma \tag{24}$$

In summary, for longitudinal motion of a hypervelocity vehicle, the variables are conveniently selected as

$$R,\ V,\ \gamma,\ q,\ \theta$$

with equations

$$\frac{dR}{dt} = V\sin\gamma$$

$$\frac{dV}{dt} = \frac{F_T}{m} - g\sin\gamma$$

$$V\frac{d\gamma}{dt} = \frac{F_N}{m} - (g - \frac{V^2}{R})\cos\gamma \tag{25}$$

$$I_y\frac{dq}{dt} = M_\gamma$$

$$\frac{d\theta}{dt} = q + \frac{V}{R}\cos\gamma$$

The auxiliary variables are α, u, and w with the relations

$$\theta = \gamma + \alpha$$

$$u = V\cos\alpha \tag{26}$$

$$w = V\sin\alpha$$

$$\tan\alpha = w/u$$

III. CONTROLS EFFECTIVENESS

In the pitching moment equation in system (25), the total pitching moment is represented by

$$M_Y = M + M_t - \frac{3g}{2R}(I_x - I_z)\sin 2\theta \qquad (27)$$

where M is the aerodynamic moment, M_t is the pitching moment due to reaction control system and the last term expresses the gravity torque. A complete discussion of gravity torques has been given by Roberson (ref. 10) and Beletskii (ref. 11). Because R is large, the effect of this term is small whenever aerodynamic and thrusting moments are effective. But the term should be retained in the case of orbital flight when $M \to 0$.

Effectiveness of Reaction Control System

The thrusting moment is an arbitrary function of the time. If f(t) is the thrust magnitude applied at a distance ℓ_t from the center-of-gravity, for the duration τ of the firing it can be represented by an average constant value (Fig. 4)

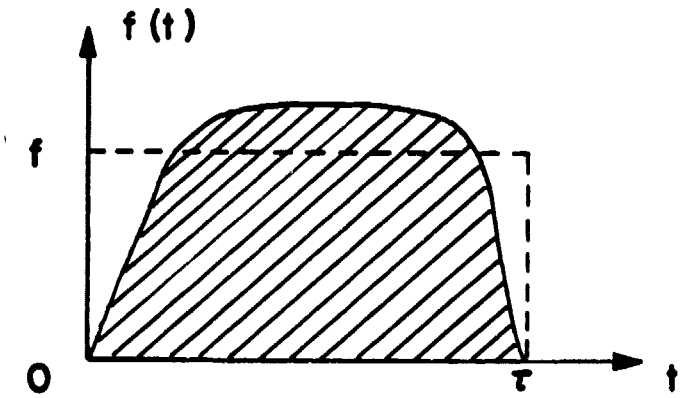

$$M_t = \frac{\ell_t}{\tau}\int_o^\tau f(t)dt \qquad (28)$$

Fig. 4. Average thrusters force.

This average value accounts for the effects of thrust built up with time and thrust loss due to back pressure increases with decreasing altitude.

The total pitching moment coefficient is defined as

$$C_{m_{tot}} = \frac{M_Y}{\frac{1}{2}\rho SV^2\bar{c}} = C_m + \frac{M_t}{\frac{1}{2}\rho SV^2\bar{c}} - \frac{3g(I_x - I_z)\sin 2\theta}{R\rho SV^2\bar{c}} \qquad (29)$$

where C_m is the aerodynamic moment coefficient and the reference length $\bar{c}$ used is the mean aerodynamic chord. To trim at $C_{m_{tot}} = 0$, the use of thrusters (RCS) is effective at high altitude, while at high dynamic pressure, aerodynamic moment is the main ingredient for control. Let f be the average constant thrusters force. The thrust moment coefficient is

$$C_{m_t} = \frac{M_t}{\frac{1}{2}\rho SV^2\bar{c}} = (\ell_t/\bar{c})(f/\tfrac{1}{2}\rho SV^2) \tag{30}$$

Introducing the load factor

$$n = \frac{L}{W} = \frac{\rho SV^2 C_L}{2W} = \frac{\bar{q}SC_L}{W} \tag{31}$$

where $\bar{q}$ is the dynamic pressure, we write Eq.(30) as

$$C_{m_t} = (\ell_t/\bar{c})(f/W)(C_L/n) \tag{32}$$

This formula makes explicit the effectiveness of reaction control system. On the right-hand-side of the equation, the first ratio is obviously a design parameter while the second term, which is simply the thrust-to-weight ratio, concerns the sizing of the engines. The last term depends on the trajectory to be flown. As a rule, in an optimum fashion, jet firings can be used as an effective means of pitch control whenever the load factor, or proportionally the dynamic pressure, remains small. For a reentry trajectory, RCS jets can be used to supplement pitch control during the early part of the entry at low dynamic pressure, but under severe trim condition their use may also be mandatory at lower altitude with significant penalty in fuel consumption. Also for a skip trajectory, at high load factor, the use of RCS requires high thrusting force if aerodynamic pitch control is constrained by aerodynamic heating consideration.

Effect of the Aerodynamic Center

For the aerodynamic moment, consider a wing-body combination (Fig. 5)

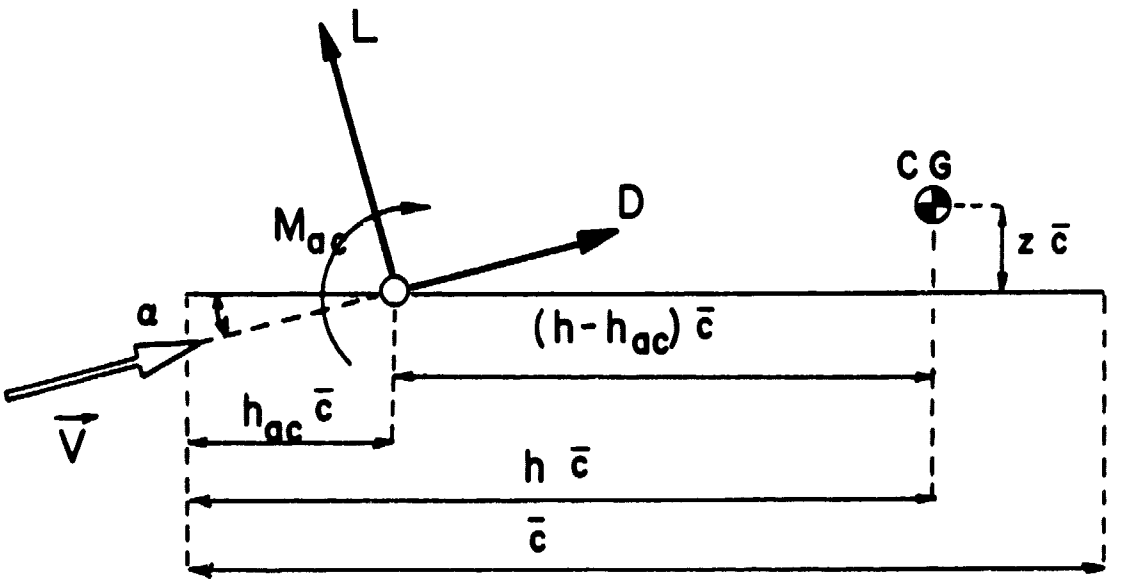

Fig. 5. Aerodynamic forces and moment.

The force system acting in symmetric flight can be represented as a lift L and a drag D acting at a reference point, the mean aerodynamic center, together with a pitching moment M_{ac}. Then, the aerodynamic moment about the vehicle center-of-gravity is

$$M = M_{ac} + (L\cos\alpha + D\sin\alpha)(h - h_{ac})\bar{c} + (L\sin\alpha - D\cos\alpha)z\bar{c} \qquad (33)$$

where h and h_{ac}, expressed in fraction of the mean aerodynamic chord $\bar{c}$, indicate the location of the center-of-gravity and the aerodynamic center, respectively. If the last term which is small is neglected, the aerodynamic pitching moment coefficient is

$$C_m = C_{m_{ac}} + (h - h_{ac})C_N \qquad (34)$$

where

$$C_N = C_L\cos\alpha + C_D\sin\alpha \qquad (35)$$

is the normal aerodynamic force coefficient.

The inviscid theory of thin wing at small α predicts that $C_{m_{ac}}$ is invariant with α, but in general it varies with both the angle-of-attack and the Mach number. Likewise, the location of the aerodynamic center which is here expressed as h_{ac} in fraction of the mean aerodynamic chord is a function of the angle-of-attack and the Mach number. It is particularly sensitive to the variation of the Mach number in the case of the CCV because of the large ratio of the body-planform to wing-planform area.

For small angle-of-attack, and considering that $C_{D\alpha} << C_L$, we have the classical formula for use in the case of airplane dynamics

$$C_m = C_{m_{ac}} + (h - h_{ac})C_L \qquad (36)$$

Hence, on the basis that $C_{m_{ac}}$ is independent of the angle-of-attack, and in the case where h_{ac} is also insensitive to variation in α we have the formula

$$C_{m_\alpha} = (h - h_{ac})C_{L_\alpha} \qquad (37)$$

which provides an excellent way of finding h_{ac} from test results, that is from measurements of the stability derivatives C_{m_α} and C_{L_α}. Since $C_{L_\alpha} > 0$ and for static stability, $C_{m_\alpha} < 0$, the quantity $(h - h_{ac})$, in fraction of the mean aerodynamic chord $\bar{c}$, is meaningfully called the stability static margin.

Since in the case of hypersonic reentry, in the early part of the trajectory, the angle-of-attack is large, we retain the more rigorous expression (34) and measure the stability static margin according to

$$K = h - h_{ac} = \partial C_m/\partial C_N \qquad (38)$$

Since C_N is a positive and increasing function of α and at the trim condition $C_m = 0$, a $C_{m_\alpha} < 0$ provides the condition for the vehicle to be statically stable, a positive K denotes a level of static instability. An aft shift of the center-of-gravity, or during an entry a shift forward of the aerodynamic center will increase this level.

Equation (37) is only appropriate for the computation of the value of K at low angle-of-attack and low Mach number when K is insensitive to the variations of these variables. In general, from Eq.(34), we have the equation

$$K = \frac{C_m}{C_N} - \frac{C_{m_{ac}}}{C_N} \tag{39}$$

which shows that, at a given Mach number, K is a function of the angle-of-attack through the functions $C_m(\alpha)$, and $C_N(\alpha)$. These functions can be modeled based on wind tunnel test data but the small and nearly constant value $C_{m_{ac}}$ can only be estimated with certain degree of arbitrariness. As a first approximation, we can neglect this term and take

$$K \simeq \bar{K} = C_m/C_N \tag{40}$$

Typical plots of K and $\bar{K}$ are shown in Fig. 6.

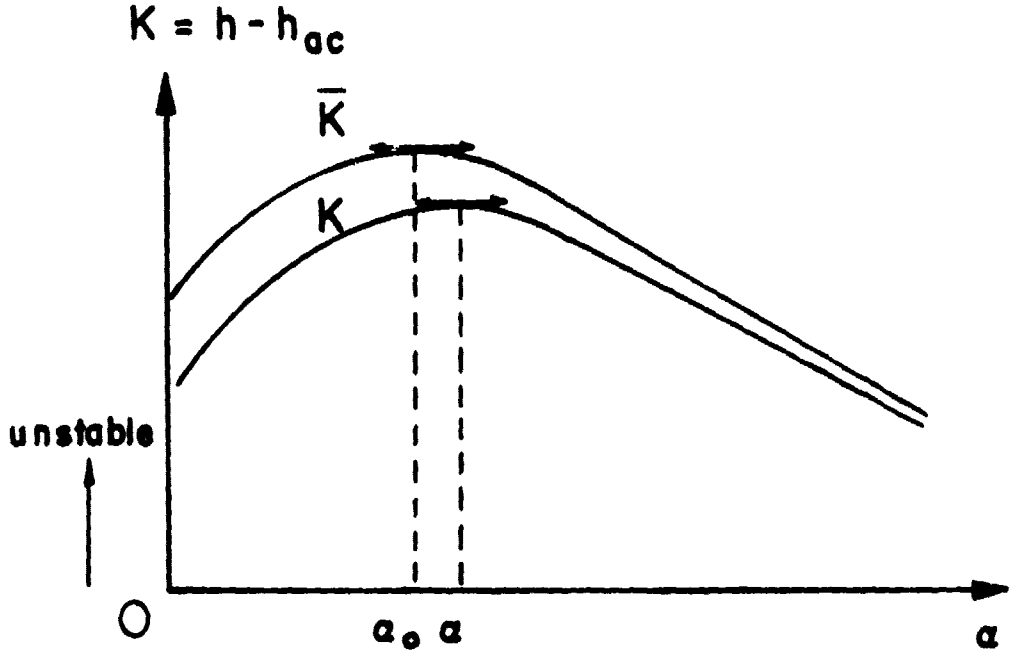

Fig. 6. Maximum shift of the aerodynamic center at hypersonic speeds.

The difference $\bar{K} - K = Cm_{ac}/C_N$ becomes small at high angle-of-attack with large values of C_N. It is seen that for both K and $\bar{K}$ there exists angle-of-attack providing the maximum shift forward of the aerodynamic center yielding the maximum level of static margin. This leads to the following procedure for evaluating Cm_{ac}. On the basis of the invariance of Cm_{ac} and by taking the successive partial derivatives of the equation

$$C_m = C_{m_{ac}} + KC_N \tag{41}$$

with respect to α we have

$$C_{m_\alpha} = K_\alpha C_N + KC_{N_\alpha} \tag{42}$$

and

$$C_{m_{\alpha\alpha}} = K_{\alpha\alpha} C_N + 2K_\alpha C_{N_\alpha} + KC_{N_{\alpha\alpha}} \tag{43}$$

At the point α where K is maximized, $K_\alpha = 0$, and we have

$$K = \frac{C_{m_\alpha}}{C_{N_\alpha}} \tag{44}$$

and hence, combining this equation with Eq.(43)

$$\frac{C_{m_\alpha}}{C_{N_\alpha}} = \frac{C_{m_{\alpha\alpha}}}{C_{N_{\alpha\alpha}}} - \frac{K_{\alpha\alpha} C_N}{C_{N_{\alpha\alpha}}} \tag{45}$$

At the point α_o where $\bar{K}$ is maximized we have

$$(C_m/C_N)_{\alpha=\alpha_o} = (C_{m_\alpha}/C_{N_\alpha})_{\alpha=\alpha_o} \tag{46}$$

The partial derivatives can be evaluated if $C_m(\alpha)$ and $C_N(\alpha)$ are accurately modeled as continuous functions of α. Equation (46), upon solving, provides α_o but not the value α where K is maximized. Since the difference $C_{m_{ac}}/C_N$ between the two curves $\bar{K}$ and K is small, we can assume that the behaviors of the two curves, respectively near the two stationary values are the same, that is they have the same slope and the same curvature. Since $\bar{K}_\alpha(\alpha_o) = K_\alpha(\alpha) = 0$, we have the condition for the same curvature

$$K_{\alpha\alpha}(\alpha) = \bar{K}_{\alpha\alpha}(\alpha_o) = \left(\frac{C_{m_{\alpha\alpha}}}{C_N} - \frac{C_m C_{N_{\alpha\alpha}}}{C_N^2} \right)_{\alpha=\alpha_o} \tag{47}$$

Upon substituting this approximation in Eq.(45) we have the equation for evaluating α where K is maximized

$$\frac{C_{m_\alpha}}{C_{N_\alpha}} = \frac{C_{m_{\alpha\alpha}}}{C_{N_{\alpha\alpha}}} - \left(\frac{C_{m_{\alpha\alpha}}}{C_N} - \frac{C_m C_{N_{\alpha\alpha}}}{C_N^2} \right)_{\alpha=\alpha_e} \frac{C_N}{C_{N_{\alpha\alpha}}} \tag{48}$$

Once this value of α has been computed, we obtain from Eqs.(41) and (44) the constant value

$$C_{m_{ac}} = C_m - \frac{C_{m_\alpha}}{C_{N_\alpha}} C_N \tag{49}$$

For a typical reentry profile, a constant and high angle-of-attack is maintained through the hypersonic range. Since at hypersonic speeds, the aerodynamic characteristics are nearly independent of the Mach number the value of K is nearly constant (ref. 5) and can be kept at a low level of instability by selecting a high enough angle-of-attack (Fig. 6). Below Mach 5.0, the aerodynamic characteristics are strongly influenced by the Mach number. This, coupled with the rapid decrease in the angle-of-attack for a transition from entry to glide configuration may create unsteady phenomena resulting in large static instability. The function K is now function of the two variables α and M. Since it is not convenient to analyze a three-dimensional plot we consider the intersections of the surface $K = K(\alpha, M)$ by the planes α = constant.

Aerodynamic data for the example CCV are taken from references 2 and 8. The reference dimensions are given in Fig. 7 with the center-of-gravity located at 0.69 of the body length. Aerodynamic forces and moment are controlled by a combination of a body flap and an elevon system. With $\delta_F = 0$, and $\delta_e = 0$ and for different values of the angle-of-attack, the variations of C_L and C_N as functions of the Mach number are shown in Fig. 8. At low angle-of-attack, C_N can be approximated by C_L but at high angle-of-attack especially in the vicinity of sonic speeds, due to a sharp rise in the drag, the two curves can be quite distinct. Hence, we continue to evaluate K through the use of Eq.(39) but now with an estimate value for $C_{m_{ac}}$ based on the assumption that at each Mach number, it is independent of the angle-of-attack. Hence, we can take $C_{m_{ac}} = C_m$ when $C_N = 0$. But this evaluation has to be used with care because the point corresponds to nearly zero angle-of-attack where the aerodynamic center is not well defined. The value for $C_{m_{ac}}$ obtained is compared with the value of $C_{m_{ac}}$ estimated by using Eq.(49) at low angle-of-attack ($\alpha = 2.5°$) and this provides excellent agreement. The result is plotted in Fig. 9 in dashed line as function of the Mach number. In the same figure, we have plotted the variation of C_m for different values of the angle-of-attack. From the data in Figs. 8 and 9, the location of the aerodynamic center, now expressed in percentage of the body length is evaluated through the formula

$$\frac{x_{ac} - x_{cg}}{\ell} = \frac{(C_{m_{ac}} - C_m)}{C_N} \left(\frac{\bar{c}}{\ell} \right) \tag{50}$$

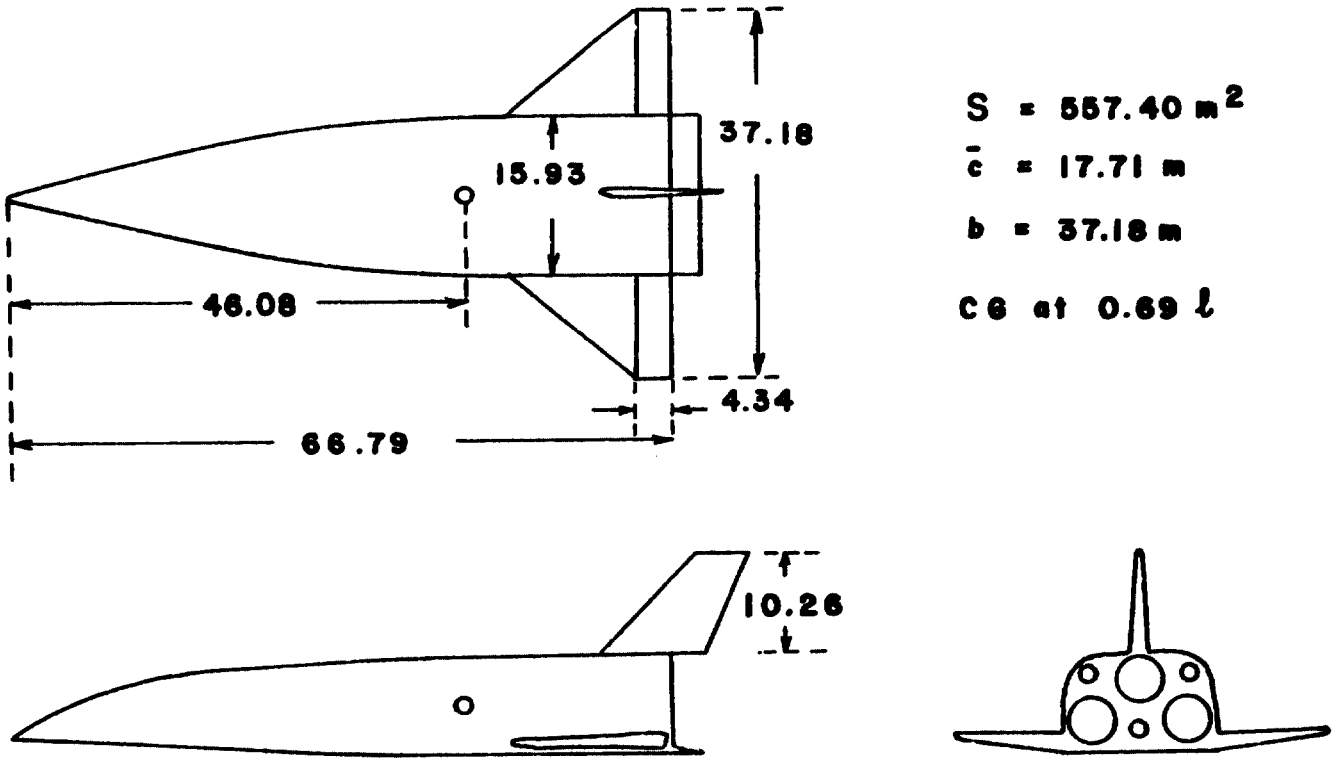

Fig. 7. Reference dimensions of the vehicle.

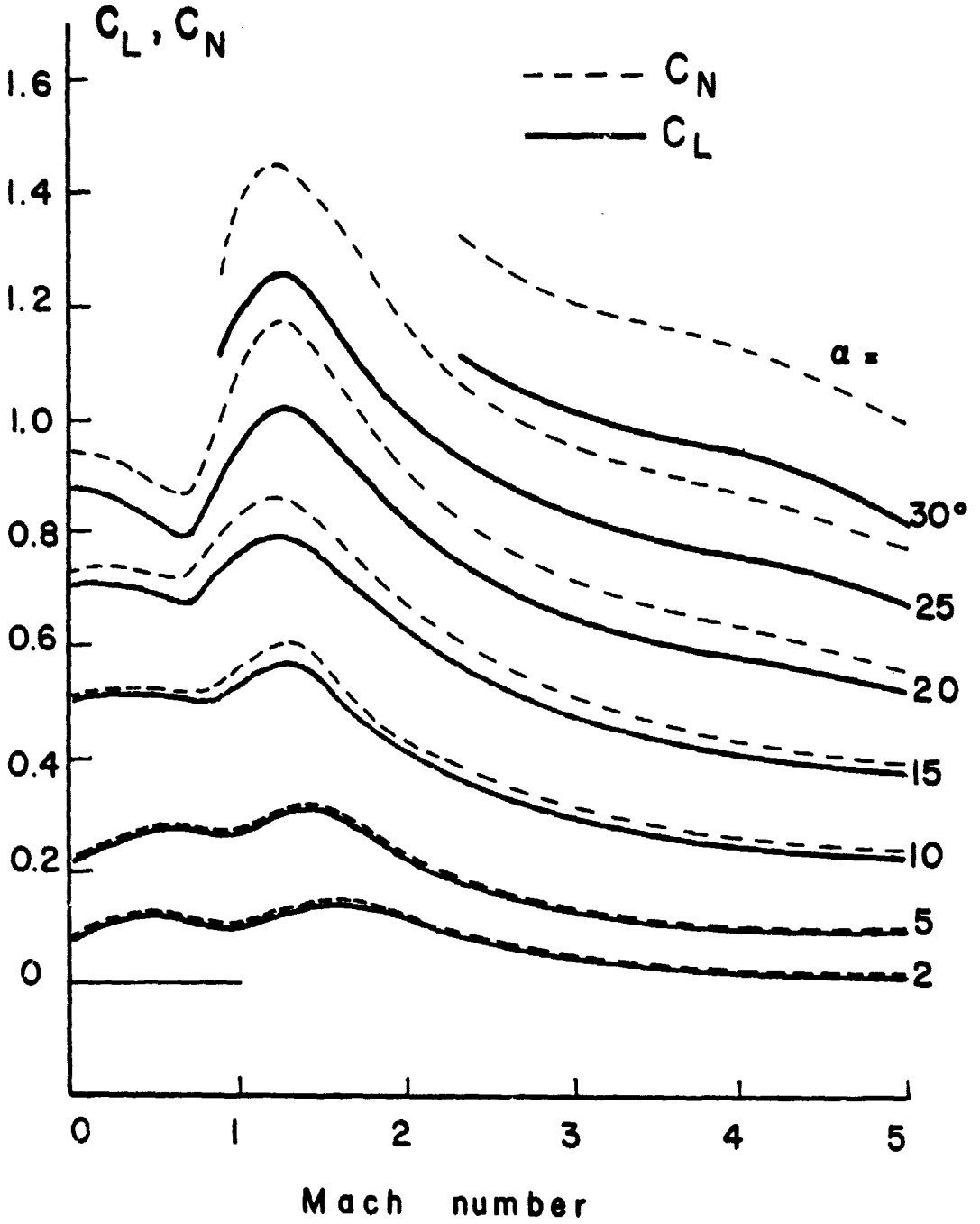

Fig. 8. Lift and normal force coefficients as functions of the Mach number for $\delta_F = 0$, $\delta_e = 0$.

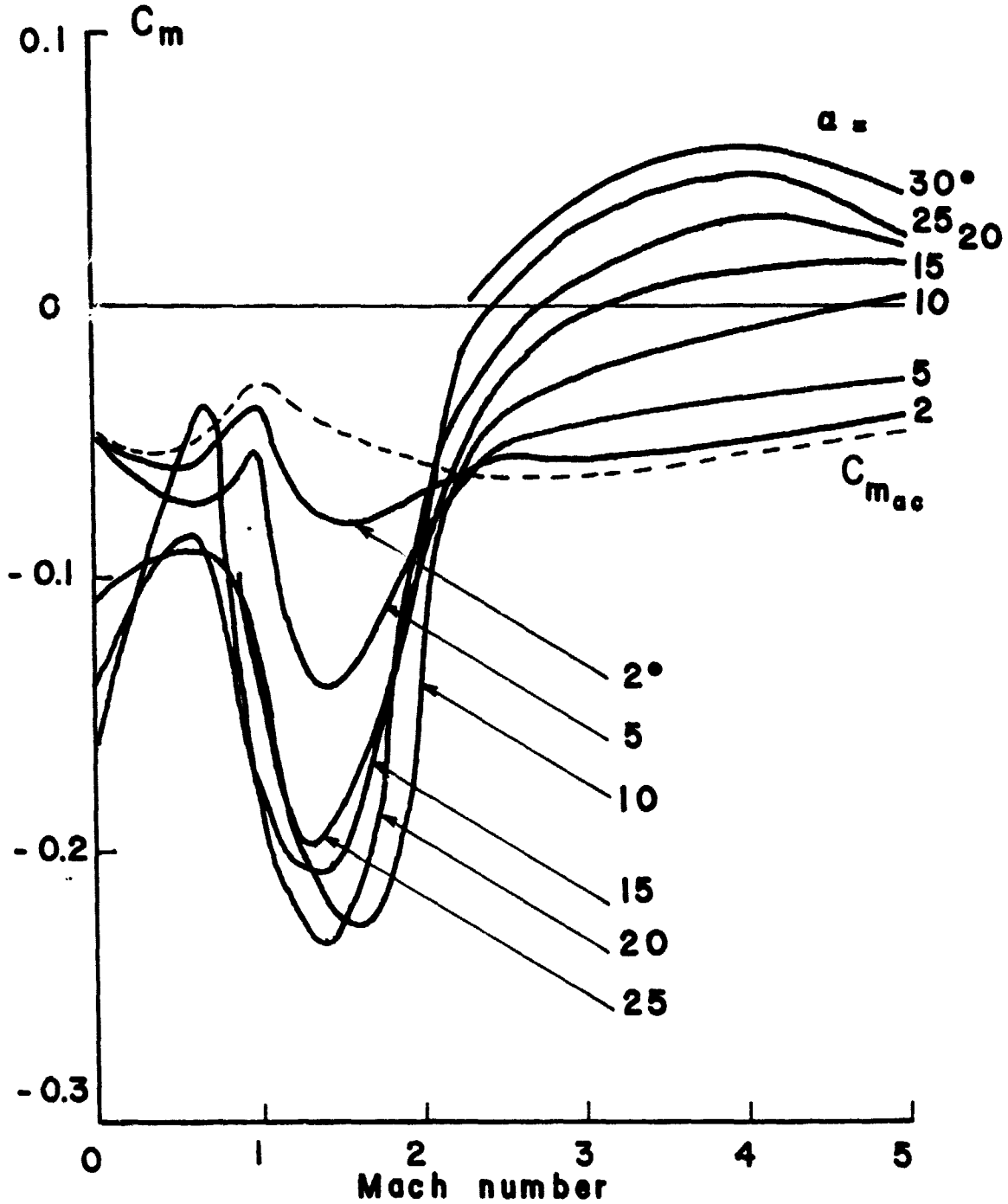

Fig. 9. Aerodynamic pitching moment coefficient as function of the Mach number.

With a $x_{cg}/\ell = 0.69$, the location of the aerodynamic center as function of the Mach number is shown in Fig. 10 for low angle-of-attack and in Fig. 11 for high angle-of-attack. These figures make explicit the influence of the Mach number on the longitudinal stability characteristic.

During entry, the vehicle is slightly unstable at hypersonic speeds. It can even be made slightly stable with the selection of high angle-of-attack for entry. Below Mach 5.0, the aerodynamic center shifts forward and the vehicle becomes more unstable. Then at lower Mach number, the aerodynamic center begins to shift aft and the neutral point, defined as $x_{ac} = x_{cg}$, is reached at a Mach number slightly above 2.0. For all the angles-of-attack considered, the maximum level of stability which corresponds to the maximum aft-location of the aerodynamic center occurs in the transonic region. This is due to a sharp rise in transonic drag. At Mach number in the vicinity of 0.7, the vehicle becomes much less stable and remains slightly stable at the lowest Mach number. This behavior is a characteristic of hypervelocity vehicle and the quantitative results agree with the results obtained from a simulation study presented in reference 5.

The Mach number for neutral point, $K = 0$, is evaluated from Fig. 9 at the intersections of the dashed line representing the variation of $C_{m_{ac}}$ and the solid lines for the variations of C_m at different angles-of-attack. The evaluation of the Mach numbers which correspond to the stationary location of the aerodynamic center can be easily achieved if the aerodynamic characteristics are modeled as functions of the Mach number for each angle-of-attack of interest. By taking the derivative of Eq.(41) with respect to M, we have

$$C_{m_M} = C_{m_{ac_M}} + K_M C_N + K C_{N_M} \tag{51}$$

When $K_M = 0$, substituting back into Eq.(41), we deduce the equation

$$\frac{C_m - C_{m_{ac}}}{(C_m - C_{m_{ac}})_M} = \frac{C_N}{C_{N_M}} \tag{52}$$

which can be solved for two values of M, one near 0.7 and one near 1.2. The first value corresponds to a relative minimum level of stability while the second value corresponds to the absolute maximum level of stability.

Hypersonic Trim

During entry, the trajectory is controlled by the angle-of-attack. With only the aerodynamic moment involved, longitudinal trim at $C_m = 0$ is effected through body-flap and elevon deflections, denoted by δ_F and δ_e respectively, with positive value when the trailing edge is down. For the example CCV, aerodynamic characteristics at hypersonic speed, M = 20.3, are presented in Figs. 12-14. Figure 12 plots the normal force coefficient C_N as function of the angle-of-attack for various body-flap and elevon deflections. The variations of the moment coefficient as function of the angle-of-attack are presented in Fig. 13. To show the trimmable condition

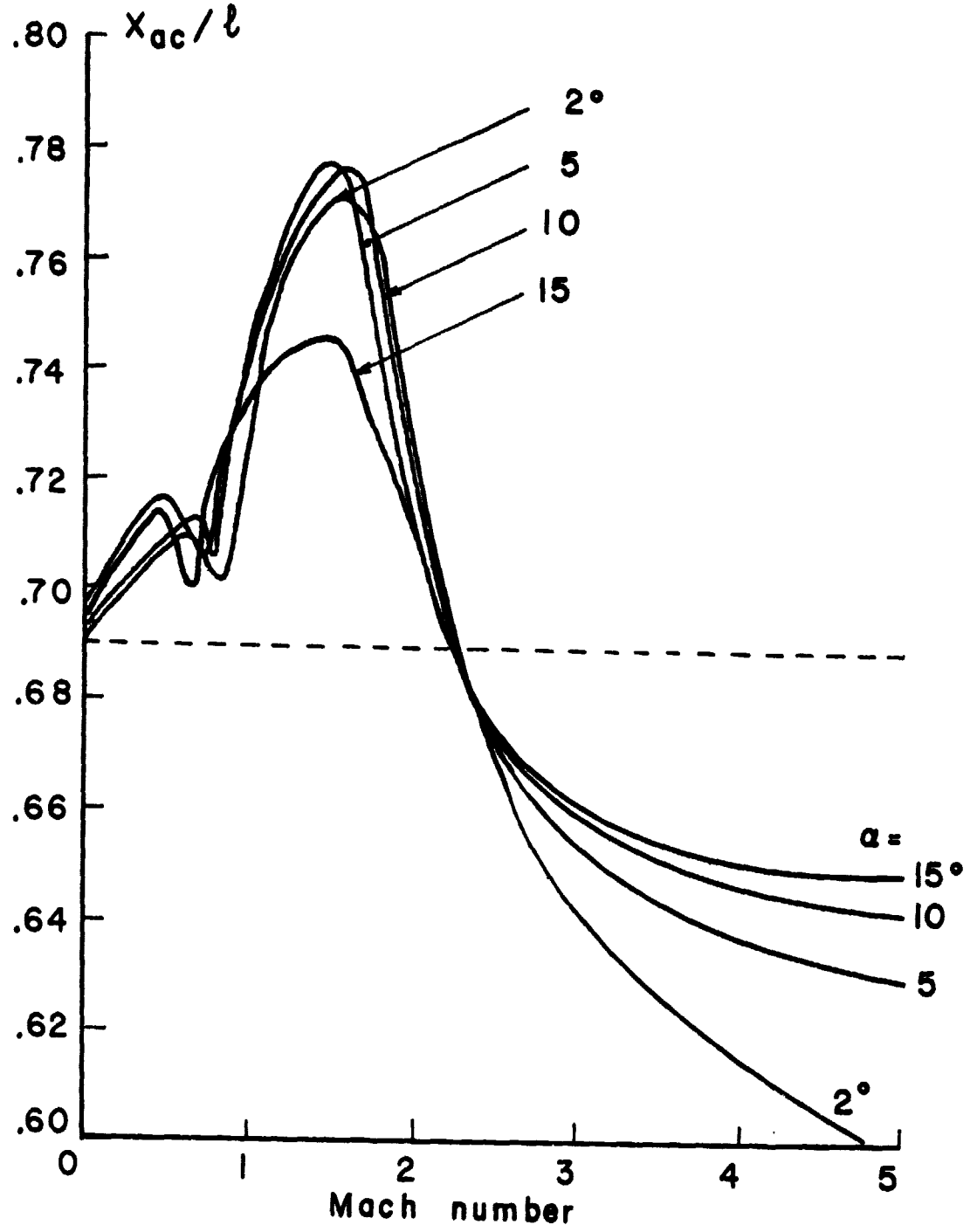

Fig. 10. Location of the aerodynamic center as function of the Mach number (low angle-of-attack).

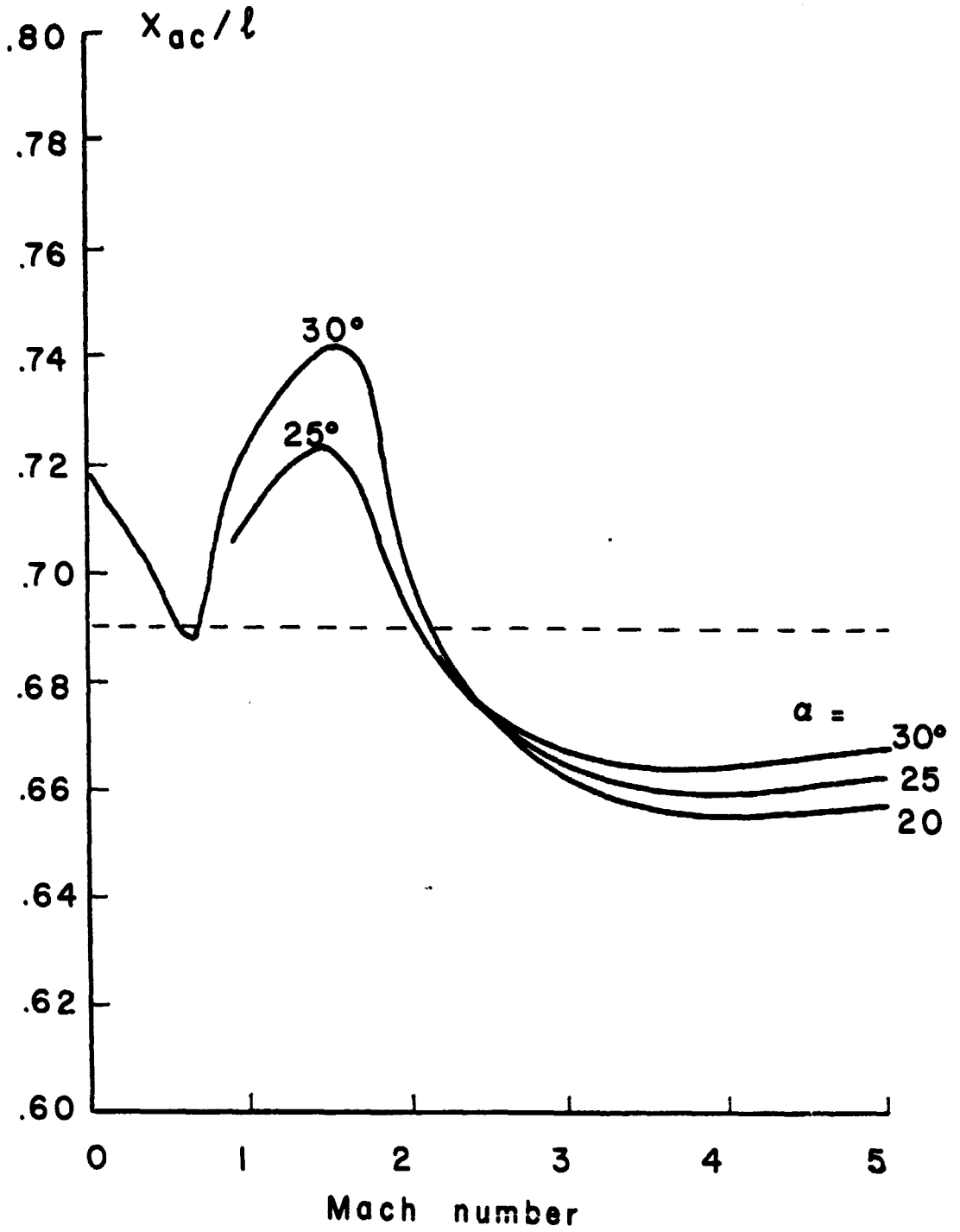

Fig. 11. Location of the aerodynamic center as function of the Mach number (high angle-of-attack).

as function of the location of the center of gravity, the values of C_m are evaluated for a center-of-gravity at 0.715 of the body length. For any given angle-of-attack, with different location of the center-of-gravity, the new C_m curve can be deduced by using the relation (50) written as

$$C_{m_2} - C_{m_1} = \frac{(x_2 - x_1)}{\ell} \left(\frac{\ell}{c} \right) C_N \tag{53}$$

where x_1/ℓ and x_2/ℓ denote any two locations of the center-of-gravity in percentage of the body length with corresponding moment coefficients C_{m_1} and C_{m_2}. It is seen in Fig. 13 that at $x_{cg}/\ell = 0.715$, with $\delta_F = 10°$, a small elevon deflection, negative when $\alpha > 42.5°$ and positive when $\alpha < 42.5°$ is sufficient for hypersonic trim. Based on Eq.(53), if the center-of-gravity is moved further aft, a positive nose up increment ΔC_m is introduced, proportional to C_N and hence large at high angle-of-attack. This will require larger positive deflections of both δ_F and δ_e. On the other hand, a move forward of the center-of-gravity can result in a negative pitching moment coefficient and a negative elevon deflection is required for trim. For any allowable deflections of the control surfaces, in both positive and negative limits, there exists trimmable center-of-gravity range, function of the angle-of-attack in the hypersonic range and also function of the Mach number in the transonic and supersonic range.

In general, in the hypersonic range, at any angle-of-attack, for a specified location of the center-of-gravity, the function $C_m(\alpha, \delta_F, \delta_e)$ can be linearized and we have

$$C_m = C_m(\alpha, 0, 0) + \left(\frac{\partial C_m}{\partial \delta_F} \right)_o \delta_F + \left(\frac{\partial C_m}{\partial \delta_e} \right)_o \delta_e \tag{54}$$

The stability derivatives $(\partial C_m/\partial \delta_F)_o$ and $(\partial C_m/\partial \delta_e)_o$ are evaluated for $x_{cg}/\ell = 0.715$ and plotted in Fig. 14 as functions of the angle-of-attack. At any angle-of-attack, for any selected body-flap deflection, δ_F, the elevon deflection, δ_e, required for trim is computed from $C_m = 0$, and subsequently the trimmed lift coefficient is deduced from

$$C_{L_{trim}} = C_L(\alpha, 0, 0) + \left(\frac{\partial C_L}{\partial \delta_F} \right)_o \delta_F + \left(\frac{\partial C_L}{\partial \delta_e} \right)_o \delta_e \tag{55}$$

Similarly, the corresponding normal force coefficient is obtained from

$$C_{N_{trim}} = C_N(\alpha, 0, 0) + \left(\frac{\partial C_N}{\partial \delta_F} \right)_o \delta_F + \left(\frac{\partial C_N}{\partial \delta_e} \right)_o \delta_e \tag{56}$$

The stability derivatives in Eqs.(55) and (56) are positive and using positive δ_F and δ_e for trim increases the lift coefficient and the normal force coefficient.

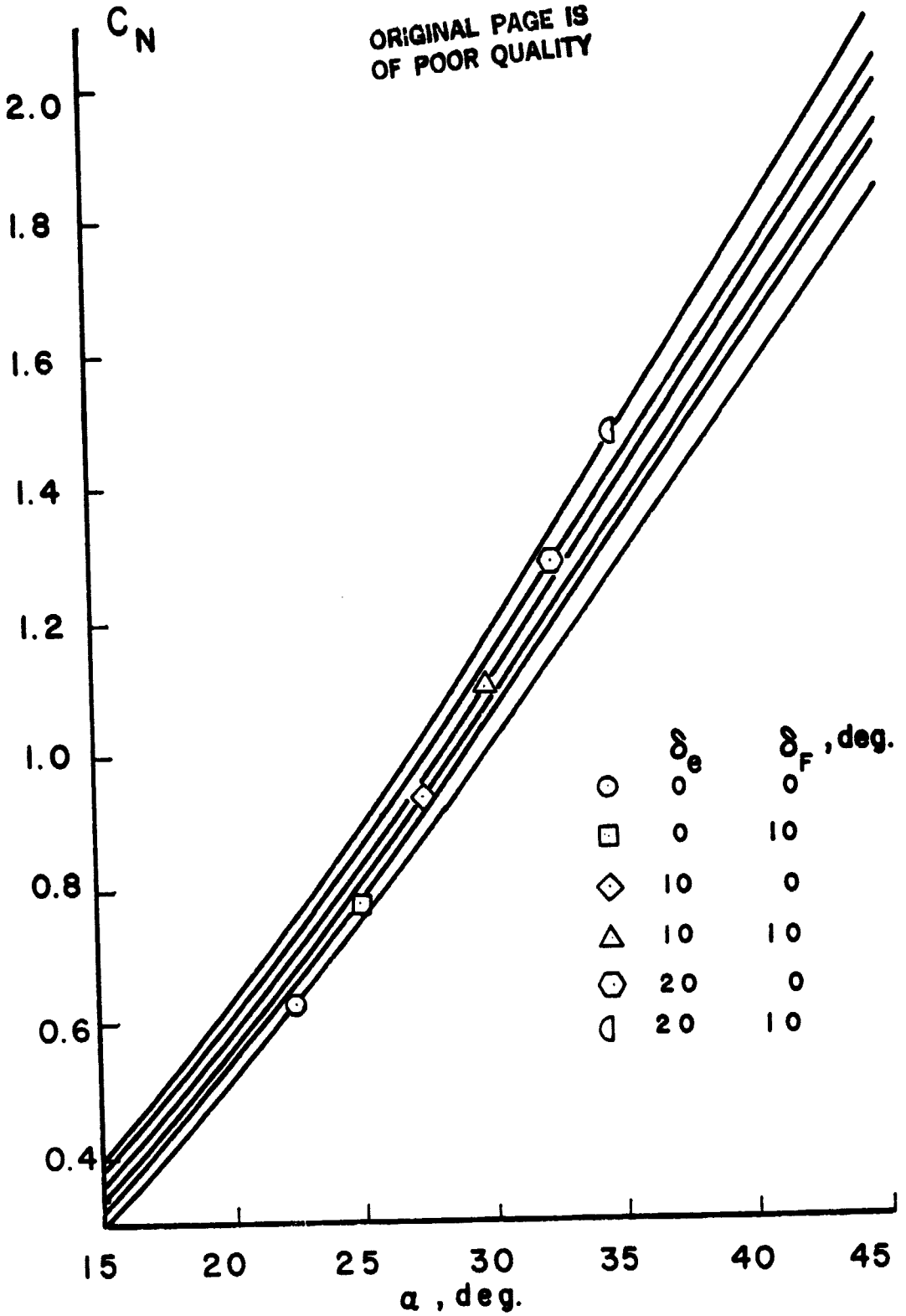

Fig. 12. Normal force coefficient at hypersonic speed, M = 20.3, for various control surfaces deflections.

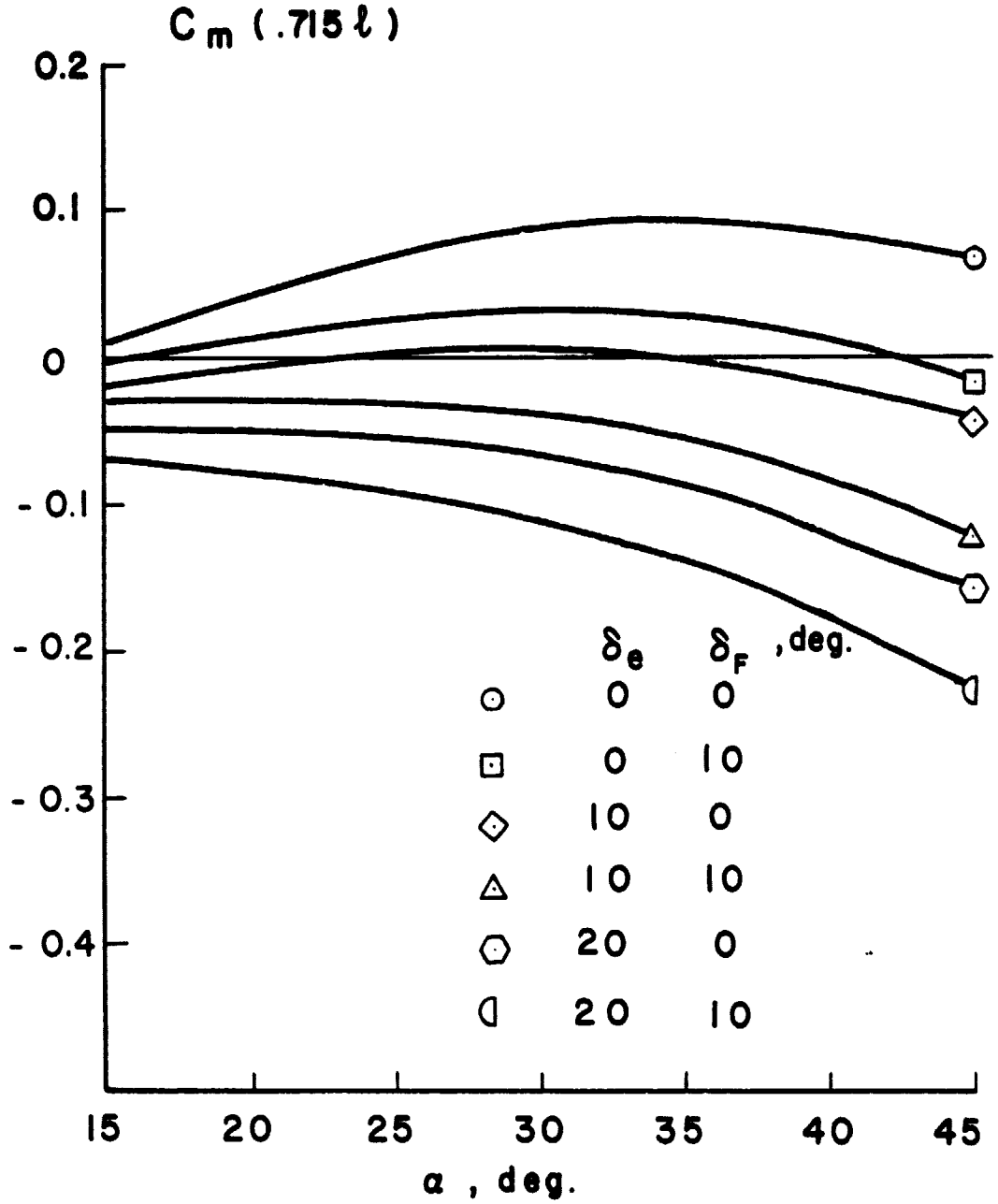

Fig. 13. Aerodynamic pitching moment coefficient at hypersonic speed, M = 20.3, with x_{cg}/ℓ = 0.715 and various control surfaces deflections.

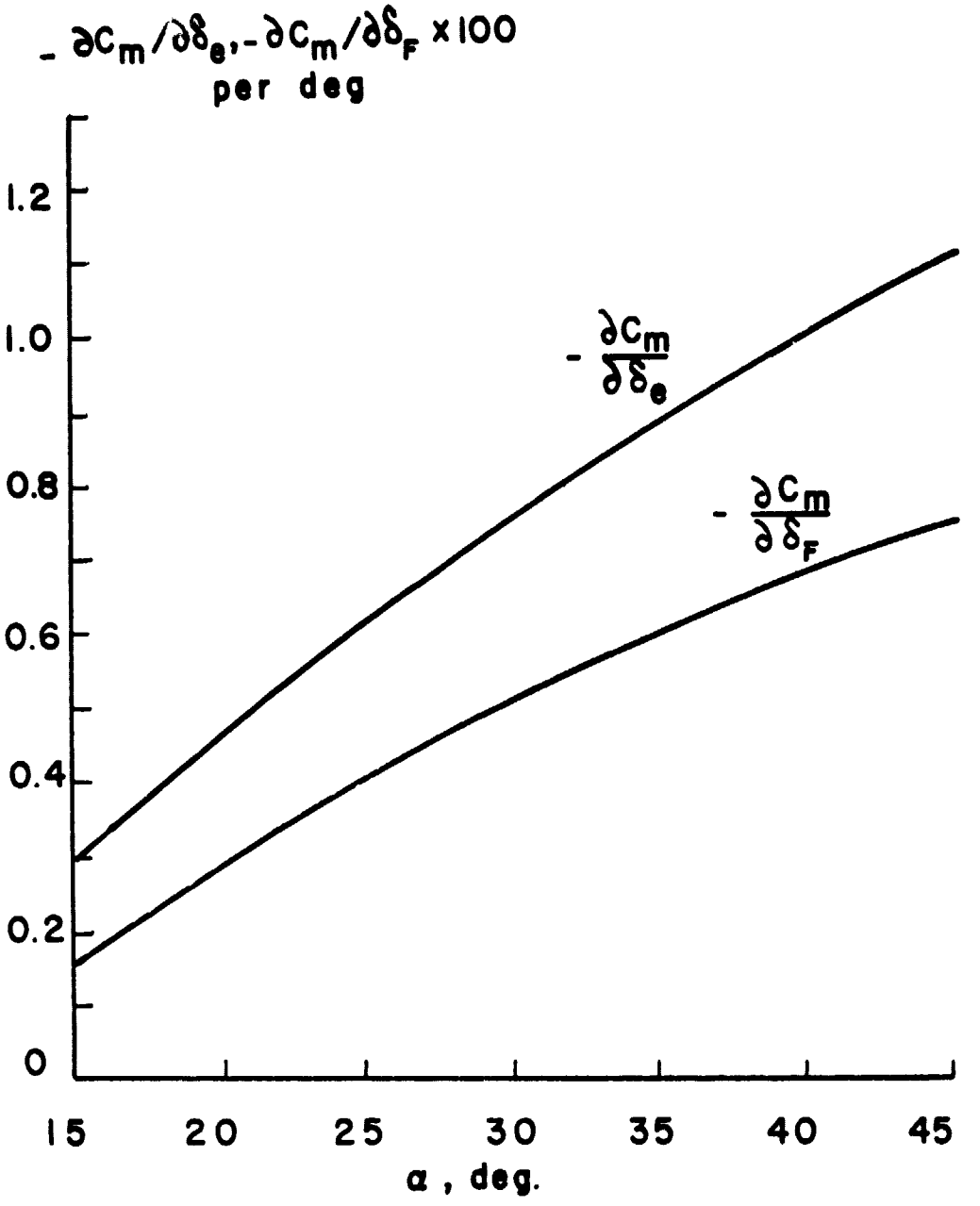

Fig. 14. Sensitivity coefficients for body-flap and elevon deflections at hypersonic speed.

For a SSTO vehicle, an aft center-of-gravity location resulting from large engine mass at the rear of the vehicle creates challenging problems for the designer. Due to thermal and structural constraints, both the body-flap and elevon deflections have allowable limits. With these limits, as mentioned above, there exists trimmable center-of-gravity range. To assess this range, we follow Freeman and Powell (ref. 5) and consider the plot of C_m versus C_N for $x_{cg} = 0.715\ell$ in Fig. 15. The lowest curve corresponds to maximum positive deflections of the control surfaces, with $\delta_F = 10°$, $\delta_e = 20°$. In general, at any location of the center-of-gravity, for any δ_F and δ_e, the equation of the C_m versus C_N curve is obtained by eliminating α between the two equations

$$\begin{aligned} C_m &= C_m(\alpha, \delta_F, \delta_e) \\ C_N &= C_N(\alpha, \delta_F, \delta_e) \end{aligned} \tag{57}$$

which results in

$$C_m = C_m(C_N, \delta_F, \delta_e) \tag{58}$$

From Fig. 15, in the range of angle-of-attack of interest, since at maximum control surfaces deflections, $C_m < 0$, while $C_m > 0$ for zero deflection angles, the vehicle is trimmable at this location of the center-of-gravity. For another aft location, from Eq.(53), we have an increment ΔC_m such that

$$\Delta C_m = \zeta C_N \tag{59}$$

where the constant factor is given by

$$\zeta = \frac{\Delta x}{\ell} \left(\frac{\ell}{\bar{c}} \right) \tag{60}$$

with $\Delta x/\ell$ expressing the shift in percentage of body length of the center-of-gravity. With $\Delta x > 0$, all the C_m curves move upward according to the increment given in Eq.(59). It suffices to analyze the shift of the lowest curve for the determination of the most aft of the center-of-gravity for trimmability. This is done in Fig. 16 from which the assessment for the example vehicle can be made.

In general, for any vehicle having similar behaviors for the aerodynamic characteristics, consider the interval of angle-of-attack of interest $\alpha \varepsilon [\alpha_1, \alpha_2]$ which corresponds to the interval $C_N \varepsilon [C_{N_1}, C_{N_2}]$. The critical center-of-gravity is reached when, with maximum deflections of the control surfaces, either $C_m = 0$ for $\alpha = \alpha_1$ or when C_m curve has a maximum value $C_m = 0$ at a certain angle-of-attack.

The first case occurs when

$$C_m(\alpha_1) + \zeta C_N(\alpha_1) = 0 \tag{61}$$

where $C_m(\alpha_1)$ denotes the pitching moment coefficient evaluated at α_1, with maximum control surfaces deflection at reference center-of-gravity location.

From Eq.(61) we deduce ζ and then the critical location of the center-of-gravity. Beyond this position, the vehicle is trimmable only at high angle-of-attack and for each ζ beyond this critical value, the lowest value of the trimmable angle-of-attack is obtained by solving Eq.(61) with α_1 replaced by α. Of course the absolute limit for trimmability is obtained when this α reaches α_2.

The second case occurs when the following conditions are satisfied simultaneously

$$C_m(C_N, \delta_F, \delta_e) + \zeta C_N = 0$$
$$\frac{\partial C_m}{\partial C_N} + \zeta = 0 \qquad (62)$$

for a value C_N within the interval $[C_{N_1}, C_{N_2}]$. In this system of equations δ_F and δ_e have their maximum values, and hence the equations can be solved for ζ and C_N. We then deduce the critical location of the center-of-gravity, through ζ, and the critical angle-of-attack, through C_N. Beyond this position, the vehicle becomes trimmable either at high angle-of-attack or at low angle-of-attack. For each ζ, beyond the critical value, the two limiting angles-of-attack are obtained by solving Eq.(61) with α_1 replaced by α.

Graphically, since for any percentage variation in the center-of-gravity resulting in a value ζ, the increment ΔC_m from maximum deflection is given by Eq.(59), we can plot this equation as a straight line, with a change in sign for ζ and measure the new value of C_m for maximum deflection from this line (Fig. 17). Figure 17-a for a hypothetical vehicle corresponds to the first case. At $x_{cg} = 0.735\ell$, the vehicle becomes just trimmable at $\alpha = 20°$. As the center-of-gravity moves further aft, it is trimmable only at higher angle-of-attack. Figure 17-b corresponds to the case of the present example CCV. At $x_{cg} = 0.739\ell$, the vehicle becomes just trimmable at $C_N = 1.350$, $\alpha = 33.1°$. As the center-of-gravity moves further aft, the vehicle becomes trimmable either at high angle-of-attack or at low angle-of-attack.

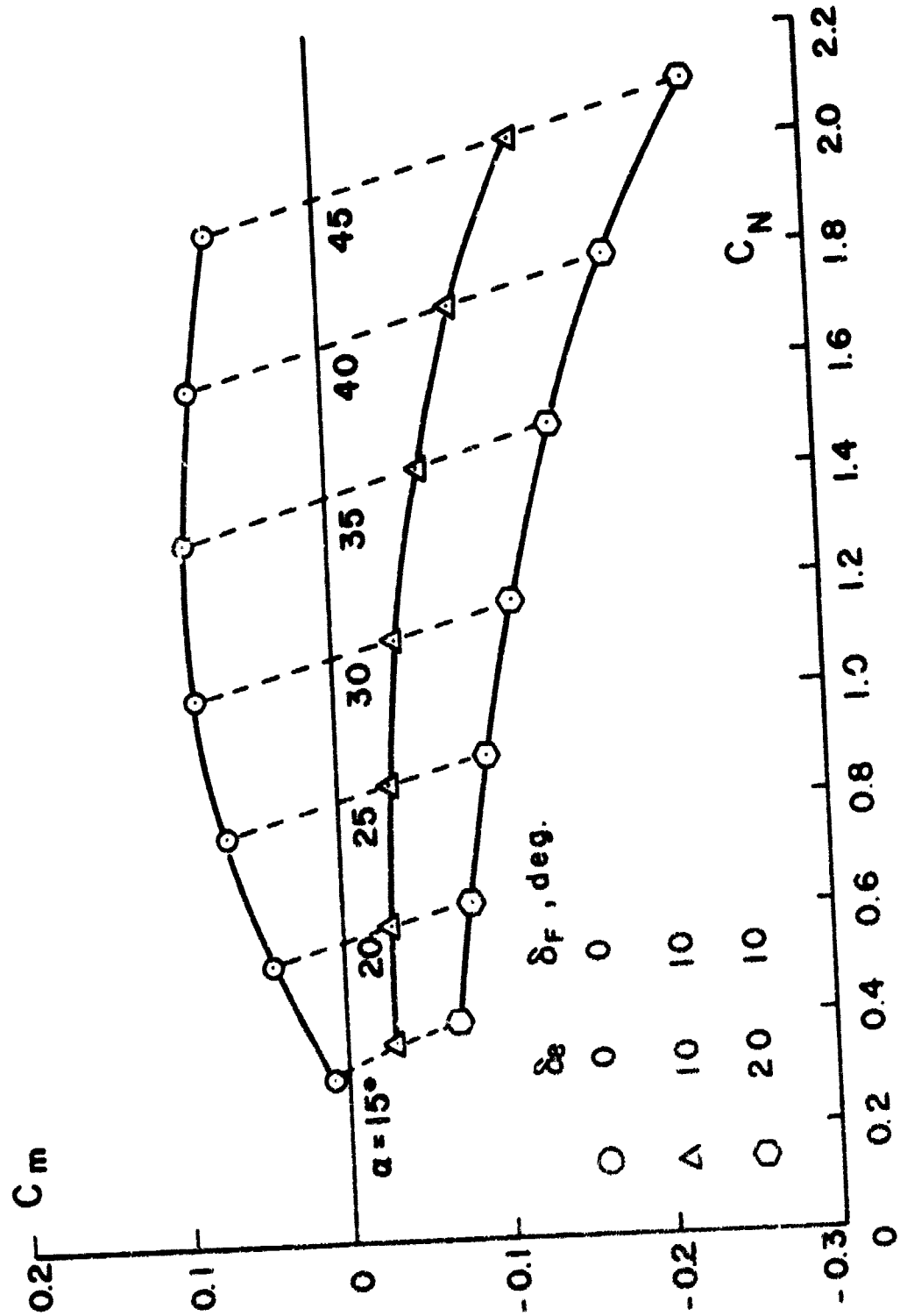

Fig. 15. Hypersonic trim characteristics of the vehicle.

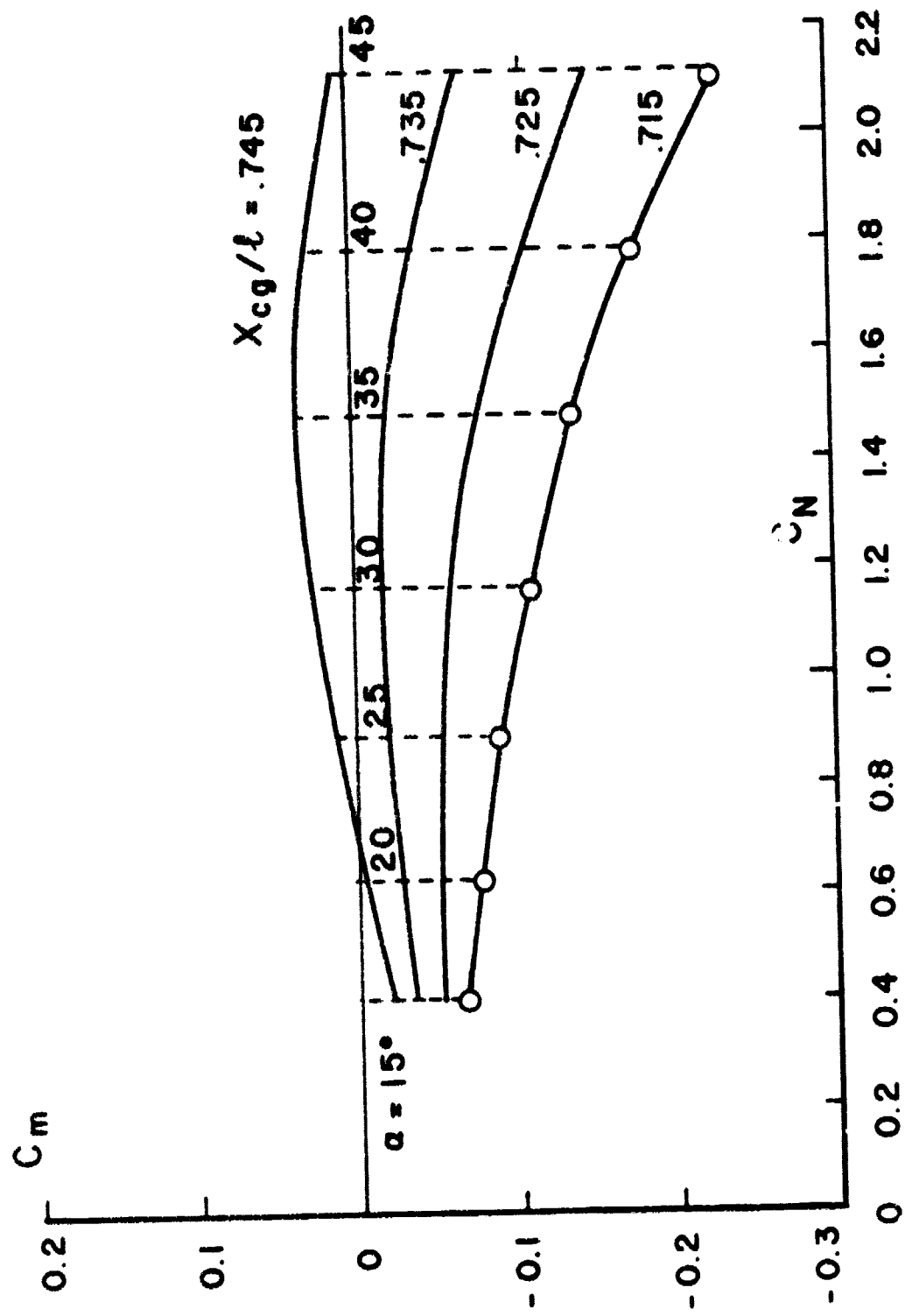

Fig. 16. Aerodynamic pitching moment coefficient at maximum control surfaces deflections for various locations of the center-of-gravity.

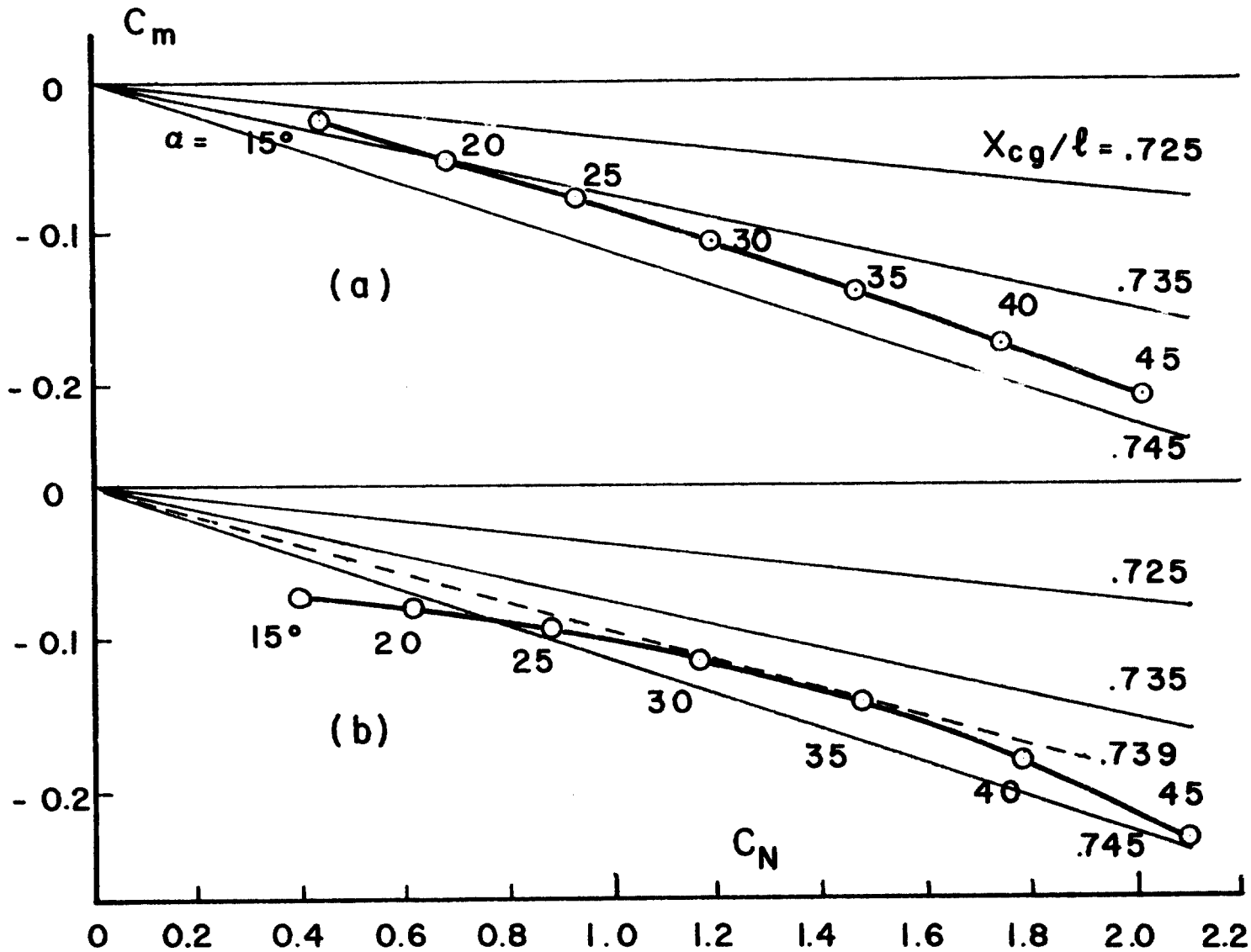

Fig. 17. Condition for hypersonic trim as function of the location of the center-of-gravity.

IV. PHUGOID OSCILLATIONS

With the static stability assessed, we now investigate the dynamic stability in longitudinal motion.

In low speed flight, when perturbed from a reference flight condition, longitudinal dynamics is characterized by a phugoid oscillation with long period and an angle-of-attack oscillation with short period. The phugoid mode is a trajectory mode along which the angle-of-atttack remains nearly constant while the center-of-gravity of the vehicle oscillates about a reference flight path through an exchange between the potential energy and the kinetic energy. By extension, we shall use this decoupling to analyze the first order effect of density gradient and centrifugal force on phugoid motion at nearly constant angle-of-attack.

The phugoid, or trajectory oscillations for the three typical cases of cruising flight, ballistic entry and glide entry are the subjects of investigation in this chapter. In Chapter V we shall analyze the angle-of-attack oscillations during entry for these cases.

Cruising Flight

The simplest motion can be envisaged when the vehicle is perturbed from a steady-state condition. From Eq.(25), at very high altitude, this can be achieved by using a small thrusting force to balance the drag and maintain a constant orbital altitude. With the thrust aligned with the velocity and considering a cruising flight at constant angle-of-attack α_o resulting in a lift and drag coefficients, C_{L_o} and C_{D_o}, we have the equations of motion

$$\frac{dR}{dt} = V \sin\gamma$$

$$m \frac{dV}{dt} = T - \tfrac{1}{2} \rho S C_{D_o} V^2 - mg \sin\gamma \tag{63}$$

$$mV \frac{d\gamma}{dt} = \tfrac{1}{2} \rho S C_{L_o} V^2 - m\left(g - \frac{V^2}{R}\right)\cos\gamma$$

At the reference constant-altitude cruise

$$R = R_o,\ V = V_o,\ \gamma = 0$$

$$T = \tfrac{1}{2} \rho_o S C_{D_o} V_o^2 \tag{64}$$

$$\tfrac{1}{2} \rho_o S C_{L_o} V_o^2 = m\left(g_o - \frac{V_o^2}{R_o}\right)$$

It is convenient to use a time transformation

$$\tau = \frac{1}{R_o} \int_0^t V(t)dt \tag{65}$$

to rewrite the equations. We notice that this new independent variable denotes the dimensionless arc length. Then, with the prime denoting the derivative with respect to τ, the system of equations (63), with the constant thrust replaced by its expression in Eqs.(64), becomes

$$\frac{R'}{R_o} = \sin\gamma$$

$$\frac{V'}{V} = \delta_o C_{D_o} \frac{V_o^2}{V^2} - \delta C_{D_o} - \left(\frac{gR_o}{V^2} \right)\sin\gamma \tag{66}$$

$$\gamma' = \delta C_{L_o} - \left(\frac{gR_o}{V^2} - \frac{R_o}{R} \right)\cos\gamma$$

where we have defined the dimensionless atmospheric density

$$\delta = \frac{\rho S R_o}{2m} \tag{67}$$

From the reference steady-state orbital cruise, we have the small perturbations

$$\begin{aligned} R &= R_o + \Delta R \\ V &= V_o + \Delta V \\ \gamma &= 0 + \gamma \end{aligned} \tag{68}$$

The gravity acceleration g(R) and the density $\delta(R)$ are functions of R. For an inverse-square force field we have the linearized acceleration of the gravity

$$g = g_o\left(1 - 2\frac{\Delta R}{R_o}\right) \tag{69}$$

The density function δ is more complex. In general, by Taylor's series expansion

$$\delta = \delta_o + R_o\left(\frac{d\delta}{dR}\right)_o \frac{\Delta R}{R_o} + \ldots \tag{70}$$

where $(d\delta/dR)_o$ is the first order density gradient. The system (66) can be linearized and using the reference condition (64) for simplification, we have the equations for the perturbations ΔR, ΔV and γ

$$\frac{\Delta R'}{R_o} = \gamma$$

$$\frac{\Delta V'}{V_o} = -C_{D_o} R_o\left(\frac{d\delta}{dR}\right)_o \frac{\Delta R}{R_o} - 2\delta_o C_{D_o} \frac{\Delta V}{V_o} - \frac{g_o R_o}{V_o^2}\gamma \tag{71}$$

$$\gamma' = \left[C_{L_o} R_o\left(\frac{d\delta}{dR}\right)_o + \frac{2g_o R_o}{V_o^2} - 1\right]\frac{\Delta R}{R_o} + \frac{2g_o R_o}{V_o^2}\frac{\Delta V}{V_o}$$

Any merit of an analytical study results from the fact that certain parameters governing the physical phenomena can be displayed explicitly. From the linearized system (71), it is seen that the characteristic roots depend on the constant parameters

$$\delta_o C_{D_o} = \frac{\rho_o S R_o C_{D_o}}{2m}$$

$$\delta^2 = \frac{V_o^2}{g_o R_o} \tag{72}$$

$$\sigma = \frac{R_o}{\rho_o}\left(\frac{d\rho}{dR}\right)_o = \frac{R_o}{\delta_o}\left(\frac{d\delta}{dR}\right)_o$$

The first term is the drag parameter at the reference altitude. It is function of the angle-of-attack selected and the orbital altitude. The parameter δ is the ratio of the reference cruising speed V_o to the orbital speed in the vacuum $\sqrt{g_o R_o}$ at the reference altitude. We notice that $\delta \to 1$ as $\rho \to 0$ at very high altitude. The parameter σ is termed the atmospheric density gradient. From the reference condition (64) we deduce the relation

$$\delta_o C_{L_o} = \frac{(1 - \delta^2)}{\delta^2} \tag{73}$$

Hence, ultimately, phugoid oscillation, for any vehicle considered, depends on the flight altitude, which provides the values σ and δ_o, and the trimmed angle-of-attack α_o, which gives the values C_{D_o} and C_{L_o}. The speed parameter δ is deduced from Eq.(73). The effect of the altitude is entered through both the values ρ_o (or δ_o) and the density gradient σ which is not negligible at orbital flight. The effect of the orbital speed is due to the fact that Eqs.(73) account for the effect of the curvature of the Earth.

Using the vector perturbation

$$X = \left[\frac{\Delta R}{R_o}, \frac{\Delta V}{V_o}, \gamma\right]^T \tag{74}$$

we can write the linear system (71) in matrix form

$$\frac{dX}{d\tau} = AX \tag{75}$$

with the constant square matrix A being

$$A = \begin{pmatrix} 0 & 0 & 1 \\ -\delta_o C_{D_o}\sigma & -2\delta_o C_{D_o} & -\frac{1}{\delta^2} \\ \frac{(1-\delta^2)}{\delta^2}\sigma + \frac{2}{\delta^2} - 1 & \frac{2}{\delta^2} & 0 \end{pmatrix} \tag{76}$$

The resulting stability characteristic equation is a cubic equation which can be obtained by expanding the equation

$$\det.\ [A - \lambda I] = 0 \tag{77}$$

We have

$$\lambda^3 + 2\delta_o C_{D_o}\lambda^2 + \frac{1}{\delta^4}[(1-\delta^2)(2-\delta^2\sigma)+\delta^4]\lambda - \frac{2\delta_o C_{D_\alpha}}{\delta^2}[2-\delta^2-\delta^2\sigma] = 0 \tag{78}$$

For reason which will be clear later, we define

$$\omega^2 = \frac{[(1-\delta^2)(2-\delta^2\sigma) + \delta^4]}{\delta^4}$$

$$\xi^2 = \frac{[2-\delta^2-\delta^2\sigma]}{\delta^2} \tag{79}$$

Numerical values for the density gradient, σ, as function of the altitude are given in Appendix A. In the altitude range of interest, σ is oscillating in the vicinity of the value -900. On the other hand, the speed parameter δ varies in the range $0 \leq \delta \leq 1$, close to zero at low altitude and tending to unity in orbital flight. Hence, the positiveness of the parameters ω^2 and ξ^2 is assessed. With the definition (79), we rewrite the characteristic equation as

$$\lambda^3 + 2\delta_o C_{D_o}\lambda^2 + \omega^2\lambda - 2\delta_o C_{D_o}\xi^2 = 0 \tag{80}$$

This stability cubic equation for the trajectory mode has three roots, one real and small root and one pair of complex conjugate roots. The real root is obtained by observing that the last term of the cubic equation is small. Hence, we have approximately

$$\lambda_{spiral} \simeq 2\delta_o C_{D_o} \left(\frac{\xi}{\omega}\right)^2 \tag{81}$$

Since this real root is positive, hence unstable, the name of spiral mode is justified. The exact root, to any order of accuracy, is obtained through series expansion by putting

$$\lambda_{spiral} = 2\delta_o C_{D_o} \left(\frac{\xi}{\omega}\right)^2 a \tag{82}$$

where a is a constant near unity to be determined. By substituting into Eq.(80) we obtain

$$a = 1 - \left(\frac{2\delta_o C_{D_\alpha}}{\omega}\right)^2 \left(\frac{\xi}{\omega}\right)^2 a^2 \left[1 + \left(\frac{\xi}{\omega}\right)^2 a\right] \tag{83}$$

The equation is in the form

$$a = p + \varepsilon f(a) \tag{84}$$

where, with a small ε, Lagrange expansion

$$a = p + \sum_{n=1}^{\infty} \frac{\varepsilon^n}{n!} \left(\frac{d}{dp} \right)^{n-1} [f(p)]^n \tag{85}$$

is dictated. Here, the small term $(2\delta_o C_{D_o}/\omega)^2$ plays the role of ε. Hence, we have explicitly

$$\begin{aligned} a = 1 &- \left(\frac{2\delta_o C_{D_o}}{\omega} \right)^2 \left(\frac{\xi}{\omega} \right)^2 \left[1 + \left(\frac{\xi}{\omega} \right)^2 \right] \\ &+ \left(\frac{2\delta_o C_{D_o}}{\omega} \right)^4 \left(\frac{\xi}{\omega} \right)^4 \left[1 + \left(\frac{\xi}{\omega} \right)^2 \right] \left[2 + 3 \left(\frac{\xi}{\omega} \right)^2 \right] \\ &- \left(\frac{2\delta_o C_{D_o}}{\omega} \right)^6 \left(\frac{\xi}{\omega} \right)^6 \left[1 + \left(\frac{\xi}{\omega} \right)^2 \right] \left[1 + 2 \left(\frac{\xi}{\omega} \right)^2 \right] \left[5 + 6 \left(\frac{\xi}{\omega} \right)^2 \right] + \ldots \end{aligned} \tag{86}$$

Since $a = 1$ already gives a good approximation, this explicit series solution is very accurate. Next, by factorizing the cubic equation, Eq.(80), using the real root (82), we have the equation for the remaining pair of complex conjugate roots

$$\lambda^2 + 2\delta_o C_{D_o} \left[1 + \left(\frac{\xi}{\omega} \right)^2 a \right] \lambda + \frac{\omega^2}{a} = 0 \tag{87}$$

where, of course, the value of a is given by Eq.(86). From this equation we have for the phugoid mode which is a damped oscillation

$$\text{Real}(\lambda_{\text{phugoid}}) = -\delta_o C_{D_o} \left[1 + \left(\frac{\xi}{\omega} \right)^2 a \right] \tag{88}$$

and

$$\text{Im}(\lambda_{\text{phugoid}}) = \omega \sqrt{\frac{1}{a} - \left(\frac{\delta_o C_{D_o}}{\omega} \right)^2 \left[1 + \left(\frac{\xi}{\omega} \right)^2 a \right]^2} \tag{89}$$

Using Eq.(83), we have another form for the phugoid frequency

$$\text{Im}(\lambda_{\text{phugoid}}) = \omega \sqrt{1 - \left(\frac{\delta_o C_{D_o}}{\omega} \right)^2 \left[1 + \left(\frac{\xi}{\omega} \right)^2 a \right] \left[1 - 3 \left(\frac{\xi}{\omega} \right)^2 a \right]} \tag{90}$$

Returning to the dimensionless time, τ, as defined in Eq.(65), if the small speed perturbation is neglected, it is simply

$$\tau = \frac{V_o}{R_o} t \tag{91}$$

Then, the time to double for the spiral mode is

$$t_{double} = \frac{m \log 2}{\rho_o S C_{D_o} V_o a} \left(\frac{\omega}{\xi} \right)^2 \tag{92}$$

The spiral mode is a new mode inherent in near orbital flight. Since we assume a small constant thrust which exactly balances the drag in cruising flight at constant altitude, any perturbation causing an increase in the altitude with smaller drag will create an excess of thrust which has the effect of increasing the radial distance, hence sending the vehicle into an outward spiral. The reverse effect is true for any decrease in the altitude.

Now, since the phugoid mode is a damped oscillation, we consider the spiral effect on the change in the flight path angle and the speed. We start with the solution for the radial distance

$$\frac{\Delta R}{R_o} = \varepsilon e^{\lambda \tau} \tag{93}$$

where λ is the spiral root and ε is the initial perturbation with $\varepsilon > 0$ for an outward spiral. From the first equation in the linear system (71), we have

$$\gamma = \varepsilon \lambda e^{\lambda \tau} \tag{94}$$

which shows that γ varies as ΔR. On the other hand, from the last equation of the system, we have

$$\frac{\Delta V}{V_o} = \frac{\varepsilon}{2} \left[\lambda^2 \delta^2 - (1-\delta^2)\sigma + \delta^2 - 2 \right] e^{\lambda \tau} \tag{95}$$

Since λ^2 is small and $\sigma \simeq -900$ (see Appendix A) while $\delta \to 1$ when $\rho \to 0$, the bracketed coefficient is negative at very high altitude and is positive at low altitude. Hence, at very high altitude, the speed varies in the opposite direction as the radial distance, that is the speed decreases along an outward spiral and increases along an inward spiral. At lower altitude, the speed varies in the same direction as the radial distance. Neglecting the small term $\lambda^2 \delta^2$, the condition for the speed to vary in the same direction as the radial distance is

$$-(1-\delta^2)\sigma + \delta^2 - 2 > 0 \tag{96}$$

In terms of ω^2, as defined in Eq.(79), we rewrite this condition as

$$\omega^2 \delta^4 > 2 \tag{97}$$

In a more explicit form, using Eq.(73) to calculate the speed parameter δ^2, we rewrite the condition (96)

$$-(2+\sigma)\delta_o C_{L_o} > 1$$

Since $-\sigma$ is large, we simply have

$$\frac{(W/S)}{C_{L_o}} < -\frac{g_o R_o}{2} R_o \left(\frac{d\rho}{dR} \right)_o \tag{98}$$

If the equality sign is used in this equation, upon solving we have the altitude where the speed inversion occurs. Graphically, since the right-hand side of the condition (98) is purely a function of the altitude, for any planetary atmosphere, the function can be plotted versus the altitude. Then, for any wing loading condition (W/S), and lift coefficient, C_{L_o}, the altitude for speed inversion for the corresponding vehicle can be assessed.

Concerning the phugoid oscillation, from Eq.(88), we have for the damping, in real time

$$t_{half} = \frac{2m \log 2}{\rho_o S C_{D_o} V_o} \times \frac{1}{1 + (\frac{\xi}{\omega})^2 a} \tag{99}$$

The period of oscillation is

$$P = \frac{2\pi}{\omega} \frac{R_o}{V_o} \{1 - (\frac{\delta_o C_{D_o}}{\omega})^2 [1 + (\frac{\xi}{\omega})^2 a][1 - 3(\frac{\xi}{\omega})^2 a]\}^{-\frac{1}{2}} \tag{100}$$

Expliciting for ω, we obtain

$$\omega = (\frac{g_o R_o}{V_o^2}) \sqrt{(\frac{V_o^2}{g_o R_o})^2 + \frac{L_o}{m g_o} [2 - \frac{V_o^2}{g_o R_o} \frac{R_o}{\rho_o} (\frac{d\rho}{dR})_o]} \tag{101}$$

where L_o is the lift force in reference cruise. Then, the period of oscillation in phugoid motion has the final form

$$P = \frac{2\pi V_o}{g_o} \{(\frac{V_o^2}{g_o R_o})^2 + \frac{L_o}{m g_o} [2 - \frac{V_o^2}{g_o R_o} \frac{R_o}{\rho_o} (\frac{d\rho}{dR})_o]\}^{-\frac{1}{2}} \times$$
$$\{1 - (\frac{\delta_o C_{D_o}}{\omega})^2 [1 + (\frac{\xi}{\omega})^2 a][1 - 3(\frac{\xi}{\omega})^2 a]\}^{-\frac{1}{2}} \tag{102}$$

If we neglect the small term $(\delta_o C_{D_o})^2$, and take the second bracketed term as unity we obtain an expression that is identical to Laitone and Chou's (Ref. 12). Eq.(102) which takes into account the effect of the density gradient and the centrifugal force correctly predicts the phugoid period in the entire range of cruise altitude from low altitude for airplane dynamics to high altitude orbital flight. Asymptotically, in orbital flight with $\delta_o \to 0$, $L_o \to 0$, $V_o^2 \to g_o R_o$ the period tends to

$$P \text{ (orbit)} = \frac{2\pi V_o}{g_o} = 2\pi \sqrt{R_o / g_o} \tag{103}$$

which is precisely the orbital period along a circular orbit at distance R_o.

The relative balancing effect between the speed and the density gradient on phugoid period can be displayed by considering the simplified formula

$$P = \frac{2\pi V_o}{g_o} \{(\frac{V_o^2}{g_o R_o})^2 + \frac{L_o}{mg_o} [2 - (\frac{V_o^2}{g_o R_o})\sigma]\}^{-\frac{1}{2}} \tag{104}$$

For flight at very high altitude in the near vacuum, $V_o^2/g_o R_o$ is near unity and, although $-\sigma$ is large, because L_o/mg_o is near zero, the effect of orbital speed is predominant. At medium altitude, as V_o decreases and L_o becomes larger, the effect of the density gradient becomes more pronounced and should be included. At lower altitude, for airplane-type dynamics, we write the bracketed term

$$\{\ \} = 2\frac{L_o}{mg_o} + (\frac{V_o^2}{g_o R_o})[(\frac{V_o^2}{g_o R_o}) - (\frac{L_o}{mg_o})\sigma] \tag{105}$$

At sonic speed, taking $V_o = 340$ m/sec, $\sqrt{g_o R_o} = 7919$ m/sec, we have $V_o^2/g_o R_o = 1.843 \times 10^{-3}$ while L_o/mg_o is near unity. Hence, for all practical purpose, we can take

$$\{\ \} = \frac{L_o}{mg_o}(2 - \frac{V_o^2}{g_o R_o}\sigma) \tag{106}$$

Then, by setting $L_o = mg_o$ as condition for equilibrium steady-state flight, a condition which can be deduced from the last equation in system (64) by using the same approximation, that is with $V_o^2/g_o R_o << 1$, Eq.(104) becomes

$$P\ (\text{airplane}) = \frac{2\pi V_o}{g_o \sqrt{2 - \frac{V_o^2}{g_o R_o}\sigma}}$$

or

$$P\ (\text{airplane}) = \frac{2\pi}{\sqrt{g_o\ (\frac{2g_o}{V_o^2} - \frac{1}{\rho}\frac{d\rho}{dH})}} \tag{107}$$

It is shown in Appendix A that the density gradient term is equal to -1.577×10^{-4}/m for an isothermal atmosphere while for sonic speed, $M = 1$, $V_o = 295$ m/sec in the stratosphere we have $2g_o/V_o^2 = 2.255 \times 10^{-4}$/m. The speed and density gradient effects are now of the same order of magnitude. For very low speed, the density gradient effect can be neglected and we have the classical formula

$$P\ (\text{airplane}) = \frac{\sqrt{2}\pi V_o}{g_o} \tag{108}$$

which, as well known, gives the phugoid period within 10% of the value obtained by considering the full set of linearized equations taking into account the coupling between the phugoid and the angle-of-attack modes.

From the physical discussion above, we have seen that the density gradient effect is most pronounced at the intermediate range of speed. Mathematically, since

$$\frac{L_o}{mg_o} = 1 - \frac{V_o^2}{g_o R_o} = 1 - \delta^2 \tag{109}$$

we express the bracketed term in Eq.(104) as

$$\{\ \}^{\frac{1}{2}} = \omega\delta^2 = \bar{\omega} = \sqrt{\delta^4 + (1-\delta^2)(2-\delta^2\sigma)} \tag{110}$$

We have seen that near orbital flight, we have asymptotically

$$\{\ \}^{\frac{1}{2}} = \bar{\omega}_1 = \delta^2 \tag{111}$$

while at very low speed we take

$$\{\ \}^{\frac{1}{2}} = \bar{\omega}_2 = \sqrt{2} \tag{112}$$

The three functions $\bar{\omega}$ above are plotted versus the speed parameter $\delta = V_o/\sqrt{g_o R_o}$ in Fig. 18 using an average value $-\sigma = 900$. It is seen that the influence of the density gradient is important and has the effect of shortening the phugoid period. The approximation $\bar{\omega}_1$ and $\bar{\omega}_2$ can only be used near the limiting cases either near orbital flight or at very low speed.

Ballistic Entry

We now consider the important case of ballistic entry. With $T = 0$ and $C_{L_o} = 0$, the system of equations (66) is reduced to

$$\begin{aligned} \frac{R'}{R_o} &= \sin\gamma \\ \frac{V'}{V} &= -\delta C_{D_o} - \left(\frac{gR_o}{V^2}\right)\sin\gamma \\ \gamma' &= -\left(\frac{gR_o}{V^2} - \frac{R_o}{R}\right)\cos\gamma \end{aligned} \tag{113}$$

In the second equation of this system, the drag force during entry is large as compared to the small component of the gravity along the tangent to the flight path. Furthermore, we shall use the approximation $R_o/R \simeq 1$ in the last equation. Then, we have the simplified system

$$\begin{aligned} \frac{R'}{R_o} &= \sin\gamma \\ \frac{V'}{V} &= -\delta C_{D_o} \\ \gamma' &= \left(1 - \frac{gR_o}{V^2}\right)\cos\gamma \end{aligned} \tag{114}$$

It has been verified in reference 13 that the numerical solution of this system is accurate as compared to the solution obtained from the integration of the exact equations. Following the analysis in that reference, we use the Chapman-Yaroshevskii variables

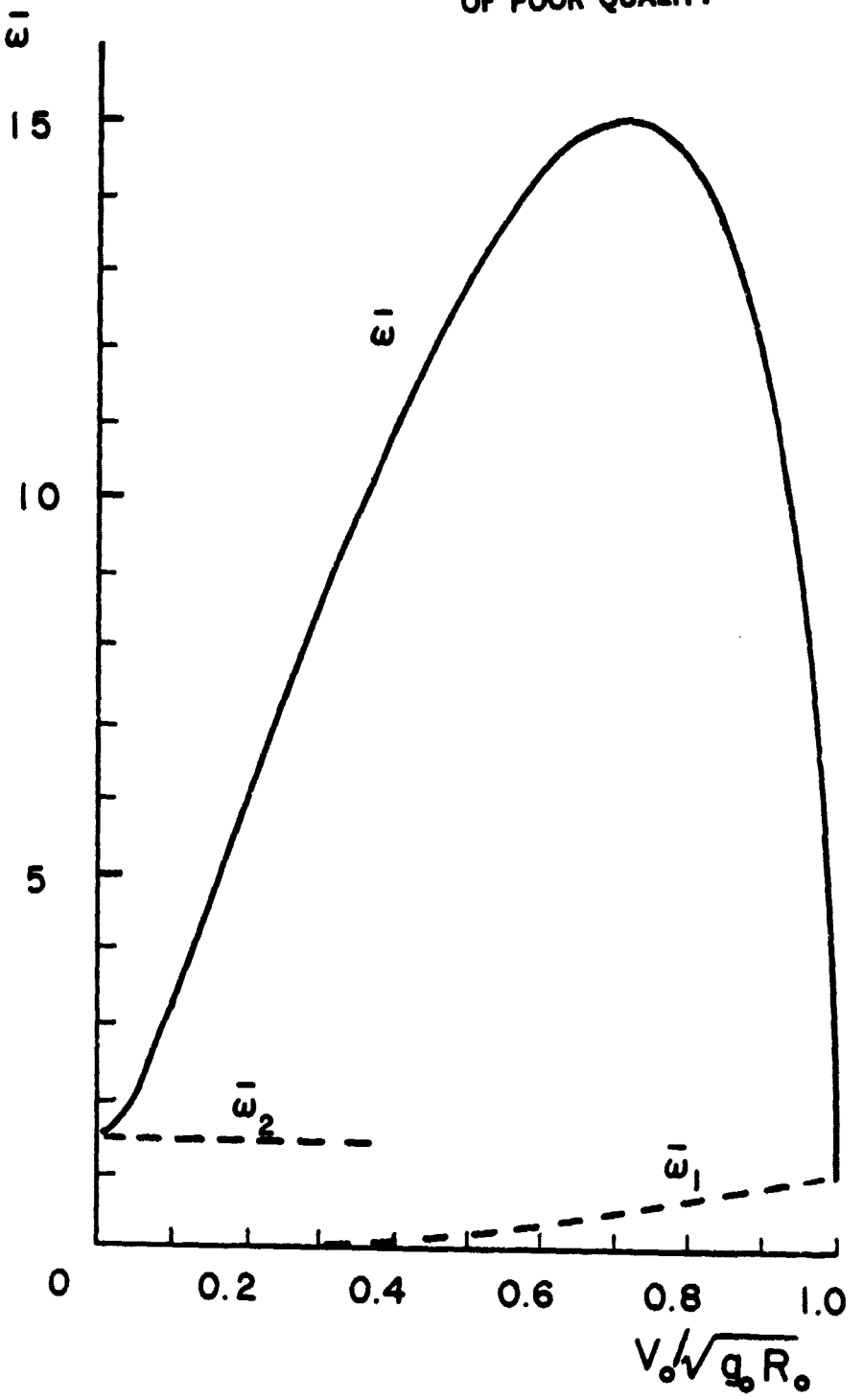

Fig. 18. The modified frequency $\bar{\omega}$ and its asymptotic approximations as functions of the cruising speed.

$$Y = \frac{\rho S C_{D_o}}{m}\sqrt{R_o/\beta} = 2\delta C_{D_o}/\sqrt{\beta R_o}$$

$$\Phi = -\sqrt{\beta R_o}\,\sin\gamma \tag{115}$$

$$x = \log\,(gR_o/V^2)$$

where $\bar{\beta}$ is the inverse of the scale height in a locally exponential atmosphere, that is

$$d\rho = -\bar{\beta}\rho dR \tag{116}$$

Then, we have the equation for the altitude which is here represented by the new dimensionless density Y

$$Y' = -\bar{\beta}R_o Y\sin\gamma \tag{117}$$

For the flight path angle which is represented by the variable Φ, we have

$$\Phi' = -\sqrt{\beta R_o}\,(1 - \frac{gR_o}{V^2})\cos^2\gamma \tag{118}$$

Changing the independent variable to V and then to x, we have successively

$$\frac{dY}{dV} = -\frac{2}{V}\Phi$$

$$\frac{d\Phi}{dV} = \frac{2}{YV}\,(1 - \frac{gR_o}{V^2})\cos^2\gamma \tag{119}$$

and

$$\frac{dY}{dx} = \Phi$$

$$\frac{d\Phi}{dx} = \frac{(e^x - 1)\cos^2\gamma}{Y} \tag{120}$$

Because of the physical constraint on the deceleration during entry, ballistic entry is generally effected at small flight path angles. Hence, we have the dimensionless equations for ballistic entry at small and medium angles by taking $\cos^2\gamma \approx 1$, that is

$$\frac{dY}{dx} = \Phi$$

$$\frac{d\Phi}{dx} = \frac{(e^x - 1)}{Y} \tag{121}$$

For ballistic entry from circular speed, the independent variable x increases from the initial value zero to about 6.3 when the speed has decreased to the order of the speed of sound at low altitude. On the other hand, the altitude

variable Y, which is proportional to the density, starts with near zero value at the top of the sensible atmosphere. For most vehicle physical parameters, the value of Y at sea level is near 60. Expressed in the change in the altitude, we can consider the change in an exponential atmosphere

$$\bar{\beta}\Delta H = \log \frac{Y}{Y_1} \tag{122}$$

where Y_1 is the initial value of Y and $\Delta H = H_1 - H$ is the variation in the altitude from the initial height. This formulation is convenient in that it is independent of the physical characteristics of the vehicle.

Accurate series solutions for the system (121) have been given in reference 13. For the case of ballistic entry from a decaying orbit such as the case of the reentry of the skylab, we have the initial condition

$$Y(0) = 0, \qquad \Phi(0) = 0 \tag{123}$$

with the solution

$$Y = \frac{2}{\sqrt{3}} x^{3/2} \left[1 + \frac{1}{3}\left(\frac{x}{4}\right) + \frac{1}{6}\left(\frac{x}{4}\right)^2 + \frac{47}{594}\left(\frac{x}{4}\right)^3 + \frac{20021}{605880}\left(\frac{x}{4}\right)^4\right] \tag{124}$$

and

$$\Phi = \sqrt{3}\, x^{1/2} \left[1 + \frac{5}{9}\left(\frac{x}{4}\right) + \frac{7}{18}\left(\frac{x}{4}\right)^2 + \frac{47}{198}\left(\frac{x}{4}\right)^3 + \frac{20021}{165240}\left(\frac{x}{4}\right)^4\right] \tag{125}$$

For entry with non zero initial flight path angle, we have the initial condition

$$Y(0) = 0, \qquad \Phi(0) = -\sqrt{\bar{\beta}R_0}\, \sin\gamma_1 = c \tag{126}$$

where γ_1 is the initial flight path angle. From the definition of σ in Eq.(72), with a locally exponential atmosphere as defined in Eq.(116), it is seen that $\bar{\beta}R_0 = -\sigma$. Hence, as shown in Appendix A, we take the average value $\bar{\beta}R_0 = 900$ for evaluating the initial parameter c.

For the solution in this case, we write the system (121) in the form of Yaroshevskii non-linear equation

$$Y \frac{d^2Y}{dx^2} = e^x - 1 = x + \frac{x^2}{2!} + \frac{x^3}{3!} + \ldots \tag{127}$$

and evaluate the formal solution

$$Y = \sum_{k=1}^{\infty} a_k x^k \tag{128}$$

satisfying the initial condition (126). It is found that

$$a_1 = c, \quad a_2 = \frac{1}{2c}, \quad a_3 = \frac{1}{12c}\left(1 - \frac{1}{c^2}\right), \quad a_4 = \frac{1}{72c}\left(1 - \frac{2}{c^2} + \frac{2}{c^4}\right) \tag{129}$$

To the same order, we have

$$\Phi = \sum_{k=0}^{\infty} b_k x^k \tag{130}$$

where

$$b_0 = c, \quad b_1 = \frac{1}{c}, \quad b_2 = \frac{1}{4c}\left(1 - \frac{1}{c^2}\right), \quad b_3 = \frac{1}{18c}\left(1 - \frac{2}{c^2} + \frac{2}{c^4}\right)$$

$$b_4 = \frac{1}{96c}\left(1 - \frac{10}{3c^2} + \frac{20}{3c^4} - \frac{17}{3c^6}\right) \tag{131}$$

The variations of the flight path angle for entry at circular speed with different initial flight path angles are presented in Fig. 19. The solid lines indicate the exact numerical solutions of Eqs.(121), while the dashed lines represent the present analytical solutions. Solution for entry from a decaying orbit is very accurate. On the other hand, for non-zero initial angle, the solution is only accurate when $-\gamma_i > 1.5°$. For very small initial angles providing small values of c, because of small radius of convergence of the series solution, the solution is restricted to the high speed range.

We now investigate the small perturbations from a reference solution Y_o, Φ_o. Let

$$Y = Y_o + \Delta Y$$

$$\Phi = \Phi_o + \Delta\Phi \tag{132}$$

By substituting into system (121) and simplifying, we have

$$\frac{d\Delta Y}{dx} = \Delta\Phi$$

$$\frac{d\Delta\Phi}{dx} = -\frac{(e^x - 1)\Delta Y}{Y_o(Y_o + \Delta Y)} \tag{133}$$

Hence, the perturbation in altitude is obtained from the non-linear differential equation of the second order

$$\frac{d^2\Delta Y}{dx^2} + \frac{(e^x - 1)\Delta Y}{Y_o(Y_o + \Delta Y)} = 0 \tag{134}$$

where the function $Y_o(x)$ used is the reference solution, that is the solution (124) for entry from decaying orbit and solution (128) for entry with non-zero initial angles. By the change of variable

$$y = \frac{\Delta Y}{\sqrt{x}} \tag{135}$$

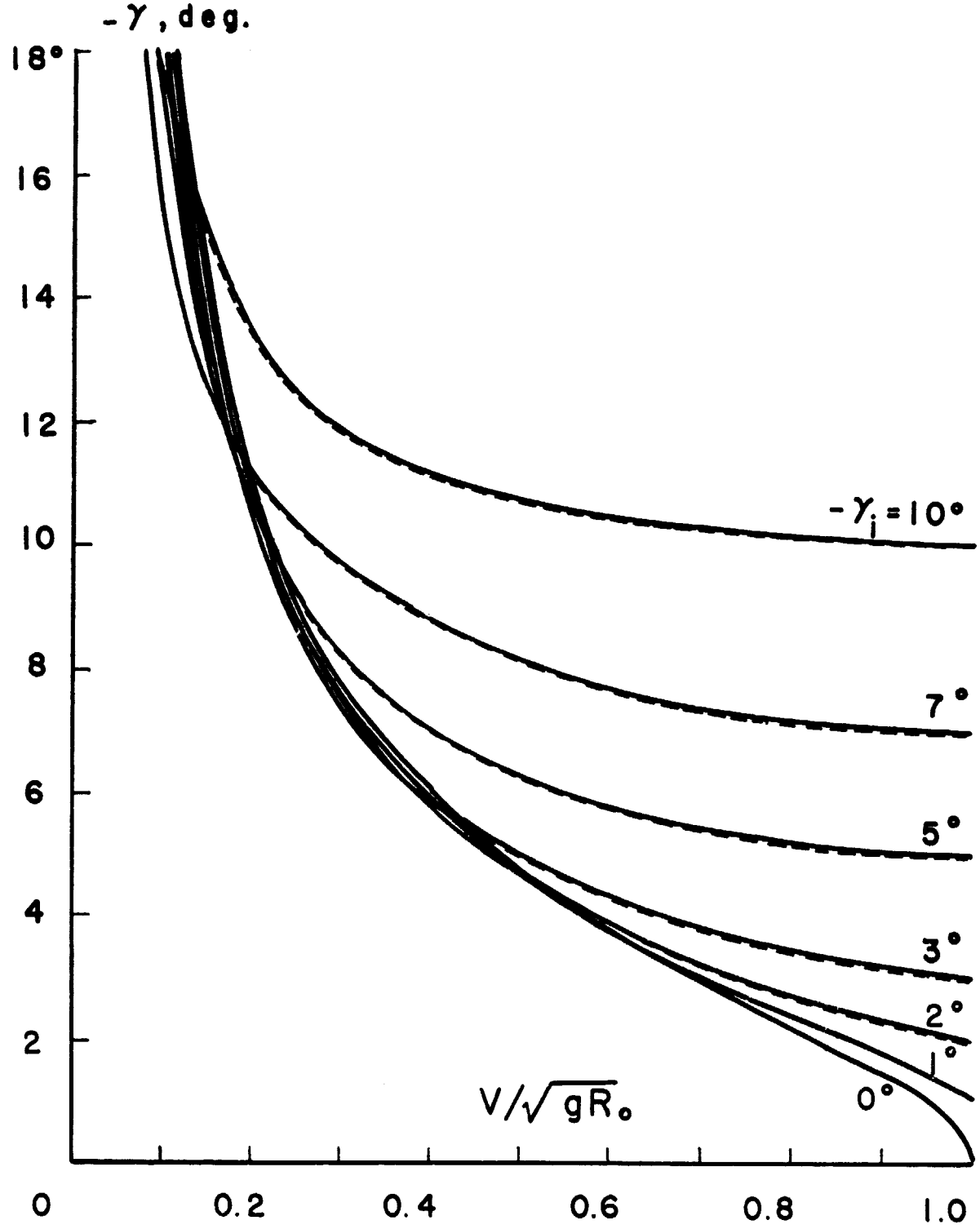

Fig. 19. Variation of the flight path angle for ballistic entry at circular speed.

we obtain the new non-linear equation

$$\frac{d^2y}{dx^2} + \frac{1}{x}\frac{dy}{dx} - \frac{y}{4x^2} + \frac{(e^x - 1)y}{Y_o^2(1 + y\sqrt{x}/Y_o)} = 0 \tag{136}$$

Going back to the initial system (121), it is seen that for large x, $e^x - 1 \simeq e^x$ and the asymptotic solution for Y is

$$Y = 2e^{x/2} \tag{137}$$

If this solution is used for Y_o in Eq.(136), we have, with the same asymptotic approximation

$$\frac{d^2y}{dx^2} + \frac{1}{x}\frac{dy}{dx} - \frac{y}{4x^2} + \frac{y}{4(1 + y\sqrt{x}/2e^{x/2})} = 0 \tag{138}$$

Hence, it appears that y is a damped oscillation, and in the linearized form we have

$$\frac{d^2y}{dx^2} + \frac{1}{x}\frac{dy}{dx} + \frac{1}{4}\left(1 - \frac{1}{x^2}\right)y = 0 \tag{139}$$

This is a special case of Bessel equation and the general solution is obviously

$$y = \frac{1}{\sqrt{x}}\left[C_1 \cos\frac{x}{2} + C_2 \sin\frac{x}{2}\right] \tag{140}$$

where C_1 and C_2 are two constants of integration. In general, since y is a damped oscillation, Eq.(136) can be linearized and we have

$$\frac{d^2y}{dx^2} + \frac{1}{x}\frac{dy}{dx} + \left[\frac{(e^x - 1)}{Y_o^2} - \frac{1}{4x^2}\right]y = 0 \tag{141}$$

For phugoid motion, perturbed from entry from a decaying orbit, we use Y_o as given by Eq.(124) with three terms

$$Y_o = \frac{2}{\sqrt{3}} x^{3/2}\left[1 + \frac{x}{12} + \frac{x^2}{96}\right] \tag{142}$$

Substituting into Eq.(141) and expanding the coefficient of y for small x, we have

$$\frac{d^2y}{dx^2} + \frac{1}{x}\frac{dy}{dx} + \frac{1}{4x^2}\left(2 + x + \frac{x^2}{4}\right)y = 0 \tag{143}$$

It can be shown that this equation can be transformed into a confluent hypergeometric equation (ref. 14). If the term $x^2/4$ is neglected, we have the equation

$$\frac{d^2y}{dx^2} + \frac{1}{x}\frac{dy}{dx} + \frac{(2+x)y}{4x^2} = 0 \qquad (144)$$

which can be transformed into a Bessel equation of imaginary order (ref. 15). For very small x, if we consider the coefficient of y as simply $1/2x^2$, we have obviously an Euler equation with general solution

$$y = C_1\cos\left(\frac{\sqrt{2}}{2}\log x\right) + C_2\sin\left(\frac{\sqrt{2}}{2}\log x\right) \qquad (145)$$

where C_1 and C_2 are constants of integration. It is enlightening to derive this solution by considering the general equation (144). By the transformation of variable

$$x = \zeta^2 \qquad (146)$$

the equation becomes

$$\frac{d^2y}{d\zeta^2} + \frac{1}{\zeta}\frac{dy}{d\zeta} + \left(1 + \frac{2}{\zeta^2}\right)y = 0 \qquad (147)$$

with general solution

$$y = C_1\, J_{i\sqrt{2}}(\sqrt{x}) + C_2\, J_{-i\sqrt{2}}(\sqrt{x}) \qquad (148)$$

where the functions $J_n(x)$ are Bessel functions of order n and argument x.

$$J_n(x) = \frac{x^n}{2^n \cdot n!}\left[1 - \frac{x^2}{2(2n+2)} + \frac{x^4}{2\cdot 4(2n+2)(2n+4)} - \ldots\right] \qquad (149)$$

To obtain the solution in the real form, we consider the two linearly independent solutions, putting $n = \pm i\sqrt{2}$, and changing x into $\sqrt{x}$ in the expression (149)

$$y_1 \sim x^{i\sqrt{2}/2}\left[1 - \frac{x}{4(1+i\sqrt{2})} + \frac{x^2}{32(1+i\sqrt{2})(2+i\sqrt{2})} - \frac{x^3}{384(1+i\sqrt{2})(2+i\sqrt{2})(3+i\sqrt{2})} + \ldots\right]$$

$$y_2 \sim x^{-i\sqrt{2}/2}\left[1 - \frac{x}{4(1-i\sqrt{2})} + \frac{x^2}{32(1-i\sqrt{2})(2-i\sqrt{2})} - \frac{x^3}{384(1-i\sqrt{2})(2-i\sqrt{2})(3-i\sqrt{2})} + \ldots\right]$$

After some manipulations

$$y_1 \sim x^{i\sqrt{2}/2}\,[f_1(x) + ig_1(x)]$$
$$y_2 \sim x^{-i\sqrt{2}/2}\,[f_1(x) - ig_1(x)] \tag{150}$$

where

$$f_1(x) = 1 - \frac{x}{12} + \frac{x^3}{12672} - \ldots$$
$$g_1(x) = \frac{\sqrt{2}\,x}{12}\left(1 - \frac{x}{16} + \frac{x^2}{704} - \ldots\right) \tag{151}$$

Since a linear combination of solutions is a solution, we combine linearly the solutions (150) to obtain new solutions in the real form

$$y_1 = f_1(x)\cos\left(\frac{\sqrt{2}}{2}\log x\right) - g_1(x)\sin\left(\frac{\sqrt{2}}{2}\log x\right)$$
$$y_2 = f_1(x)\sin\left(\frac{\sqrt{2}}{2}\log x\right) + g_1(x)\cos\left(\frac{\sqrt{2}}{2}\log x\right) \tag{152}$$

The solution (145) is obtained using the approximation $f_1(x) \simeq 1$, $g_1(x) \simeq 0$ for small x. Using the two linearly independent solutions (152), with the definition (135), we obtain the solution for the perturbation ΔY in the form

$$\Delta Y = A\sqrt{x}\,\left[f_1(x)\cos\left(\frac{\sqrt{2}}{2}\log\frac{x}{x_o}\right) - g_1(x)\sin\left(\frac{\sqrt{2}}{2}\log\frac{x}{x_o}\right)\right] \tag{153}$$

where A and x_o are now arbitrary constants of integration. By the first of the equation (133), we obtain the perturbation $\Delta\Phi$ in the form

$$\Delta\Phi = \frac{A}{2\sqrt{x}}\left[f_2(x)\cos\left(\frac{\sqrt{2}}{2}\log\frac{x}{x_o}\right) - g_2(x)\sin\left(\frac{\sqrt{2}}{2}\log\frac{x}{x_o}\right)\right] \tag{154}$$

where

$$f_2(x) = 1 - \frac{5x}{12} + \frac{x^2}{96} + \frac{x^3}{3168}$$
$$g_2(x) = \sqrt{2}\left(1 + \frac{x}{6} - \frac{5x^2}{192} + \frac{23x^3}{25344}\right) \tag{155}$$

The solutions (153) and (154) with the functions $f_i(x)$ and $g_i(x)$, $i = 1, 2$, not only provide the solution for the phugoid oscillations for entry from a decaying orbit but at the same time yield accurate analytical solutions for entry at very small angles. We recall that, as stated above, the existing solutions (128) and (130) cannot be used when the value of c is small.

It is now seen that, with a misalignment in the entry angle, $\gamma_i \neq 0$, the difference in the altitude of the perturbed motion, as compared to entry at $\gamma_i = 0$, increases. This is to be expected since entry at non-zero initial angle has the effect of drastically decreasing the range, providing a large difference in the altitude. On the other hand, the variation in the

flight path angle, as shown explicitly in Eq.(154), is a damped oscillation. Hence, in this sense, phugoid oscillation for near grazing ballistic entry is stable. To show this quantitatively, we use Eq.(154) to compute the perturbation from the reference solution as given by Eq.(125). The constants of integration A and x_o in Eq.(154) are evaluated using the initial condition (126). Because of the singularity at $x = 0$, the constants are evaluated at a certain point beyond the entry point. By convention, we take this point at $x = x_o$. For the computation at this arbitrary initial point, we refer to the definition (132) and use the following approximations:

Since in this case $c \neq 0$, the functions Y and Φ are initially given by the solutions (128) and (130) which are valid for small x, even in the case of small c. The functions Y_o and Φ_o are given by Eqs.(124) and (125) and the functions ΔY and $\Delta\Phi$ are given by Eqs.(153) and (154). Then at the point $x = x_o$, and to the order of x^3, we have

$$\frac{2}{\sqrt{3}} x^{3/2}\left(1 + \frac{x}{12} + \frac{x^2}{96}\right) + A\sqrt{x}\, f_1(x) = cx + \frac{1}{2c}x^2 + \frac{1}{12c}\left(1 - \frac{1}{c^2}\right)x^3 \qquad (156)$$

and

$$\sqrt{3}\, x^{1/2}\left(1 + \frac{5x}{36} + \frac{7x^2}{288}\right) + \frac{A}{2\sqrt{x}} f_2(x) = c + \frac{1}{c}x + \frac{1}{4c}\left(1 - \frac{1}{c^2}\right)x^2 \qquad (157)$$

where, from the expressions for $f_1(x)$ and $f_2(x)$, it suffices to take

$$f_1(x) = 1 - \frac{x}{12}$$
$$f_2(x) = 1 - \frac{5x}{12} \qquad (158)$$

In these equations, subscript zero in x_o has been omitted for convenience. Then, by solving the system of equations (156) and (157), the initial value x_o is obtained from

$$\frac{x^{1/2}}{\sqrt{3}}\left(4 + x + \frac{x^2}{8} - \frac{x^3}{288}\right) = c\left(1 + \frac{x}{4}\right) + \frac{x}{2c}\left(3 + \frac{x}{12}\right) + \frac{x^2}{12c}\left(1 - \frac{1}{c^2}\right)\left(5 - \frac{x}{12}\right) \qquad (159)$$

and subsequently the constant A is given by

$$A = \frac{12}{\sqrt{3}}\left(1 + \frac{x}{6} + \frac{x^2}{32}\right) - \frac{3}{\sqrt{x}}\left[c + \frac{3x}{2c} + \frac{5x^2}{12c}\left(1 - \frac{1}{c^2}\right)\right] \qquad (160)$$

where we recall that, in the two equations above, $c = -\sqrt{\beta R_o}\, \sin\gamma_i = -30 \sin\gamma_i$, and $x = x_o$. The solution for $\Delta\Phi$, computed for $-\gamma_i$ in the interval from 0° to 2°, displays, as expected, a damped oscillation with long period. Furthermore, when added to the nominal value $\Phi_o(x)$, it gives

accurate solution for shallow ballistic entry. The result is plotted in Fig. 19 and is indistinguishable from the exact numerical solution.

Half of the period of oscillation can be defined as the interval between two consecutive zeros, x_1 and x_2 of $\Delta\Phi$, as given explicitly in Eq.(154). Let

$$\tan[\psi(x)] = g_2(x)/f_2(x) \tag{161}$$

Then, the zeros of $\Delta\Phi$ are also the zeros of the function

$$\overline{\Delta\Phi} = \cos[\frac{\sqrt{2}}{2} \log \frac{x}{x_o} + \psi(x)] \tag{162}$$

Hence, if x_1 is the first zero and x_2 is the next one, we have

$$\frac{\sqrt{2}}{2} \log \frac{x_2}{x_1} + \psi(x_2) - \psi(x_1) = \pi \tag{163}$$

Similarly, we define

$$\tan[\bar{\psi}(x)] = \frac{g_1(x)}{f_1(x)} \tag{164}$$

For the oscillation in the altitude, if x_1 and x_2 are the first and the second zero of the function ΔY, respectively, we have the relation

$$\frac{\sqrt{2}}{2} \log \frac{x_2}{x_1} + \bar{\psi}(x_2) - \bar{\psi}(x_1) = \pi \tag{165}$$

Figure 20 plots x_2 versus x_1 for the Eqs.(163) and (165). The value x_1 increases from zero as $-\gamma_i$ increases from zero. Since the practical range of x is between 0 and 6, except for near zero values of x_1, which correspond to very small values of γ_i, the value of x_2 is large. Hence practically the plots of the variations of the flight path angle for $\gamma_i \neq 0$ cross the plot for the case of orbit decay, $\gamma_i = 0$, only once (Fig. 19).

Next, we consider the phugoid motion as perturbed from entry at medium and large angles. As seen in Fig. 19, with an initial perturbation

$$\Delta\phi(0) = -\sqrt{\beta R_o}\,(\sin\gamma_i - \sin\gamma_{i0}) = \Delta c \tag{166}$$

where γ_{i0} is the initial reference angle and $\gamma_i = \gamma_{i0} + \Delta\gamma_i$ is the initial perturbed angle, the function $-\Delta\gamma$, and hence $\Delta\Phi$, is a slowly decreasing function. Again, in the $(-\gamma, V)$ space, the two neighboring trajectories cross each other once at low speed. Hence, the phugoid motion is a slowly damped oscillation with long period. Since accurate analytical solution has been given in Eqs.(130) and (131), it suffices to take the difference between two neighboring solutions to obtain the solution for phugoid motion.

To display the damping characteristic of the phugoid motion, we consider the linearized perturbed equation (141), with the reference solution $Y_o(x)$

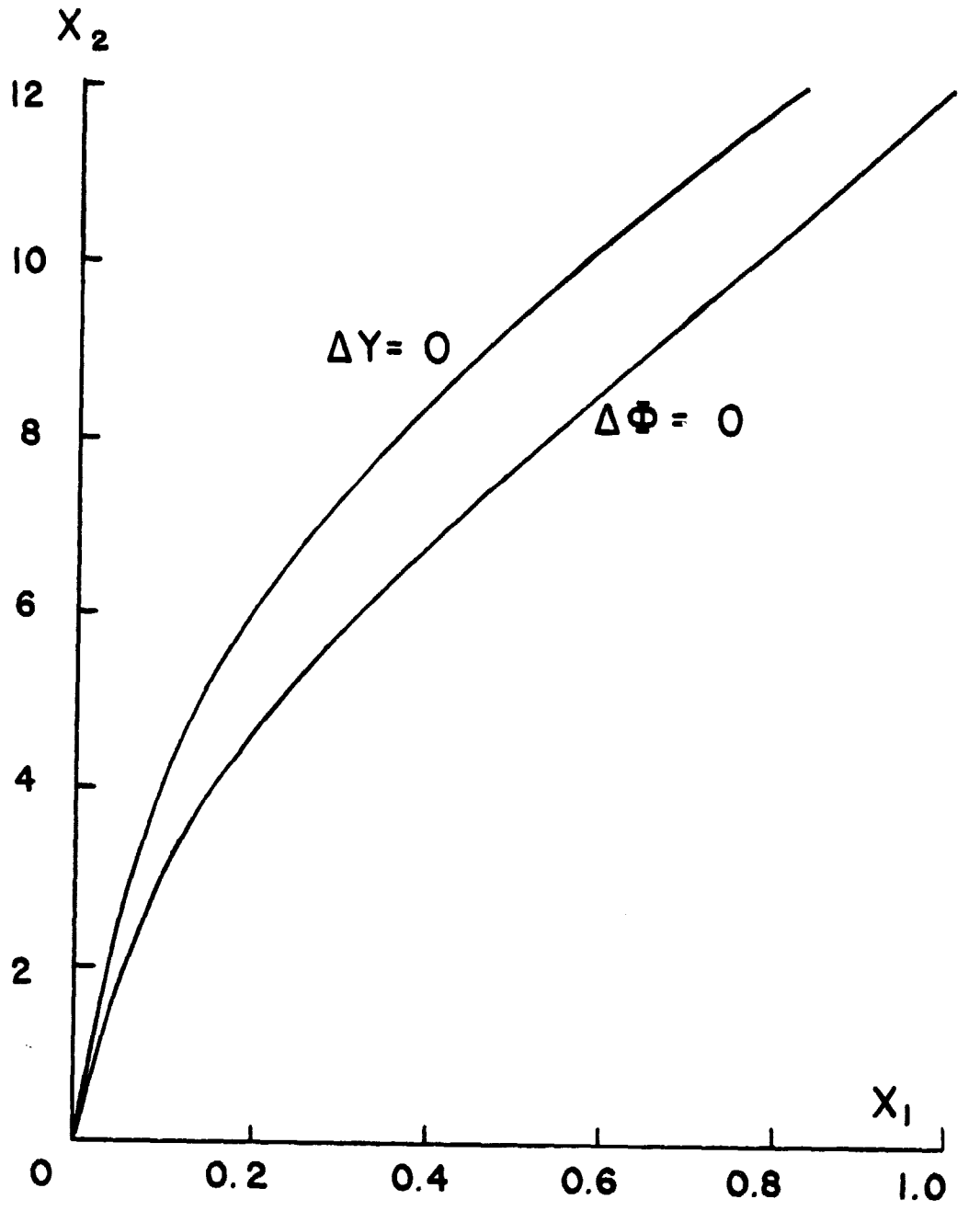

Fig. 20. Relation between the first two zeros of the functions $\Delta Y(x)$ and $\Delta\Phi(x)$.

given by two terms of the series (128). Then we have the equation, to the same order as Eq.(143)

$$\frac{d^2y}{dx^2} + \frac{1}{x}\frac{dy}{dx} + [\frac{(c^2 - 2)}{2c^4} + \frac{1}{c^2x} - \frac{1}{4x^2}]y = 0 \tag{167}$$

Again, this equation can be transformed into a confluent hypergeometric equation. For medium and large initial entry angle, c^2 is relatively large and we can neglect the constant term, which is small, in the coefficient of y. Then, by the transformation of the independent variable

$$\zeta = \frac{2\sqrt{x}}{c} \tag{168}$$

we obtain a Bessel equation of order 1

$$\frac{d^2y}{d\zeta^2} + \frac{1}{\zeta}\frac{dy}{d\zeta} + (1 - \frac{1}{\zeta^2})y = 0 \tag{169}$$

From the definition (135), we have the solution

$$\Delta Y = \sqrt{x}\ [C_1 J_1(\frac{2\sqrt{x}}{c}) + C_2 Y_1(\frac{2\sqrt{x}}{c})] \tag{170}$$

where the general Bessel function $J_n(x)$ is given by the series (149) and $Y_1(x)$ is Neumann's Bessel function of the second kind of order 1. By considering the relation

$$Y_1 = J_1 \log x - \frac{1}{x} - \frac{1}{2} J_1 + \frac{9}{4} J_3 - \ldots \tag{171}$$

and from the condition $\Delta Y(0) = 0$, it is clear that $C_2 = 0$. From the first of the equations (133) we have the solution for $\Delta\Phi$. Using the relation

$$\zeta J_1'(\zeta) = - J_1(\zeta) + \zeta J_0(\zeta) \tag{172}$$

for the derivative of the Bessel function with respect to its argument, we have

$$\Delta\Phi = \frac{C_1}{c} J_0\ (\frac{2\sqrt{x}}{c}) \tag{173}$$

Using the initial condition (166), we have the final solution for the perturbation in the flight path angle

$$\Delta\Phi = \Delta c\ J_0\ (\frac{2\sqrt{x}}{c}) \tag{174}$$

Since Bessel function of order zero is a damped oscillation, the characteristic behavior of phugoid motion perturbed from ballistic entry is established. Furthermore, Eq.(174) gives accurate solution for $\Phi(x)$ when added to the reference solution $\Phi_0(x)$. Since the first zero of $J_0(\zeta)$ is $\zeta_1 = 2.40482\ldots$ two neighboring trajectories, in the $(-\gamma, V)$ space cross each other for the first time at the value

$$x_1 = 1.4458\ c^2 \tag{175}$$

For medium and large entry angles, this corresponds to a very low speed.

Glide Entry

For glide entry, we consider the system (66) with T = 0. By neglecting the small component of the gravity along the tangent to the flight path and using small angle approximation we have

$$\frac{R'}{R_o} = \gamma$$

$$\frac{V'}{V} = -\delta C_{D_o} \tag{176}$$

$$\gamma' = \delta C_{L_o} - \left(\frac{gR_o}{V^2} - 1\right)$$

In the last equation, the approximation $R_o/R \simeq 1$ has been made. Then, using the density function Y as defined in Eq.(115) and the new speed variable

$$\bar{v} = \frac{V^2}{gR_o} \tag{177}$$

as the independent variable, we obtain the equations for glide entry at small flight path angle

$$\frac{d\gamma}{d\bar{v}} = \frac{\sqrt{\beta R_o}\,\gamma}{\bar{v}}$$

$$\bar{v}\,\frac{d\gamma}{d\bar{v}} = -\frac{1}{2}\left(\frac{L}{D}\right) + \frac{1}{\sqrt{\beta R_o}\,\gamma}\left(\frac{1}{\bar{v}} - 1\right) \tag{178}$$

For small flight path angle, the dimensionless arc length τ, as defined in Eq.(65), is the same as the longitudinal range. From the second equation in system (176), we have

$$\frac{d\tau}{d\bar{v}} = -\frac{1}{\sqrt{\beta R_o}\,\gamma\,\bar{v}} \tag{179}$$

For the value of the lift-to-drag ratio, L/D = 1, 1.5, the equations are integrated for glide entry from circular speed, $\bar{v} = 1.0$, and an entry altitude which corresponds to $\gamma_i = 0.001$ with an initial angle $\gamma_i = -4°$. The variation in the altitude during the glide is shown in Fig. 21. The figure displays the oscillatory character of phugoid motion. For an average value of the altitude, we can use the equilibrium solution which expresses the fact that the variation in the flight path angle is small, that is $d\gamma/d\bar{v} \simeq 0$. Hence, from the second equation in system (178), we have

$$\gamma = \frac{2(1-\bar{v})}{\sqrt{\bar{\beta}R_o}\,(L/D)\,\bar{v}} \tag{180}$$

This average solution is plotted in dashed line in Fig. 21. To have an explicit solution of the deviation from this line, we use the new dependent variable

$$z = \frac{\sqrt{\bar{\beta}R_o}\,(L/D)\gamma\bar{v}}{2(1-\bar{v})} - 1 \tag{181}$$

As a result of this definition, except at the beginning of the entry trajectory where z can be large, the perturbation in z is a small quantity. By substituting into the system (178), we have the equations

$$\begin{aligned} \frac{dz}{d\bar{v}} &= \frac{\bar{\beta}R_o\,(L/D)\gamma}{2(1-\bar{v})} + \frac{(z+1)}{\bar{v}(1-\bar{v})} \\ \frac{d\gamma}{d\bar{v}} &= -\frac{(L/D)z}{2\bar{v}(z+1)} \end{aligned} \tag{182}$$

By eliminating γ between the two equations, we have a second order non-linear differential equation for z

$$\bar{v}(1-\bar{v})\frac{d^2z}{d\bar{v}^2} - (1+\bar{v})\frac{dz}{d\bar{v}} + \frac{\bar{\beta}R_o\,(L/D)^2 z}{4(\bar{z}+1)} + \frac{(z+1)}{\bar{v}} = 0 \tag{183}$$

The equilibrium solution (180) does not provide the oscillation in the altitude but gives an average value with good accuracy. Hence, the function z gives this correct oscillation and tends to zero near the end of the trajectory. By linearizing Eq.(183) we obtain

$$\bar{v}(1-\bar{v})\frac{d^2z}{d\bar{v}^2} - (1+\bar{v})\frac{dz}{d\bar{v}} + \left[\frac{\bar{\beta}R_o\,(L/D)^2}{4} + \frac{1}{\bar{v}}\right]z = -\frac{1}{\bar{v}} \tag{184}$$

Since $\bar{\beta}R_o \simeq 900$ is large, in the homogeneous equation, when $\bar{v}$ is not too small, we can neglect the term $1/\bar{v}$ and obtain a hypergeometric equation. In general, with the change of variables

$$z = \frac{U}{(\tan\mu)^{3/2}}, \qquad \bar{v} = \cos^2\mu, \qquad 0 \le \mu \le \frac{\pi}{2} \tag{185}$$

the linear equation (184) is transformed into

$$\frac{d^2U}{d\mu^2} + \left[\bar{\beta}R_o\left(\frac{L}{D}\right)^2 + \frac{1 - 4\cos^2\mu}{4\sin^2\mu\cos^2\mu}\right]U = -\frac{4\sin\mu\,(\tan\mu)^{\frac{1}{2}}}{\cos^3\mu} \tag{186}$$

In the homogeneous equation, the non-constant term in the coefficient of U is

$$\frac{1 - 4\cos^2\mu}{4\sin^2\mu\cos^2\mu} = \frac{1-4\bar{v}}{4\bar{v}(1-\bar{v})} \tag{187}$$

In the range of speed of interest, when $\bar{v}$ decreases from 0.95 to 0.01, this coefficient increases from a negative value -14.737 to a positive value 24.242. On the other hand, the term $\beta R_o(L/D)^2$ is very large. Hence, the solution of the homogeneous equation in z is practically

$$z = \frac{1}{(\tan\mu)^{3/2}} \{C_1 \cos[\sqrt{\beta R_o}\,(\tfrac{L}{D})\mu] + C_2 \sin[\sqrt{\beta R_o}\,(\tfrac{L}{D})\mu]\} \tag{188}$$

To this equation, we add a particular solution of Eq.(186). Considering the solution (188), when $\bar{v} \to 0$, $\tan\mu \to \infty$ and $z \to 0$ as expected. Furthermore, z, and hence the altitude Y by Eq.(181), has an oscillatory motion in μ with frequency $\sqrt{\beta R_o}\,(L/D)$. Actually, this should be viewed as an oscillation about the average altitude as given by the equilibrium relation (180) which has been used as the reference solution in the linearization. When μ varies from 0 to $\pi/2$, the argument of the trigonometric functions in Eq.(188) varies from 0 to $\sqrt{\beta R_o}\,\pi(L/D)/2$. Hence, the number of oscillations is approximately

$$N = \frac{\sqrt{\beta R_o}}{4}\,(\frac{L}{D}) \tag{189}$$

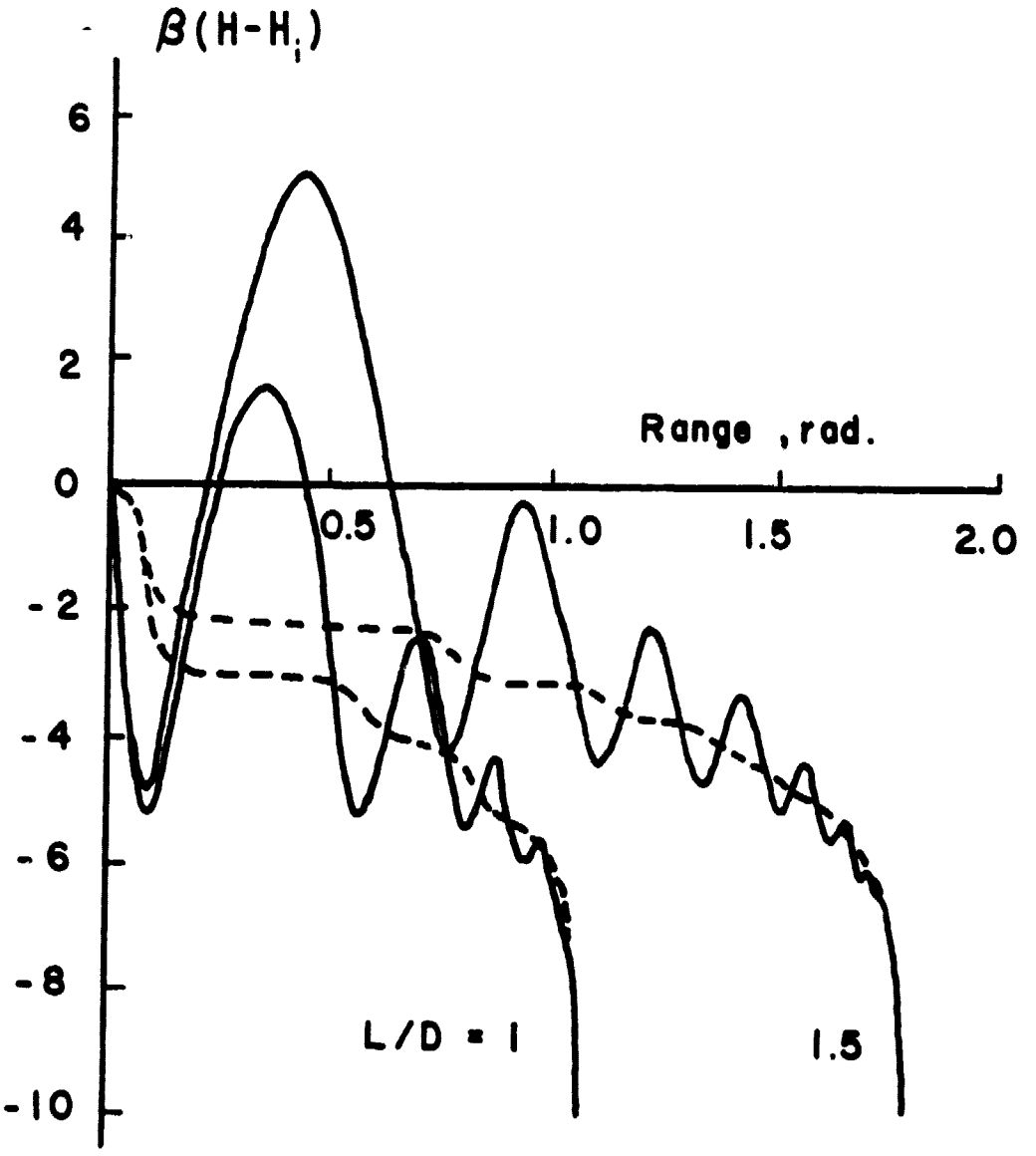

Fig. 21. Oscillations in altitude during glide entry.

V. ANGLE OF ATTACK OSCILLATIONS

For the angle-of-attack oscillation during entry, we consider the full set of equations, rewritten here for convenience

$$\frac{dR}{dt} = V\sin\gamma$$

$$\frac{dV}{dt} = \frac{T}{m} - \frac{\rho S C_D V^2}{2m} - g\sin\gamma$$

$$V\frac{d\gamma}{dt} = \frac{\rho S C_L V^2}{2m} - \left(g - \frac{V^2}{R}\right)\cos\gamma \tag{190}$$

$$\frac{dq}{dt} = \frac{\rho S\bar{c} C_m V^2}{2I_y} - \frac{3g}{2R}\left(\frac{I_x - I_z}{I_y}\right)\sin 2\theta$$

$$\frac{d\theta}{dt} = q + \frac{V}{R}\cos\gamma$$

$$\theta = \gamma + \alpha$$

The elimination of θ and q results in the following exact equation for the angle-of-attack α

$$\frac{d^2\alpha}{dt^2} + \frac{SC_L V}{2m}\frac{d\rho}{dt} + \frac{\rho SV}{2m}\frac{dC_L}{dt} - \frac{\rho S\bar{c} C_m V^2}{2I_y} + \frac{3g}{2R}\left(\frac{I_x - I_z}{I_y}\right)\sin 2(\gamma+\alpha)$$

$$+ \left(\frac{3}{R} - \frac{2g}{V^2}\right)g\sin\gamma\cos\gamma - \frac{\rho S C_D}{2m}g\cos\gamma - \left(\frac{\rho S}{2m}\right)^2 C_L C_D V^2 \tag{191}$$

$$+ \frac{T}{m}\left(\frac{\rho S C_L}{2m} + \frac{g}{V^2}\cos\gamma\right) = 0$$

In deriving this equation we have used an inverse-square gravitational attraction to preserve the correct behavior of the motion in orbital flight. If the time transformation (65) is applied, we have

$$\tau = \frac{1}{R_o}\int_0^t V(t)dt, \quad \frac{d\tau}{dt} = \frac{V(t)}{R_o}, \quad \frac{d}{d\tau}(\,) = (\,)'$$

$$\frac{d}{dt}(\,) = \frac{V}{R_o}(\,)', \quad \frac{d^2}{dt^2}(\,) = \left(\frac{V}{R_o}\right)^2(\,)'' + \left(\frac{VV'}{R_o^2}\right)(\,)' \tag{192}$$

where the prime denotes derivative with respect to τ. Then, upon using in Eq.(191) we have the non-linear equation for α

$$\alpha'' + \frac{V'}{V}\alpha' + \frac{R_e S C_L}{2m}\rho' + \frac{R_e S \rho}{2m}C_L' - \frac{\rho S \bar{c}}{2m}\left(\frac{mR_e^2}{I_y}\right)C_m$$

$$+ \frac{3gR_e^2}{2RV^2}\left(\frac{I_x - I_z}{I_y}\right)\sin 2(\gamma+\alpha) + \left(3\frac{R_e}{R} - \frac{2gR_e}{V^2}\right)\left(\frac{gR_e}{V^2}\right)\sin\gamma\cos\gamma \qquad (193)$$

$$-\left(\frac{R_e \rho S C_D}{2m}\right)\left(\frac{gR_e}{V^2}\right)\cos\gamma - \left(\frac{R_e \rho S}{2m}\right)^2 C_L C_D + \frac{R_e T}{mV^2}\left(\frac{R_e \rho S C_L}{2m} + \frac{gR_e}{V^2}\cos\gamma\right) = 0$$

By the display of this equation, it is natural to use the following dimensionless variables and parameters

$$\delta = \frac{\rho S R_e}{2m}, \quad \bar{v} = \frac{V^2}{gR_e}, \quad B = 3\left(\frac{I_x - I_z}{I_y}\right), \quad k_y = \frac{I_y}{m\bar{c}^2} \qquad (194)$$

Notice that the density δ and the kinetic energy $\bar{v}$ are the same as have been defined in the equations (67) and (177), respectively. Then, we have the equation in the final form

$$\alpha'' + \frac{\bar{v}'}{2\bar{v}}\alpha' + \delta' C_L + \delta C_L' - \delta\left(\frac{R_e}{\bar{c}}\right)\frac{C_m}{k_y} + \frac{B}{2\bar{v}}\left(\frac{R_e}{R}\right)\sin 2(\gamma+\alpha)$$

$$+ \left(3\frac{R_e}{R} - \frac{2}{\bar{v}}\right)\left(\frac{1}{\bar{v}}\right)\sin\gamma\cos\gamma - \frac{\delta C_D}{\bar{v}}\cos\gamma - \delta^2 C_L C_D \qquad (195)$$

$$+ \frac{(T/mg)}{\bar{v}}\left(\delta C_L + \frac{\cos\gamma}{\bar{v}}\right) = 0$$

It is more enlightening to linearize this equation separately for the different cases of reentry considered.

Cruising Flight

To show the correct behavior of the angle-of-attack oscillation in the asymptotic case of orbital flight, we consider the case of circular orbit in the vacuum with $T = 0$, $\delta = 0$, $\gamma = 0$, $\bar{v} = 1$. Then the non-linear equation (195) is reduced to

$$\alpha'' + \frac{|B|}{2}\sin 2\alpha = 0 \qquad (196)$$

This is the equation of a compound pendulum, and while in orbit, in its stable equilibrium position, the vehicle points its axis of minimum moment of inertia toward the center of the Earth. The equation is integrable by the use of elliptic integral. Since in this case, $\tau = V_e t/R_e$, the period of oscillation, in real time, is

$$P = \frac{2\pi R_e}{V_e\sqrt{|B|}}\left(1 + \frac{1}{4}\alpha_o^2 + \frac{11}{192}\alpha_o^4 + \ldots\right) \qquad (197)$$

where α_o is the initial, perturbed angle-of-attack. Neglecting order of α_o^2 and higher, and noticing that $V_o = \sqrt{g_o R_o}$, upon comparing with the expression for the phugoid orbital period as given in Eq.(103), we see that the ratio of the two periods is

$$\frac{P(\text{orbit})}{P(\text{pitch})} = \sqrt{|B|} \tag{198}$$

Depending on the inertia characteristic $|B|$, the period for the angle-of-attack mode can be greater than the period for the phugoid mode. Hence, the names of long and short period modes, traditionally employed in airplane longitudinal dynamic stability analysis, are no longer appropriate in reentry dynamics. For the example SSTO vehicle with physical characteristics given in Appendix B, we have $|B| = 2.3596$. Hence, the period of oscillation for the angle-of-attack is equal to 65% of the orbital period.

For cruising flight at lower altitude, aerodynamic moment is restored. Using a thrust to balance the drag and the lift to maintain constant altitude flight, we recall the equilibrium condition (64), now written as

$$\frac{T}{mg} = \delta\delta^2 C_{D_o}, \quad \delta\delta^2 C_{L_o} = 1 - \delta^2, \quad \delta^2 = \frac{V_o^2}{g_o R_o} \tag{199}$$

On the other hand, with a perturbed angle-of-attack α, we have the linearized expressions

$$\begin{aligned} C_D &= C_{D_o} + C_{D_\alpha}\alpha \\ C_L &= C_{L_o} + C_{L_\alpha}\alpha \end{aligned} \tag{200}$$

while for the pitching momemt coefficient C_m, experience has shown that we must express it as

$$C_m = C_{m_\alpha}\alpha + C_{m_{\dot\alpha}}\dot\alpha + C_{m_q}(\dot\gamma+\dot\alpha) \tag{201}$$

where q is the vehicle pitch rate referred to the local horizontal. In all the cases considered, either cruising flight, ballistic entry or equilibrium glide, the condition $\dot\gamma \simeq 0$ is enforced. On the other hand, the stability derivatives $C_{m_{\dot\alpha}}$ and C_{m_q} written in dimensionless form are based on the body length, or wing chord $\bar c$ as reference length. Hence, from the term in C_m in Eq.(195) and using the time transformation (192) for the derivative we consider

$$\left(\frac{R_o}{\bar c}\right)C_m = \left(\frac{R_o}{\bar c}\right)C_{m_\alpha}\alpha + \left(\frac{R_o}{\bar c}\right)\frac{\partial C_m}{\partial \dot\alpha}\left(\frac{V_o}{R_o}\right)\alpha' + \left(\frac{R_o}{\bar c}\right)\frac{\partial C_m}{\partial q}\left(\frac{V_o}{R_o}\right)\alpha'$$

Changing notation, we write

$$\left(\frac{R_o}{\bar c}\right)C_m = \left(\frac{R_o}{\bar c}\right)C_{m_\alpha}\alpha + C_{m_{\dot\alpha}}\alpha' + C_{m_q}\alpha' \tag{202}$$

with the definition

$$C_{m_{\dot{\alpha}}} = \frac{V_o}{\bar{c}} \frac{\partial C_m}{\partial \dot{\alpha}}, \quad C_{m_q} = \frac{V_o}{\bar{c}} \frac{\partial C_m}{\partial q} \tag{203}$$

Using the equations above in the basic non-linear equation (195), and noticing that $\bar{v} = \delta^2$, $R = R_o$, $\gamma = 0$ and linearizing α, we have the equation for the angle-of-attack oscillation in circular orbit

$$\alpha'' + 2\eta\alpha' + n^2\alpha = 0 \tag{204}$$

where

$$\eta = \frac{\delta}{2}\left[C_{L_\alpha} - \frac{(C_{m_{\dot{\alpha}}} + C_{m_q})}{k_y}\right]$$
$$n^2 = \frac{B}{\delta^2} - \frac{\delta(2-\delta^2)}{\delta^2} C_{D_\alpha} - \left(\frac{R_o}{\bar{c}}\right)\frac{\delta}{k_y} C_{m_\alpha} \tag{205}$$

The viscous damping term is always positive. Hence the condition for stability of the angle-of-attack mode is that n^2 is strictly positive. By inspection of this term, for slender type vehicle $B < 0$ such as in the case of the present SSTO vehicle. On the other hand, as has been analyzed in Chapter IV, for cruising flight the speed parameter δ is in the range $[0, 1]$, with near zero value for airplane flight mode at low altitude and close to unity near orbital flight. Hence, the negative effect of the second term is diminished with smaller drag curve slope C_{D_α}. Finally, the stabilizing effect is due to the static stability derivative C_{m_α} which must be negative for stability in cruising flight. Otherwise, thrusters control must be introduced. With a negative value for C_{m_α}, a smaller pitch moment of inertia, k_y, contributes more to stability. It is obvious that a large value of δ contributes to the positiveness of the term n^2. Physically, this means that, at low altitude a restoring aerodynamic moment overcomes the pitch down effect of the gravity gradient. The altitude, below which the vehicle is stable, is obtained by solving the equation $n^2 = 0$, that is

$$\frac{B}{\delta^2} - \frac{\delta(2-\delta^2)}{\delta^2} C_{D_\alpha} - \left(\frac{R_o}{\bar{c}}\right)\frac{\delta}{k_y} C_{m_\alpha} = 0 \tag{206}$$

This altitude s very high so that we can use the approximation $\delta = 1$, and also neglect the small term in C_{D_α} to rewrite the equation as

$$R_o^2\rho = \frac{6(I_x - I_z)}{S\bar{c}C_{m_\alpha}} \tag{207}$$

which separates vehicle and atmospheric characteristics. For the vehicle to be stable at nearly all altitudes, that is for very small value of ρ in this equation, this requires large negative value for C_{m_α} and small difference in moments of inertia about the axes in the plane of symmetry. The left-

hand-side of this equation is plotted versus the altitude in Fig. 22, while the right-hand-side is used to locate the limiting altitude for stability for any vehicle. The small circle in the figure represents the present example vehicle.

In the altitude range where the vehicle is stable, from the damping term η and with the definition of τ, we have the time to damp to half

$$t_{half} = \frac{4m \log 2}{\rho_o S V_o \left[C_{L_\alpha} - \frac{(C_{m_\dot{\alpha}} + C_{m_q})}{k_y}\right]} \tag{208}$$

It is seen that small wing loading, low altitude, high lift curve slope, strong damping in pitch and small pitch moment of inertia, all contribute to shorten this time constant.

At high altitude where η is small, the frequency for the angle-of-attack oscillation is practically n. Hence, we have for the period in real time

$$P = \frac{2\pi R_o}{V_o n} \tag{209}$$

With the approximation $\delta^2 = V_o^2/g_o R_o \simeq 1$, we have the expression

$$P = \frac{2\pi V_o}{g_o\left[B - \delta C_{D_\alpha} - \left(\frac{R_o}{\bar{c}}\right)\frac{\delta}{k_y} C_{m_\alpha}\right]^{\frac{1}{2}}} \tag{210}$$

As a consequence, near the altitude where the vehicle becomes unstable, $n \simeq 0$ and the period for the pitching mode is infinitely large. Since the period of oscillation for the phugoid mode is finite, with the limit being the orbital period, and the period oscillation for the angle-of-attack mode is short at low altitude, there exists an altitude where the two periods are equal. Cruising at this altitude, the vehicle is subject to unstable resonance effect. The resonance altitude was detected by Etkin (ref. 16) and the resonance effect was discussed by Vinh and Dobrzelecki (ref. 17). It has been shown in Chapter IV that the phugoid frequency in cruising flight is ω as given by Eq.(79). Hence, the resonance altitude is obtained by setting $n = \omega$. This altitude is high so that we can use the approximation $\delta = 1$. This amounts to simply using $\omega = 1$. Neglecting the term C_{D_α} in the expression for n, and separating vehicle and atmospheric characteristics as has been done in the case of limiting stable altitude, we obtain the equation

$$R_o^2 \rho = \frac{2[3(I_x - I_z) - I_y]}{S\bar{c}\, C_{m_\alpha}} \tag{211}$$

Plotting the right-hand-side of this equation in Fig. 22, we have the resonance altitude. It is obvious that this altitude is below the limiting altitude for stability. If a strictly exponential atmosphere with height

scale $1/\bar{\beta}$ is considered, by taking the ratio of the two equations (207) and (211), we have the difference between the resonance altitude and the limiting altitude for stability

$$\bar{\beta}\Delta H = \log\left(\frac{B-1}{B}\right) \tag{212}$$

This is quite an interesting formula since the altitude difference is purely a function of the inertia property B. For the example SSTO vehicle, we have $\bar{\beta}\Delta H = 0.3533$. Using Chapman's approximation for the atmosphere, $\bar{\beta}R_o = 900$, we can write the equation as

$$\Delta H = \frac{R_o}{900}\log\left(\frac{B-1}{B}\right) \tag{213}$$

With an average value $R_o = 6467$ km at the flight altitude, for the vehicle considered, we obtain $\Delta H = 2.539$ km.

A final note to close this section is in order. For the phugoid mode, as has been discussed in detail in Chapter IV, the period, customarily called the long period, increases from small values, of the order of a few minutes, for airplane-type cruise at low altitude and tends asymptotically to the orbital period when the atmospheric density tends to zero at very high altitude. On the other hand, for the angle-of-attack mode, the period, mistakenly called the short period, also increases from very small values, of the order of a second, to infinity at the unstable altitude where the gravity torque and the aerodynamic moment are equal. This altitude is above the resonance altitude, where the two periods for phugoid and angle-of-attack modes are equal, by an altitude difference as given by Eq.(213). The motion is unstable above the limiting altitude but after a pitch down to point the x-axis along the vertical, the gravity gradient torque becomes predominant and the pitch motion is again stable with the asymptotic period being finite as given by Eq.(197). The motion during this whole range of transition altitude is non-linear and a separate study should be undertaken to analyze all the inherent phenomena. This would include the frequency resonance and the eccentricity effect of the orbit. One simplifying aspect which significantly alleviates the difficulty in the analysis is that, at high altitude, the motion is nearly Keplerian. Hence, this leads to the pitch motion subject to gravity gradient and aerodynamic moments along an elliptic orbit.

It should also be noticed that, if the orbit is strictly circular, then from the linear equation (204), resonance effect is not detected. But, if the orbit is perturbed, it becomes slightly elliptic. In this case, by going back to Eq.(195) and expressing δ, $\bar{v}$, γ and R_o/R as periodic functions in τ, with period 2π, in the linearized form, we obtain a Mathieu's equation with a periodic forcing function having a period exactly equal to the pitch period. This will create resonance phenomenon which would ultimately build up larger amplitude for the perturbed angle-of-attack if the motion is uncontrolled.

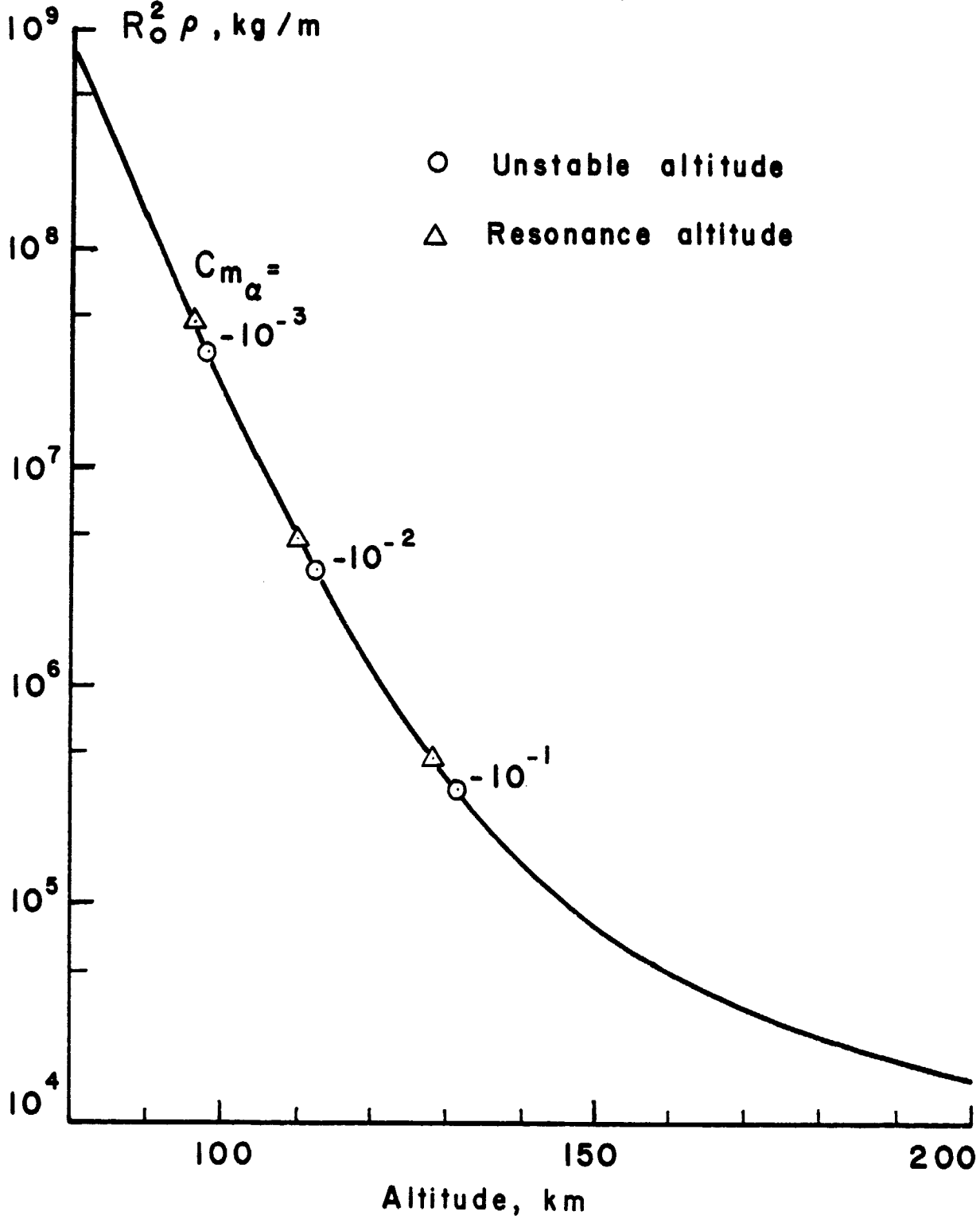

Fig. 22. Limiting unstable altitude and resonance altitude in cruising flight.

Ballistic Entry

Unlike the case of cruising flight, in which the speed either remains constant or has a periodic variation with small amplitude, for ballistic or glide entry, effective entry is being made and as a consequence the speed decreases along the trajectory. In addition, the atmospheric density increases. This creates unsteady effects and, in the linearized form, the equation for the angle-of-attack oscillation is a linear second order differential equation with varying coefficients.

We shall simplify the basic equation (195) to a form valid for both cases of ballistic and glide entry. First, we observe that the gravity gradient term in B and the following term in $\sin\gamma\cos\gamma$ are of the same order of magnitude. On the other hand, during effective entry, gravity gradient is small as compared to aerodynamic moment. Hence, with $T = 0$ and neglecting the two small terms mentioned, we are led to the equation

$$\alpha'' + \frac{\bar{v}'}{2\bar{v}}\alpha' + \delta' C_L + \delta C_L' - \delta\left(\frac{R_o}{\bar{c}}\right)\frac{C_m}{k_y} - \frac{\delta C_D}{\bar{v}}\cos\gamma - \delta^2 C_L C_D = 0 \qquad (214)$$

Of the last three terms in this equation, because of the large factor $R_o/\bar{c}$, the moment term is larger than the drag term. Therefore, we have the resulting equation

$$\alpha'' + \frac{\bar{v}'}{2\bar{v}}\alpha' + \delta' C_L + \delta C_L' - \delta\left[\left(\frac{R_o}{\bar{c}}\right)\frac{C_m}{k_y} + \delta C_L C_D\right] = 0 \qquad (215)$$

Using the linearized expressions (200) and (202) for C_D, C_L and C_m we have the linear equation governing the variation of the angle-of-attack

$$\alpha'' + b(\tau)\alpha' + c(\tau)\alpha = -\delta' C_{L_o} + \delta^2 C_{L_o} C_{D_o} \qquad (216)$$

where

$$b(\tau) = \delta\left[C_{L_\alpha} - \frac{(C_{m_{\dot{\alpha}}} + C_{m_q})}{k_y}\right] + \frac{\bar{v}'}{2\bar{v}}$$

$$c(\tau) = \delta' C_{L_\alpha} - \frac{\delta}{k_y}\left(\frac{R_o}{\bar{c}}\right) C_{m_\alpha} - \delta^2(C_{L_o} C_{D_\alpha} + C_{D_o} C_{L_\alpha}) \qquad (217)$$

are two coefficients to be evaluated as functions of the independent variable τ depending on the type of reentry trajectory.

For the present case of ballistic entry, $C_{L_o} = 0$. On the other hand, from Eq.(114)

$$\frac{V'}{V} = \frac{\bar{v}'}{2\bar{v}} = -\delta C_{D_o} \qquad (218)$$

Furthermore, from Eq.(117)

$$\frac{\gamma'}{\gamma} = \frac{\delta'}{\delta} = -\bar{\beta}R_o \sin\gamma \tag{219}$$

where $\bar{\beta}R_o = -\sigma = 900$ for the Earth's atmosphere. Hence, from Eq.(217) we have

$$b(\tau) = \delta\left[C_{L_\alpha} - C_{D_o} - \frac{(C_{m_\alpha} + C_{m_q})}{k_y}\right]$$

$$c(\tau) = \delta\left[C_{L_\alpha}\sigma \sin\gamma - \left(\frac{R_o}{\bar{c}}\right)\frac{C_{m_\alpha}}{k_y} - \delta C_{D_o} C_{L_\alpha}\right] \tag{220}$$

For ballistic entry at medium and large flight path angle, during the main portion of the reentry trajectory where the effect of deceleration is important, it has been shown in Chapter IV that the flight path angle remains nearly constant, that is $\sin\gamma = \sin\gamma_o$. Hence $b(\tau)$ and $c(\tau)$ are purely function of the dimensionless atmospheric density δ. This naturally leads to the change of independent variable from τ to δ through Eq.(219). Upon using this transformation we have the linear differential equation of the second order governing the angle-of-attack

$$\frac{d^2\alpha}{d\delta^2} + b_1(\delta)\frac{d\alpha}{d\delta} + c_1(\delta)\alpha = 0 \tag{221}$$

where

$$b_1 = \frac{1}{\delta} + k_1$$

$$c_1 = \frac{k_2}{\delta} + k_3 \tag{222}$$

with

$$k_1 = \frac{1}{\sigma \sin\gamma_o}\left[C_{L_\alpha} - C_{D_o} - \frac{(C_{m_\alpha} + C_{m_q})}{k_y}\right] > 0$$

$$k_2 = \frac{1}{(\sigma \sin\gamma_o)^2}\left[C_{L_\alpha}\sigma \sin\gamma_o - \left(\frac{R_o}{\bar{c}}\right)\frac{C_{m_\alpha}}{k_y}\right] > 0 \tag{223}$$

$$k_3 = -\frac{C_{D_o} C_{L_\alpha}}{(\sigma \sin\gamma_o)^2} < 0$$

Concerning the signs of the constant coefficients k_1, it is trivial that k_3 is negative. Since for entry $\sigma \sin\gamma_o = -900 \sin\gamma_o$ is positive, the coefficient k_1 is usually positive unless the damping in pitch C_{m_q}, which is always negative, is negligibly small and the lift curve slope C_{L_α} is also small. For the coefficient k_2, a negative C_{m_α} assures its positiveness but an unstable, positive C_{m_α} can make this coefficient negative.

Since the linear differential equation (221) has varying coefficients, the positiveness of $b_1(\delta)$ and $c_1(\delta)$ is not sufficient for the stability of the motion. To derive criteria for stability the recommended procedure is to transform the equation into a well known equation in mathematical physics. In this respect, Allen has considered a type of reentry missile such that upon some simplification the equation is reduced to a Bessel's equation of order zero (ref. 18). On the other hand, Vinh and Laitone have transformed the equation into a more general form of a confluent hypergeometric equation (ref. 19). In both these references the independent variable used is the altitude variable which necessitates the introduction of exponential function into the equation as an adequate representation for the atmospheric density. This inconvenience has been removed in the present formulation. Furthermore, we shall now use a general transformation of both independent and dependent variables to globally discuss the stability of the angle-of-attack mode during ballistic entry for different aerodynamic characteristics. For this purpose, we consider the transformation

$$\alpha = e^{k\delta} y(\eta)$$
$$\delta = h\eta \tag{224}$$

where k and h are two constants to be selected such that the resulting equation has the desired form. Upon substituting into Eq.(221), we obtain

$$\frac{d^2y}{d\eta^2} + \left[h(2k+k_1) + \frac{1}{\eta}\right]\frac{dy}{d\eta} + \left[h^2(k^2+kk_1+k_3) + \frac{h(k+k_2)}{\eta}\right]y = 0 \tag{225}$$

By selecting

$$k = -\frac{k_1}{2} \tag{226}$$

we have the equation

$$\frac{d^2y}{d\eta^2} + \frac{1}{\eta}\frac{dy}{d\eta} + \left[h^2\left(k_3 - \frac{k_1^2}{4}\right) + \left(k_2 - \frac{k_1}{2}\right)\frac{h}{\eta}\right]y = 0 \tag{227}$$

If $-C_{m_\alpha}$ is not too small, the coefficient k_2 is much larger than k_1 and $-k_3$. In this case, by neglecting the constant term in the coefficient of y in Eq.(227), and using the transformation

$$\eta = \mu^2 \tag{228}$$

we are led to the equation

$$\frac{d^2y}{d\mu^2} + \frac{1}{\mu}\frac{dy}{d\mu} + 2h(2k_2 - k_1)y = 0 \tag{229}$$

By taking h such that

$$2h(2k_2 - k_1) = 1 \tag{230}$$

we have a Bessel's equation of order zero. Hence, for the type of ballistic entry bodies such that $k_2 >> k_1, -k_3$, the approximate solution for the oscillation of the angle-of-attack is

$$\alpha(\delta) = e^{-k_1\delta/2}[C_1 J_o(2\sqrt{[k_2 - (k_1/2)]\delta}) + C_2 Y_o(2\sqrt{[k_2 - (k_1/2)]\delta})] \tag{231}$$

where k_1 and k_2 are given in Eq.(223) and J_o and Y_o are the zero order Bessel's functions of the first and second kind, respectively.
Since the Bessel's functions of order zero are oscillatory functions with decreasing amplitude and the density δ increases during ballistic entry, the condition for stability is $k_1 > 0$, that is

$$C_{L_\alpha} - C_{D_o} - \frac{(C_{m_\alpha} + C_{m_q})}{k_y} > 0 \tag{232}$$

Going back to the more general equation (225), we now select the constants k and h such that

$$h(2k + k_1) = -1$$
$$k^2 + k_1 k + k_3 = 0 \tag{233}$$

The second equation in k has one positive and one negative root. We choose the negative root yielding

$$k = -\frac{k_1}{2}[1 + \sqrt{1 - 4(k_3/k_1^2)}]$$
$$\frac{1}{h} = k_1\sqrt{1 - 4(k_3/k_1^2)} \tag{234}$$

The resulting linear equation for the angle-of-attack is a confluent hypergeometric equation

$$\eta\frac{d^2y}{d\eta^2} + (b-\eta)\frac{dy}{d\eta} - ay = 0 \tag{235}$$

where b = 1 and

$$a = \frac{1}{2} - \frac{2k_2 - k_1}{2\sqrt{k_1^2 - 4k_3}} \tag{236}$$

is a constant parameter, usually negative and large. The solution of (235) that will lead to a physically valid angle-of-attack variation as defined in Eq.(224) is given by the Kummer's function

$$y(\eta) = {}_1F_1(a, b, \eta) = 1 + \frac{a\eta}{b} + \frac{a(a+1)\eta^2}{b(b+1)2!} + \ldots \tag{237}$$

which in this case where $b = 1$, is

$$y(\eta) = 1 + a\eta + \frac{a(a+1)}{(2!)^2}\eta^2 + \frac{a(a+1)(a+2)}{(3!)^2}\eta^3 + \ldots \tag{238}$$

Figure 23 shows the variation of the function $y(\eta)$ for several values of the constant a. The function becomes more oscillatory for large negative value of a. From Eq.(236), and neglecting the small term k_3, we have

$$a = 1 - (k_2/k_1) \tag{239}$$

Hence, in general the ratio k_2/k_1 influences the oscillatory character of the angle-of-attack, while from Eq.(234) with $k \simeq -k_1$ and, from the definition (224), the damping is provided by the positiveness of the constant k_1. We are led to the same condition (232) for stability. If we consider Eq.(238) as defining a family of curves depending on a parameter a, the best way to detect the oscillatory character of the function is to select integer values for $-a = n$, with $n = 0, 1, 2, \ldots$ Then we have

$$\begin{aligned} y_o &= 1 \\ y_1 &= 1 - \eta \\ y_2 &= 1 - 2\eta + \frac{1}{2}\eta^2 \\ &\ldots \end{aligned} \tag{240}$$

or in general

$$y_n(\eta) = \sum_{m=0}^{n} (-1)^m \left\{ \begin{matrix} n \\ m \end{matrix} \right\} \frac{\eta^m}{m!} \tag{241}$$

where

$$\left\{ \begin{matrix} n \\ m \end{matrix} \right\} = \frac{n(n-1)(n-2)\ldots(n-m+1)}{m!} \tag{242}$$

is the binomial coefficient. The solution is a Laguerre polynomial, and as such, a higher order polynomial provides more zeros to the function. On the other hand, using $h \simeq 1/k_1$, we have $\eta = k_1\delta$. The largest value of δ corresponds to sea level. Since the range of η is large for large value of k_1, the number of oscillations also increases with k_1.

In summary for a general type of entry body the solution for the variation in the angle-of-attack is given by

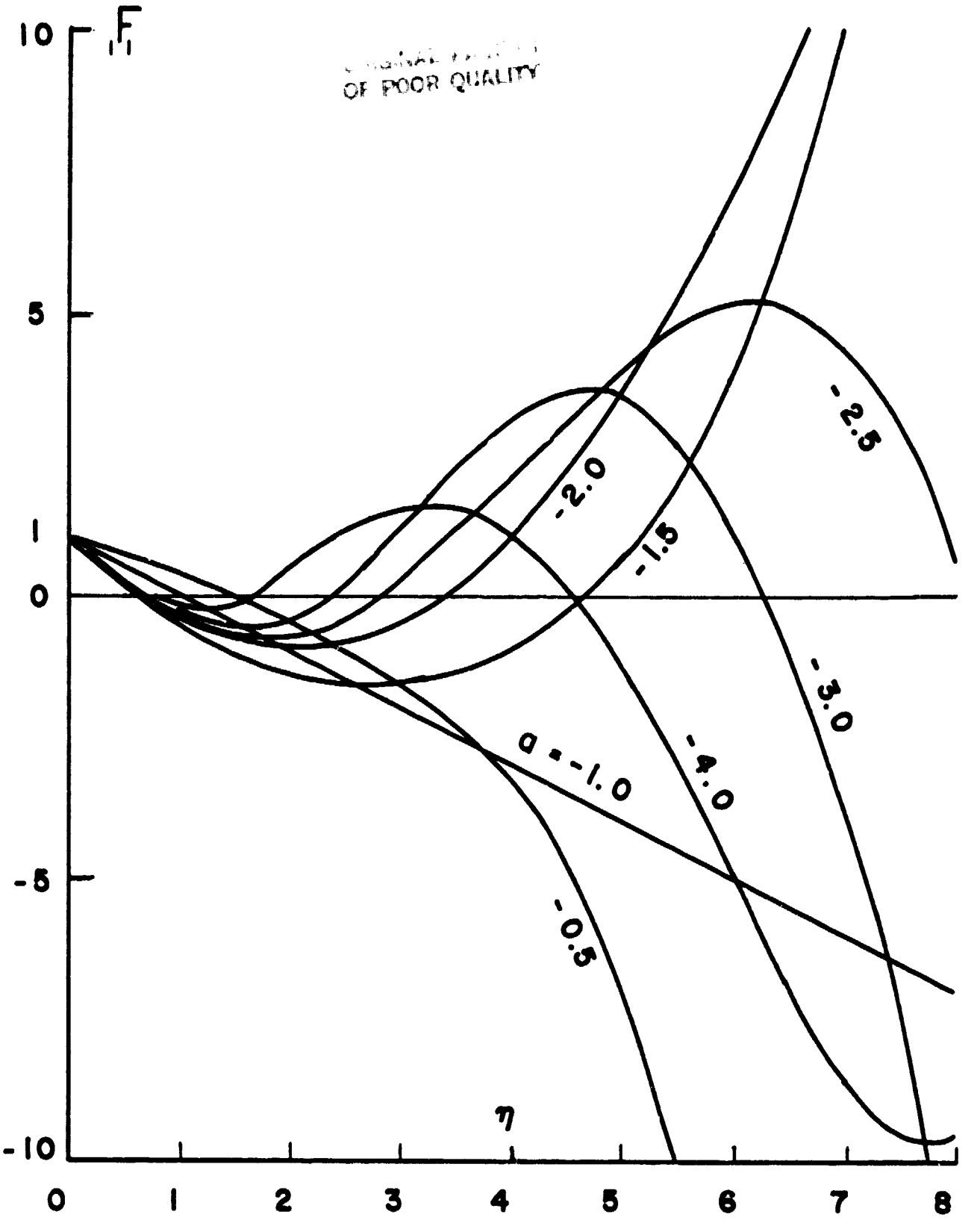

Fig. 23. Kummer's function $_1F_1(a, 1, \eta)$ for various values of a.

$$\alpha = \alpha_o e^{-k_1\delta}\, {}_1F_1[1-(k_2/k_1),\ 1,\ k_1\delta] \tag{243}$$

where k_1 and k_2 are given by Eq.(223) and the small effect of k_3 has been omitted. The fact that this solution tends to the Bessel's solution as given by Eq.(231) in the case where $k_2 >> k_1$ can be seen by using the asymptotic form for Kummer's function for large a

$$ {}_1F_1(a,\ b,\ \eta) \sim e^{\eta/2}\ (\tfrac{1}{2}b\eta - a\eta)^{(1-b)/2}\ J_{b-1}(\sqrt{2b\eta - 4a\eta}) \tag{244}$$

In the present case, $b = 1$, $\eta = k_1\delta$, $a = 1-(k_2/k_1)$. Upon using this asymptotic approximation in Eq.(243), we have the solution (231).

To verify numerically the analysis above, we integrate the linear equation (221) using the following data.

$$C_{D_o} = 0.982\ , \qquad C_{L_\alpha} = 1.06\ , \qquad C_{m_{\dot\alpha}} = 0$$

$$C_{m_\alpha} = -0.002\ , \qquad C_{m_q} = -0.68 \tag{245}$$

$$\gamma_o = -20^\circ\ , \qquad k_y = 1.129\ , \qquad R_o/\bar{c} = 3.6498 \times 10^5$$

This provides the basic numerical values

$$k_1 = 0.0022\ , \qquad k_2 = 0.010267\ , \qquad k_3 = -1.099 \times 10^{-5} \tag{246}$$

The initial conditions are $\alpha_o = 3^\circ$, $\alpha'_o = 0$, at an initial altitude such that $\delta_o C_{D_o} = 0.015$. This value is the initial deceleration in g's, due to the drag force at circular entry speed. This basic solution is plotted in dashed line in Fig. 24. Several other solutions have been generated for different values of k_2. While the damping per cycle remains essentially the same, the fact of increasing k_2, that is the effect of the static derivative C_{m_α}, produces more oscillations during the descent. This, in turn, shortens the period and leads to a stronger convergence in the angle-of-attack. For very large value of k_2 the limiting curve tends to the Bessel's solution as first derived by Allen (ref. 18).

From the definition (223) of k_2, because of the large ratio $R_o/\bar{c}$, this coefficient is very sensitive to change in the static derivative C_{m_α}, that is to the location of the center-of-gravity. We have seen that k_2 mainly governs the oscillatory character while the damping is provided by the positiveness of the coefficient k_1 as expressed in condition (232). This in turn, depends on the damping in pitch C_{m_q} which, in this case of the SSTO vehicle, in the absence of a horizontal stabilizer, must come entirely from the wing.

To show that we still have convergence in the angle-of-attack while relaxing the condition on C_{m_α}, we consider two special cases with a positive value for C_{m_α}. First, we consider the case where $k_2 = k_1$. This corresponds to the value $C_{m_\alpha} = 3.64 \times 10^{-4}$. Neglecting k_3, we have $a = 0$ in Eq.(235). With $b = 1$, the exact solution of this equation is

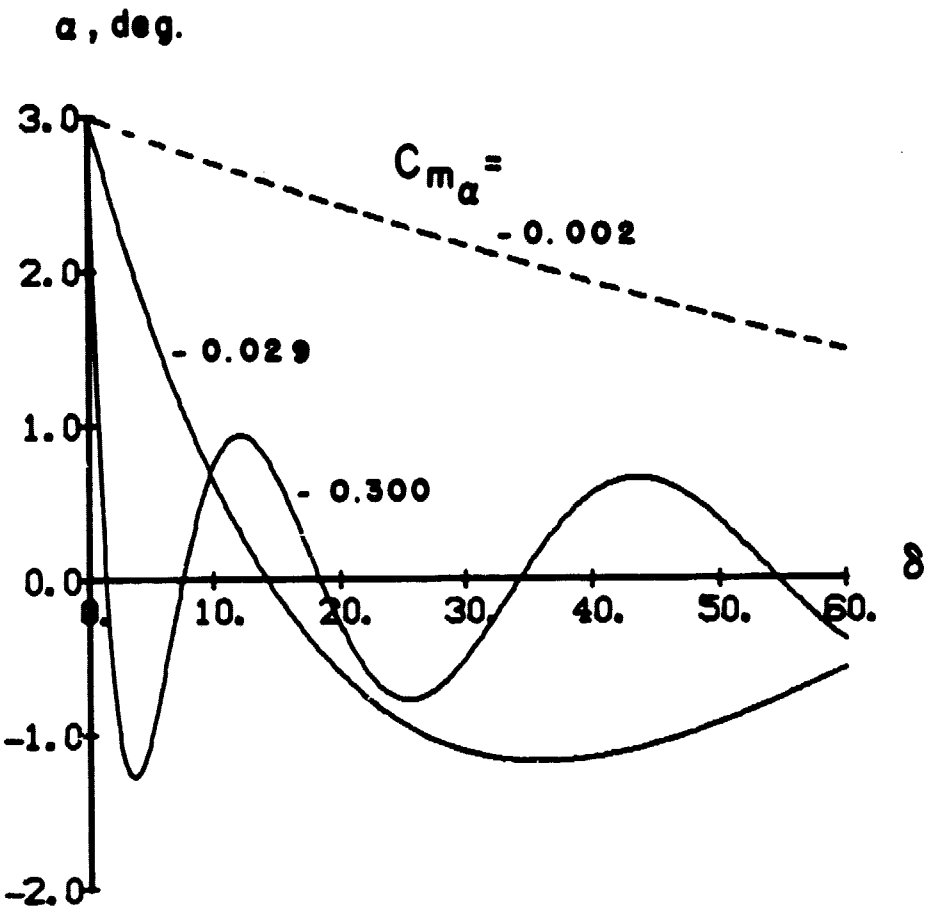

Fig. 24. Angle-of-attack oscillation during ballistic entry for various values of $k_2(C_{m_\alpha})$.

$$y(\eta) = C_1 Ei(\eta) + C_2 \tag{247}$$

where $Ei(\eta)$ is the exponential integral

$$Ei(x) = \gamma + \log x + \sum_{n=1}^{\infty} \frac{x^n}{nn!} \tag{248}$$

with $\gamma = 0.57721...$ being the Euler's constant. From Eq.(224), with $k = -k_1$, $\eta = k_1\delta$, the solution for the angle-of-attack is

$$\alpha = e^{-k_1\delta} [C_1 Ei(k_1\delta) + C_2] \tag{249}$$

This, of course, is a damped solution for $k_1 > 0$.

The second case corresponds to $k_2 = 0$, which occurs for $C_{m_\alpha} = 7.92 \times 10^{-4}$. In this case $a = 1$ in Eq.(235) and we have the exact solution

$$y(\eta) = e^{\eta} [C_1 E_1(\eta) + C_2] \tag{250}$$

where the exponential integral is now

$$E_1(x) = -\gamma - \log x - \sum_{n=1}^{\infty} \frac{(-1)^n x^n}{nn!} \tag{251}$$

The solution for the angle-of-attack is

$$\alpha = C_1 E_1(k_1\delta) + C_2 \tag{252}$$

Since the function $E_1(x)$ is decreasing, the pitch mode is convergent but non oscillatory.

Glide Entry

The coefficients b and c and the forcing function in the basic linear differential equation (216) are now evaluated for the case of glide entry.

As shown in Chapter IV, for equilibrium glide, we use the approximation $\gamma \simeq 0$ and

$$\frac{V'}{V} = \frac{\bar{v}'}{2\bar{v}} = -\delta C_{D_o} \quad , \qquad \delta C_{L_o} = \frac{(1-\bar{v})}{\bar{v}} \tag{253}$$

Hence, we deduce

$$\delta' C_{L_o} = -\frac{\bar{v}'}{\bar{v}^2} = \frac{2\delta}{\bar{v}} C_{D_o} \tag{254}$$

It appears that if the speed is not too small, δ' is of the order of δ and from Eq.(217), for the coefficient $c(\tau)$ we can simply retain the moment term

because of the large ratio $R_o/\bar{c}$. This assumption is consistent with the assumption of equilibrium glide since from the general equation (219) for the variation of the altitude, when the speed is high, the flight path angle is negligibly small and δ' is small. Then, we write Eq.(216)

$$\alpha'' + k_4\delta\alpha' + k_5\delta\alpha = -\delta' C_{L_o} + \delta^2 C_{L_o} C_{D_o} \tag{255}$$

where

$$k_4 = [C_{L_\alpha} - C_{D_o} - \frac{(C_{m_\alpha} + C_{m_q})}{k_y}]$$

$$k_5 = -(\frac{R_o}{\bar{c}}) \frac{C_{m_\alpha}}{k_y} \tag{256}$$

When C_{m_α} is not negligibly small, the coefficient k_5 is large while the damping term k_4 remains small. By Eqs.(253) and (254) it is possible to change the independent variable to δ as has been done for the case of ballistic entry. But, in order to have a comparative analysis with the phugoid mode for glide entry obtained in Chapter IV, we shall use the kinetic energy $\bar{v}$ as the new independent variable. The transformation is done through the first of the equations (253) written as

$$\bar{v}' = -\frac{2(1-\bar{v})}{E} \tag{257}$$

where

$$E = C_{L_o}/C_{D_o} \tag{258}$$

is the lift-to-drag ratio used for the glide. Upon performing this change of independent variable in Eq.(255) and expressing δ and δ' in terms of $\bar{v}$, we obtain the linear differential equation of the second order governing the perturbation of the angle-of-attack during equilibrium glide

$$\bar{v}(1-\bar{v}) \frac{d^2\alpha}{d\bar{v}^2} - [\bar{v} + \frac{k_4}{2C_{D_o}} (1-\bar{v})] \frac{d\alpha}{d\bar{v}} + \frac{Ek_5}{4C_{D_o}} \alpha = -\frac{E(1+\bar{v})}{4\bar{v}} \tag{259}$$

By the change of variable

$$\zeta = 1 - \bar{v} \tag{260}$$

with ζ increasing from zero for a starting glide at circular speed, we have the equation

$$\zeta(1-\zeta) \frac{d^2\alpha}{d\zeta^2} + [1 - (1 - \frac{k_4}{2C_{D_o}}) \zeta] \frac{d\alpha}{d\zeta} + \frac{Ek_5}{4C_{D_o}} \alpha = -\frac{E(2-\zeta)}{4(1-\zeta)} \tag{261}$$

Identifying the homogeneous equation with the hypergeometric differential equation

$$\zeta(1-\zeta)\frac{d^2\alpha}{d\zeta^2} + [c - (a+b+1)\zeta]\frac{d\alpha}{d\zeta} - ab\alpha = 0 \qquad (262)$$

we see that

$$a + b = -\frac{k_4}{2C_{D_o}}$$

$$ab = -\frac{Ek_5}{4C_{D_o}} \qquad (263)$$

$$c = 1$$

A physically valid solution of the equation is given by Gauss series with $c = 1$

$$F(a, b; 1; \zeta) = 1 + \frac{a \cdot b}{(1!)^2}\zeta + \frac{a(a+1)b(b+1)}{(2!)^2}\zeta^2 + \ldots \qquad (264)$$

In general, both k_4 and k_5 are positive with $k_5 >> k_4$. Then a and b are nearly equal with opposite sign. Hence, with the approximation $-b \simeq a > 0$, we have the solution for very large value of a

$$F(a, -a; 1; \zeta) = 1 - \frac{a^2}{(1!)^2}\zeta + \frac{a^4}{(2!)^2}\zeta^2 + \ldots \qquad (265)$$

$$= J_o(2a\sqrt{\zeta})$$

We recall that ζ varies in the range [0, 1]. The Bessel's solution is a damped solution and the number of oscillations increases proportionally with $a \simeq \sqrt{Ek_5/4C_{D_o}}$. Hence, as in the case of the phugoid mode, higher lift-to-drag ratio provides more oscillations. Here, the main influence comes from a strong positive value of k_5 requiring a stable negative value for C_{m_α}. For the case of glide entry, if the static stability derivative is relaxed thrusters reaction control must be supplemented to provide adequate stability.

To display explicitly the damping and the oscillatory characteristics, we can perform a transformation of variables in Eq.(259), in a similar way as has been done in Eq.(184) for the phugoid mode. With the change of variable

$$\alpha = \frac{y}{\sqrt{\tan\mu/(\cos\mu)^{k_4/C_{D_o}}}} \quad , \quad \bar{v} = \cos^2\mu \quad , \quad 0 \leq \mu \leq \frac{\pi}{2} \qquad (266)$$

the linear equation (259) is transformed into

$$\frac{d^2y}{d\mu^2} + \left\{ \frac{Ek_5}{C_{D_o}} - \frac{1}{4\sin^2\mu\cos^2\mu}\left[\left(2 + \frac{k_4}{C_{D_o}}\sin^2\mu\right)^2 - (1 + 4\cos^2\mu)\right]\right\} y =$$

$$- \frac{E(1 + \cos^2\mu)(\tan\mu)^{\frac{1}{2}}}{\cos^2\mu(\cos\mu)^{k_4/2C_{D_o}}} \tag{267}$$

If C_{m_α} is not negligibly small, k_5 is large. Then during the hypersonic portion of the glide where the speed is not small we can neglect the non-constant term in the coefficient of y and obtain the solution to the homogeneous equation in the form

$$\alpha = \frac{1}{\sqrt{\tan\mu/(\cos\mu)^{k_4/C_{D_o}}}}\left[C_1 \cos\left(\sqrt{\frac{Ek_5}{C_{D_o}}}\,\mu\right) + C_2 \sin\left(\sqrt{\frac{Ek_5}{C_{D_o}}}\,\mu\right)\right] \tag{268}$$

To this equation, we add a particular solution of Eq.(261) to have the general solution. For small ζ we can consider the forcing function of this equation as a constant. Then it appears that the particular solution is also a constant and is very small for large k_5. Hence, for all practical purposes, the angle-of-attack oscillation during equilibrium glide entry is given by Eq.(268). The pitch mode is oscillatory and when $\bar{v}$ varies from 1 to 0, μ varies from 0 to $\pi/2$ and the number of oscillations is approximately

$$N = \frac{1}{4}\sqrt{\frac{Ek_5}{C_{D_o}}} \tag{269}$$

As for the damping, if $k_4 > 0$ the denominator of Eq.(268) increases during the descent and the amplitude of oscillation of the angle-of-attack decreases. When $k_4 < 0$, this function increases if the only if

$$1 + \frac{k_4}{C_{D_o}}\sin^2\mu > 0 \tag{270}$$

Then, depending on the negative value of k_4, when μ is large, that is at low speed, the condition may not be verified and α can increase after an initial convergence.

To verify numerically the analysis above, we choose a low angle-of-attack for glide with the following aerodynamic data

$$C_{D_o} = 0.301 \quad , \quad C_{L_o} = 0.452 \quad , \quad C_{m_\alpha} = 0$$

$$C_{D_\alpha} = 0.186 \quad , \quad C_{L_\alpha} = 0.397 \tag{271}$$

$$C_{m_\alpha} = -0.012 \quad , \quad C_{m_q} = -1.72$$

This provides the basic numerical values

$$k_4 = 1.6195 \quad , \qquad k_5 = 3.879 \times 10^3 \quad , \qquad \frac{1}{4}\sqrt{\frac{Ek_5}{C_{D_o}}} = 34.779 \qquad (272)$$

The last number is the estimated number of oscillations if the glide is effected until sea level. Equation (261) is selected for the integration with the initial value $\alpha_o = 3°$, $\alpha_o' = 0$ at $\zeta = 0.005$ which corresponds to a slightly subcircular speed. The solution is plotted in Fig. 25 in dashed line. We notice the strong oscillatory character and damping of this pitch mode. They come mostly from the effect of C_{m_α} in the coefficient k_5. As seen from condition (270), we still can have convergence of the solution with small and even negative value of k_4. This means that if the location of the center-of-gravity is not far aft we can relax the effect of the damping in pitch C_{m_q} in the hypersonic glide mode. To test this assessment we have generated a numerical solution, plotted in solid line in Fig. 25, with $k_4 = 0$. According to the analytical solution (268) when ζ has increased from 0.005 to 0.4, which corresponds to a decrease of the speed $(\overline{v})^{\frac{1}{2}} = V_o/\sqrt{gR_o}$ from 0.9975 to 0.7746 the amplitude of oscillation is reduced to 0.2947 of the initial amplitude. This is in complete agreement with the numerical solution.

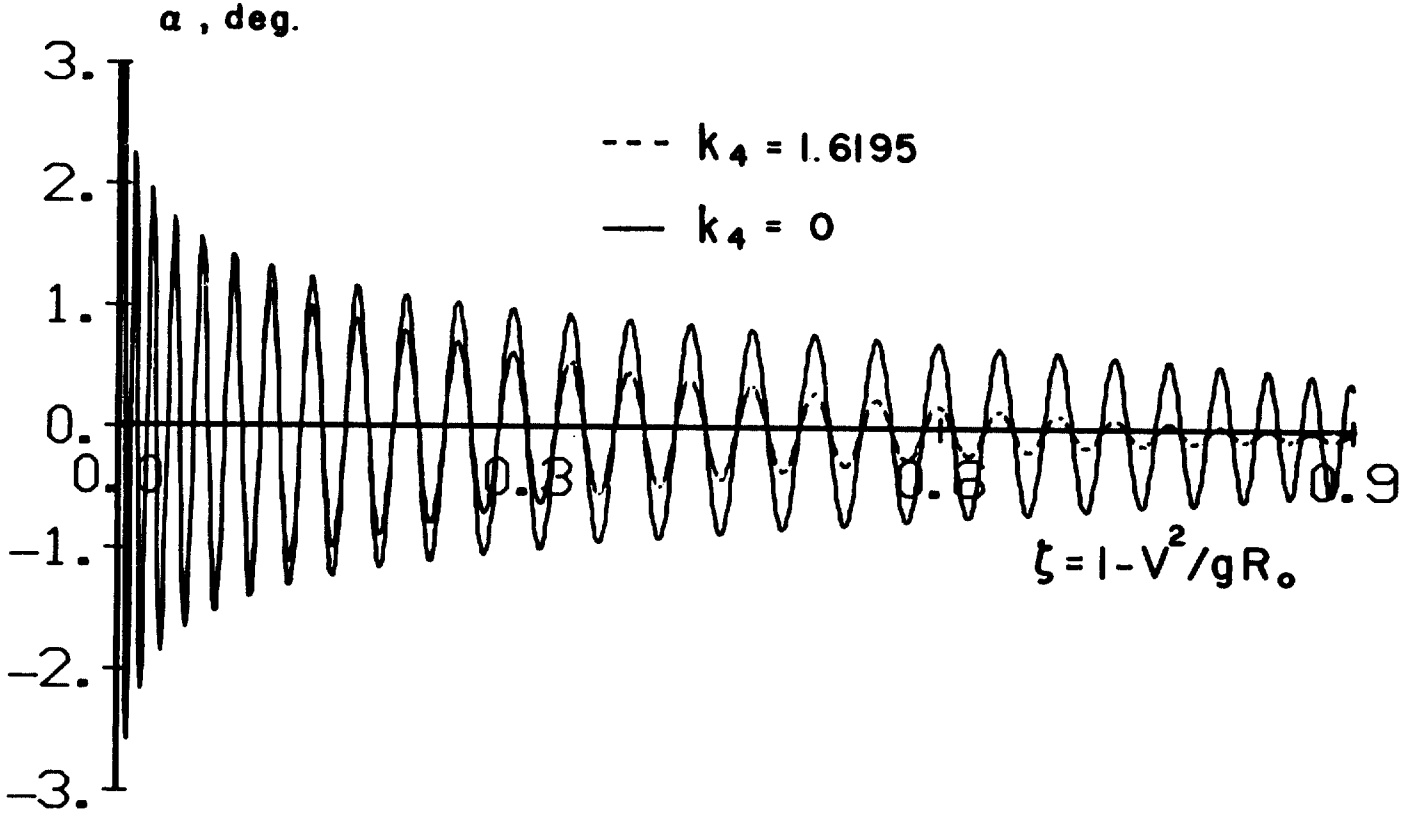

Fig. 25. Angle-of-attack oscillation during equilibrium glide.

APPENDIX A

CHARACTERISTICS OF THE ATMOSPHERE

In analytic formulation, there are two basic equations governing the density of the atmosphere as a function of the altitude. The first is the familiar equation of state for the atmosphere relating its pressure p, density ρ and temperature T

$$p = \rho R^* T \tag{A.1}$$

where R^* is the gas constant ($R^* = 287.053$ MKS for air). The second basic equation expresses that the rate of change of pressure must equal the increased weight of the atmosphere supported, as the altitude changes

$$dp = -\rho g \, dH \tag{A.2}$$

From the equation of state

$$\frac{d\rho}{\rho} = \frac{dp}{p} - \frac{dT}{T} \tag{A.3}$$

which, combined with Eqs.(A.1) and (A.2), gives

$$\frac{d\rho}{\rho} = -\left[\frac{g}{R^* T} + \frac{1}{T} \frac{dT}{dH} \right] dH \tag{A.4}$$

The density gradient has been defined as

$$\sigma = \frac{R}{\rho} \left(\frac{d\rho}{dR} \right) = \frac{R}{\rho} \left(\frac{d\rho}{dH} \right)$$

or from Eq.(A.4)

$$\sigma = -R\left[\frac{g}{R^* T} + \frac{1}{T} \frac{dT}{dH} \right] \tag{A.5}$$

For the Earth, at altitude below 120 km, $-\sigma$, which is a dimensionless quantity varies from 750 to 1350 with a weighted average of 900. Fig. A.1 plots the value of $-\sigma$ as function of the altitude. The discrete values are obtained from numerical differentiation of the tabulated U.S. Standard Atmosphere, 1962, while the smooth continuous curve is generated by using the approximate inverse polynomial representation of the atmospheric density as given in the U.S. Standard Atmosphere Supplements, 1966. It appears that the average value of $-\sigma = 900$ as proposed by Chapman in the analysis of reentry trajectories can be used.

At low altitude, the density gradient is used in the form

$$\frac{1}{\rho} \frac{d\rho}{dH} = \frac{\sigma}{R} = -\frac{1}{T} \left[\frac{g}{R^*} + \frac{dT}{dH} \right] \tag{A.6}$$

Using the standard atmosphere, in the troposphere, up to 11 km, dT/dH is equal to -6.5×10^{-3} degrees/m and above 11 km, in the stratosphere, $dT/dH = 0$. Hence we consider the values

$$H < 11{,}000 \text{ m} \quad , \qquad \frac{1}{\rho}\frac{d\rho}{dH} = -\frac{0.0276632}{T}$$

$$H > 11{,}000 \text{ m} \quad , \qquad \frac{1}{\rho}\frac{d\rho}{dH} = -1.57688 \times 10^{-4} \tag{A.7}$$

with T expressed in degrees Kelvin.

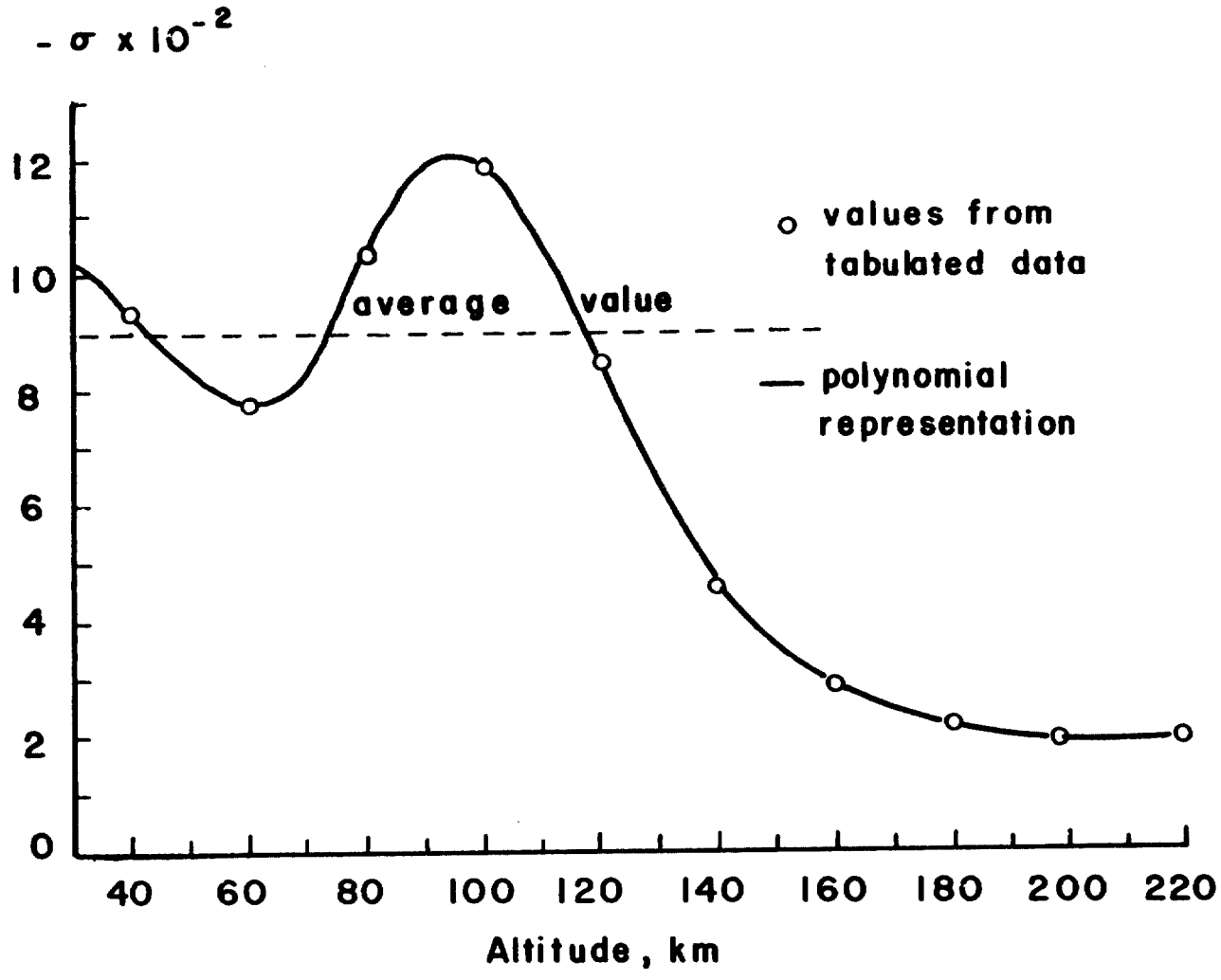

Fig. A.1. The atmospheric density gradient as function of the altitude.

APPENDIX B

VEHICLE CHARACTERISTICS

$S = 6000\ ft^2\ (557.42\ m^2)$

$\ell = 219.12\ ft\ (66.79\ m)$

$\bar{c} = 58.14\ ft\ (17.72\ m)$

$W = 429{,}613\ lbs$

$I_x = 8{,}510{,}000\ slug\text{-}ft^2$

$I_y = 50{,}970{,}000\ slug\text{-}ft^2$

$I_z = 48{,}600{,}000\ slug\text{-}ft^2$

$I_{xz} = 566{,}499\ slug\text{-}ft^2$

Dimensionless Quantities

$B = 3(I_x - I_z)/I_y = -2.359623$

$k_y = I_y/m\bar{c}^2 = 1.129$

$R_o/\bar{c} = 3.6498 \times 10^5$

Aerodynamic Characteristics

As provided in reference 8, with typical values given in Eqs.(245) and (271).

REFERENCES

1. Hepler, A.K., Zeck, H., Walker, W.H., and Shafer, D.E.: Applicability of the Control-Configured Design Approach to Advanced Earth Orbital Transportation Systems, NASA CR-2723, 1978.

2. Freeman, D.C., and Wilhite, A.W.: Effects of Relaxed Static Longitudinal Stability on a Single-Stage-To-Orbit Vehicle Design, NASA TP-1594, 1979.

3. Phillips, W.P., Decker, J.P., Rau, T.R., and Glatt, C.R.: Computer Aided Space Shuttle Orbiter Wing Design Study, NASA TN D-7478, 1974.

4. Brauer, G.L., Cornick, D.E., Habeger, A.R., Petersen, F.M., and Stevenson, R.: Program to Optimize Simulated Trajectories (POST), Volume 1 - Formulation Manual, NASA CR-132689, 1975.

5. Freeman, D.C., and Powell, R.W.: Impact of Far-Aft Center-of-Gravity for a Single-Stage-To-Orbit Vehicle, J. Spacecraft, Vol. 17, pp. 311-315, 1980.

6. Stone, H.W., and Powell, R.W.: Entry Dynamics of Space Shuttle Orbiter with Longitudinal Stability and Control Uncertainties at Supersonic and Hypersonic Speeds, NASA TP-1084, 1977.

7. Stone, H.W., and Powell, R.W.: Entry Dynamics of Space Shuttle Orbiter with Lateral-Directional Stability and Control Uncertainties at Supersonic and Hypersonic Speeds, NASA TP-1011, 1977.

8. Powell, R.W., Aerodynamic Data for the Baseline Control-Configured Vehicle from M = 0.3 to 20.3, Personal communication, September 1980.

9. Nguyen, L.T., Ogburn, M.E., Gilbert, W.P., Kemper, S.K., Brown, P.W., and Deal, P.L.: Simulator Study of Stall/Post-Stall Characteristics of a Fighter Airplane with Relaxed Longitudinal Stability, NASA TP-1538, 1979.

10. Roberson, R.E.: Gravitational Torque on a Satellite Vehicle, Journal of the Franklin Institute, No. 265, pp. 13-22, 1958.

11. Beletskii, V.V.: Motion of an Artificial Satellite About Its Center of Mass, NASA TTF-429, 1966.

12. Laitone, E.V., and Chou, Y.S.: Phugoid Oscillations at Hypersonic Speeds, AIAA Journal, Vol. 3, pp. 732-735, 1965.

13. Longuski, J.M., and Vinh, N.X.: Analytic Theory of Orbit Contraction and Ballistic Entry into Planetary Atmospheres, JPL Publication 80-58, 1980.

14. Whittaker, E.T., and Watson, G.N.: A Course of Modern Analysis, Cambridge University Press, 1963.

15. Watson, G.N.: A Treatise on the Theory of Bessel Functions, Cambridge University Press, 1966.

16. Etkin, B.: Longitudinal Dynamics of a Lifting Vehicle in Orbital Flight, J. Aerospace Sciences, Vol. 28, pp. 779-788, 1961.

17. Vinh, N.X., and Dobrzelecki, A.J.: Non-Linear Longitudinal Dynamics of an Orbital Lifting Vehicle, NASA CR-1449, 1969.

18. Allen, H.J.: Motion of a Ballistic Missile Angularly Misaligned with the Flight Path Upon Entering the Atmosphere and Its Effect Upon Aerodynamic Heating, Aerodynamic Loads, and Miss Distance, NACA TN 4048, 1957.

19. Vinh, N.X., and Laitone, E.V.: Longitudinal Dynamic Stability of a Shuttle Vehicle, J. Astronautical Sciences, Vol. 19, pp. 337-363, 1972.